

FINAL Report C

TRyy1317

**Project Title: Recycled Concrete Aggregate (RCA) for
Infrastructure Elements**

**Report C: Bond Behavior of Mild Reinforcing Steel in
RCA Concrete**

Prepared for
Missouri Department of Transportation
Construction and Materials

Missouri University of Science and Technology, Rolla, Missouri

May 2014

The opinions, findings, and conclusions expressed in this publication are those of the principal investigators and the Missouri Department of Transportation. They are not necessarily those of the U.S. Department of Transportation, Federal Highway Administration. This report does not constitute a standard or regulation.

ABSTRACT

With a growing demand for new construction and the need to replace infrastructure stretched beyond its service life, society faces the problem of an ever-rising production of construction and demolition waste. Furthermore, existing sources of natural raw materials are increasingly burdened in order to support this new construction. In recent decades, engineers have turned to a more sustainable solution of recycling the concrete from construction and demolition waste to help reduce the overall burden on sources of quality natural concrete aggregates.

The objective of this study was to determine the effect of replacing coarse natural aggregates with recycled concrete aggregates (RCA) on the bond strength between deformed mild reinforcing steel and surrounding concrete. Two different RCA replacement levels were considered, 50% and 100%, and were compared to a standard Missouri Department of Transportation (MoDOT) mix design.

To evaluate bond strength, 18 direct pull-out specimens were tested with both #4 (No. 13) and #6 (No. 19) reinforcing bars and 9 full-scale beam specimens were tested with non-confined contact lap splices located at mid-span. The construction and testing procedure of the direct pull-out specimens was based on the RILEM 7-II-128 *RC6: Bond test for reinforcing steel. 1. Pull-out test* (RILEM, 1994). The full-scale beam splice specimens were based on a non-standard test procedure that is considered to be the most realistic stress state response for bond.

Analysis of the test data indicates that replacing more than 50% of coarse natural aggregates results in diminished bond strength over concrete containing only virgin natural aggregates. This result suggests that the existing equation for development and

splice length as reported in AASHTO LRFD and ACI 318 may require additional modification factors to account for the diminished bond strength when associated with replacement of coarse aggregates with RCA at levels greater than 50%.

TABLE OF CONTENTS

	Page
ABSTRACT.....	ii
LIST OF ILLUSTRATIONS.....	vii
LIST OF TABLES.....	xi
1. INTRODUCTION.....	1
1.1. BACKGROUND AND JUSTIFICATION	1
1.1.1. General	1
1.1.2. Benefits of Recycled Aggregate Concrete	1
1.1.3. Concerns with Recycled Aggregate Concrete.....	1
1.2. OBJECTIVES AND SCOPE OF WORK	4
1.3. RESEARCH PLAN	5
1.4. OUTLINE.....	6
2. LITERATURE REVIEW.....	8
2.1. BOND CHARACTERISTICS.....	8
2.2. COMMON BOND TESTS.....	11
2.3. RCA CONCRETE BOND RESEARCH.....	13
3. MIX DESIGNS AND CONCRETE PROPERTIES	18
3.1. INTRODUCTION	18
3.2. CONCRETE PROPERTIES.....	18
3.2.1. Fresh Concrete Properties	18
3.2.2. Compressive Strength of Concrete.....	19
3.2.3. Modulus of Rupture of Concrete.....	21
3.2.4. Modulus of Elasticity of Concrete.....	21
3.2.5. Splitting Tensile Strength of Concrete	21
3.2.6. Fracture Energy of Concrete	22
3.3. RAC MIX DESIGNS	23
3.3.1. Pre-Recycled Concrete Mix Design.....	23
3.3.2. VAC Control Mix Design and Concrete Properties.....	26
3.3.3. RAC-50% Mix Design and Concrete Properties.....	28

3.3.4. RAC-100% Mix Design and Concrete Properties.....	30
3.4. CONCRETE MECHANICAL PROPERTIES	33
3.4.1. Modulus of Rupture Results.....	33
3.4.2. Modulus of Elasticity Results.....	34
3.4.3. Splitting Tensile Strength Results	34
3.4.4. Fracture Energy Results	35
3.4.5. Comparison of Mechanical Properties	36
4. EXPERIMENTAL PROGRAM.....	38
4.1. INTRODUCTION	38
4.2. RCA PRODUCTION	38
4.3. DIRECT PULL-OUT SPECIMENS	40
4.3.1. Direct Pull-Out Specimen Design	40
4.3.2. Direct Pull-Out Specimen Fabrication	42
4.3.3. Direct Pull-Out Specimen Test Set-Up	44
4.3.4. Direct Pull-Out Specimen Test Procedure	45
4.4. BEAM SPLICE SPECIMENS	46
4.4.1. Beam Splice Specimen Design.....	46
4.4.2. Beam Splice Specimen Fabrication.....	47
4.4.3. Beam Splice Specimen Test Set-Up.....	52
4.4.4. Beam Splice Specimen Test Procedure.....	54
5. TEST RESULTS AND EVALUATIONS	55
5.1. DIRECT PULL-OUT TEST RESULTS.....	55
5.2. BEAM SPLICE TEST RESULTS.....	58
5.3. REINFORCING BAR TENSION TEST RESULTS	65
5.4. ANALYSIS OF RESULTS	68
5.4.1. Methodology	68
5.4.2. Analysis and Interpretation of Direct Pull-Out Results.....	70
5.4.3. Analysis and Interpretation of Beam Splice Results	78
6. FINDINGS, CONCLUSIONS AND RECOMMENDATIONS	89
6.1. INTRODUCTION	89
6.2. FINDINGS	89

6.2.1. Material Properties Testing	89
6.2.2. Direct Pull-Out Testing	90
6.2.3. Beam Splice Testing.....	90
6.3. CONCLUSIONS	91
6.3.1. Direct Pull-Out Testing	91
6.3.2. Beam Splice Testing.....	91
6.4. RECOMMENDATIONS.....	92
APPENDIX A: DIRECT PULL-OUT TEST DATA PLOTS	94
APPENDIX B: BEAM SPLICE TEST DATA PLOTS	100
APPENDIX C: PHOTOGRAPHS OF BEAM SPLICE FAILURES.....	104
APPENDIX D: STATISTICAL ANALYSIS OF RESULTS	114
BIBLIOGRAPHY.....	127

LIST OF ILLUSTRATIONS

Figure	Page
Figure 1.1: States using RCA as Aggregate.....	3
Figure 1.2: States using RCA as Base Aggregate.....	3
Figure 1.3: States using RCA in PC Concrete	4
Figure 2.1: Bond Force Transfer Mechanisms (ACI 408, 2003).....	8
Figure 2.2: Formation of Goto Cracks (ACI 408, 2003)	9
Figure 2.3: Formation of Hoop Stresses and Resulting Splitting Cracks (ACI 408, 2003)	9
Figure 2.4: Pull-Out Failure (ACI 408, 2003)	10
Figure 2.5: Schematic Direct Pull-Out Test (ACI 408, 2003)	11
Figure 2.6: Schematic Beam-End Test (ACI 408, 2003).....	12
Figure 2.7: Schematic Beam Anchorage Test (ACI 408, 2003).....	13
Figure 2.8: Schematic Beam Splice Test (ACI 408, 2003).....	13
Figure 3.1: Compressive Strength Test.....	20
Figure 3.2: Splitting Tensile Failure Mode.....	22
Figure 3.3: Control Mix Strength Gain with Time	28
Figure 3.4: RAC-50 Mix Strength Gain with Time	30
Figure 3.5: RAC-100 Mix Strength Gain with Time	33
Figure 3.6: Comparison of Normalized Mechanical Properties	37
Figure 4.1: Formwork for Casting Pre-Recycled Concrete	39
Figure 4.2: Schematic of #4 (No. 13) Bar Direct Pull-Out Specimen	41
Figure 4.3: Schematic of #6 (No. 19) Bar Direct Pull-Out Specimen	41
Figure 4.4: Completed Direct Pull-Out Specimens in Molds	44
Figure 4.5: Test Set-Up for Direct Pull-Out Specimen.....	45
Figure 4.6: LVDT Set-Up for Direct Pull-Out Specimen.....	45
Figure 4.7: Schematic of Beam Splice Specimen Profile	48
Figure 4.8: Schematic of Beam Splice Specimen Plan.....	48
Figure 4.9: Spliced Length with Attached Strain Gauges.....	49
Figure 4.10: Completed Cage for Beam Splice Specimen	49

Figure 4.11: Steel Cages in Forms	50
Figure 4.12: Casting of Beam Splice Specimens	51
Figure 4.13: Schematic of Beam Splice Loading	53
Figure 4.14: Beam Splice Specimens in Load Test Frame	53
Figure 4.15: LVDT Set-Up for Beam Splice Test	54
Figure 5.1: Peak Bond Stresses for VAC Pull-Out Specimens	57
Figure 5.2: Peak Bond Stresses for RAC-50 Pull-Out Specimens	57
Figure 5.3: Peak Bond Stresses for RAC-100 Pull-Out Specimens	58
Figure 5.4: Typical Plot of Slip versus Applied Load	59
Figure 5.5: Peak Loads for VAC Beam Splice Specimens.....	61
Figure 5.6: Peak Loads for RAC-50 Beam Splice Specimens.....	62
Figure 5.7: Peak Loads for RAC-100 Beam Splice Specimens.....	62
Figure 5.8: Peak Stresses for VAC Beam Splice Specimens	63
Figure 5.9: Peak Stresses for RAC-50 Beam Splice Specimens	63
Figure 5.10: Peak Stresses for RAC-100 Beam Splice Specimens	64
Figure 5.11: Typical Load versus Deflection Plot (VAC-3).....	66
Figure 5.12: Typical Load versus Strain Plot (VAC-3).....	66
Figure 5.13: Beam Splice Crack Propagation at Failure (RAC50-1)	67
Figure 5.14: Beam Splice Specimen Bottom View at Failure (RAC50-1).....	67
Figure 5.15: Average #4 Pull-Out Bond Stresses by Square Root Normalization	74
Figure 5.16: Boxplot of #4 Pull-Out Bond Stresses by Square Root Normalization	74
Figure 5.17: Average #4 Pull-Out Bond Stresses by Fourth Root Normalization.....	75
Figure 5.18: Boxplot of #4 Pull-Out Bond Stresses by Fourth Root Normalization.....	75
Figure 5.19: Average #6 Pull-Out Bond Stresses by Square Root Normalization	76
Figure 5.20: Boxplot of #6 Pull-Out Bond Stresses by Square Root Normalization	76
Figure 5.21: Average #6 Pull-Out Bond Stresses by Fourth Root Normalization.....	77
Figure 5.22: Boxplot of #6 Pull-Out Bond Stresses by Fourth Root Normalization.....	77
Figure 5.23: Comparison of #4 (No.13) and #6 (No. 19) Square Root Normalized Pull-out Results	78
Figure 5.24: Comparison of #4 (No.13) and #6 (No. 19) Fourth Root Normalized Pull-out Results	79
Figure 5.25: Average Beam Splice Peak Stresses by Square Root Normalization	82

Figure 5.26: Boxplot of Peak Stresses by Square Root Normalization	82
Figure 5.27: Average Beam Splice Peak Stresses by Fourth Root Normalization.....	83
Figure 5.28: Boxplot of Peak Stresses by Fourth Root Normalization.....	83
Figure 5.29: Comparison of Prediction Ratios for Beam Splice Results.....	87
Figure 5.30: Comparison of Beam Splice Results to Database	88
Figure A.1: Bond Stresses for #4 Pull-Out Specimens, Square Root Normalization.....	95
Figure A.2: Bond Stresses for #4 Pull-Out Specimens, Fourth Root Normalization	95
Figure A.3: Bond Stresses for #6 Pull-Out specimens, Square Root Normalization	96
Figure A.4: Bond Stresses for #6 Pull-Out Specimens, Fourth Root Normalization	96
Figure A.5: Applied Load vs. Slip Plot for #4 (No. 13) VAC-PO4	97
Figure A.6: Applied Load vs. Slip Plot for #6 (No. 19) VAC-PO6	97
Figure A.7: Applied Load vs. Slip Plot for #4 (No. 13) RCA50-PO4.....	98
Figure A.8: Applied Load vs. Slip Plot for #6 (No. 19) RCA50-PO6.....	98
Figure A.9: Applied Load vs. Slip Plot for #4 (No. 13) RCA100-PO4.....	99
Figure A.10: Applied Load vs. Slip Plot for #6 (No. 19) RCA100-PO6.....	99
Figure B.1: Applied Load vs. Strain for VAC Specimens.....	101
Figure B.2: Applied Load vs. Strain for RAC-50 Specimens.....	101
Figure B.3: Applied Load vs. Strain for RAC-100 Specimens.....	102
Figure B.4: Applied load vs. Midspan Deflection for VAC	102
Figure B.5: Applied load vs. Midspan Deflection for RAC-50	103
Figure B.6: Applied load vs. Midspan Deflection for RAC-100.....	103
Figure C.1: Side View of VAC-1	105
Figure C.2: Bottom View of VAC-1.....	105
Figure C.3: Side View of VAC-2	106
Figure C.4: Bottom View of VAC-2.....	106
Figure C.5: Side View of VAC-3	107
Figure C.6: Bottom View of VAC-3.....	107
Figure C.7: Side View of RAC50-1.....	108
Figure C.8: Bottom View of RAC50-1	108
Figure C.9: Side View of RAC50-2.....	109
Figure C.10: Bottom View of RAC50-2.....	109

Figure C.11: Side View of RAC50-3.....	110
Figure C.12: Bottom View of RAC50-3.....	110
Figure C.13: Side View of RAC100-1.....	111
Figure C.14: Bottom View of RAC100-1.....	111
Figure C.15: Side View of RAC100-2.....	112
Figure C.16: Bottom View of RAC100-2.....	112
Figure C.17: Side View of RAC100-3.....	113
Figure C.18: Bottom View of RAC100-3.....	113

LIST OF TABLES

Table	Page
Table 3.1: Fresh Concrete Properties of Pre-Recycled Concrete	24
Table 3.2: Compressive Strength Results of Pre-Recycled Concrete.....	25
Table 3.3: Splitting Tensile Strength Results of Pre-Recycled Concrete	25
Table 3.4: Modulus of Rupture Results of Pre-Recycled Concrete.....	26
Table 3.5: Modulus of Elasticity Results of Pre-Recycled Concrete.....	26
Table 3.6: Control Mix Design Specifications	27
Table 3.7: Control Design Mix Proportions, Oven-Dry Basis.....	27
Table 3.8: Control Splitting Tensile Strength Results	28
Table 3.9: RAC-50 Mix Design Specifications	29
Table 3.10: RAC-50 Design Mix Proportions, Oven-Dry Basis	30
Table 3.11: RAC-50 Splitting Tensile Strength Results.....	31
Table 3.12: RAC-100 Mix Design Specifications	32
Table 3.13: RAC-100 Design Mix Proportions, Oven-Dry Basis	32
Table 3.14: RAC-100 Splitting Tensile Strength Results.....	32
Table 3.15: Modulus of Rupture Results	34
Table 3.16: Modulus of Elasticity Results.....	35
Table 3.17: Splitting Tensile Strength Results	35
Table 3.18: Fracture Energy Results.....	36
Table 5.1: Testing Matrix for Direct Pull-Out Specimens.....	55
Table 5.2: Pull-Out Test Results.....	56
Table 5.3: Testing Matrix for Beam Splice Specimens	59
Table 5.4: Beam Splice Test Results	61
Table 5.5: #6 Reinforcing Bar Tension Test Results.....	67
Table 5.6: Beam Splice Test Day Compressive Strengths	70
Table 5.7: Normalized Bond Stresses for Pull-Out Specimens	73
Table 5.8: Normalized Developed Stresses for Beam Splice Specimens.....	81
Table 5.9: Comparison of Measured to Theoretical Stress in Beam Splice Specimens	85
Table 5.10: Prediction Ratios for Beam Splice Results.....	87

Table D.1: Parametric Analysis of #4 (No.13) Pull-Out Results with Square Root Normalization between VAC and RAC-50	115
Table D.2: Non-parametric Analysis of #4 (No.13) Pull-Out Results with Square Root Normalization between VAC and RAC-50	115
Table D.3: Parametric Analysis of #4 (No.13) Pull-Out Results with Square Root Normalization between VAC and RAC-100	116
Table D.4: Non-parametric Analysis of #4 (No.13) Pull-Out Results with Square Root Normalization between VAC and RAC-100	116
Table D.5: Parametric Analysis of #6 (No.19) Pull-Out Results with Square Root Normalization between VAC and RAC-50	117
Table D.6: Non-Parametric Analysis of #6 (No.19) Pull-Out Results with Square Root Normalization between VAC and RAC-50	117
Table D.7: Parametric Analysis of #6 (No.19) Pull-Out Results with Square Root Normalization between VAC and RAC-100	118
Table D.8: Non-Parametric Analysis of #6 (No.19) Pull-Out Results with Square Root Normalization between VAC and RAC-100	118
Table D.9: Parametric Analysis of #4 (No.13) Pull-Out Results with Fourth Root Normalization between VAC and RAC-50	119
Table D.10: Non-parametric Analysis of #4 (No.13) Pull-Out Results with Fourth Root Normalization between VAC and RAC-50	119
Table D.11: Parametric Analysis of #4 (No.13) Pull-Out Results with Fourth Root Normalization between VAC and RAC-100	120
Table D.12: Non-parametric Analysis of #4 (No.13) Pull-Out Results with Fourth Root Normalization between VAC and RAC-100	120
Table D.13: Parametric Analysis of #6 (No.19) Pull-Out Results with Fourth Root Normalization between VAC and RAC-50	121
Table D.14: Non-Parametric Analysis of #6 (No.19) Pull-Out Results with Fourth Root Normalization between VAC and RAC-50	121
Table D.15: Parametric Analysis of #6 (No.19) Pull-Out Results with Fourth Root Normalization between VAC and RAC-100	122
Table D.16: Non-Parametric Analysis of #6 (No.19) Pull-Out Results with Fourth Root Normalization between VAC and RAC-100	122
Table D.17: Parametric Analysis of Beam Splice Results with Square Root Normalization between VAC and RAC-50	123
Table D.18: Non-Parametric Analysis of Beam Splice Results with Square Root Normalization between VAC and RAC-50	123
Table D.19: Parametric Analysis of Beam Splice Results with Square Root Normalization between VAC and RAC-100	124

Table D.20: Non-Parametric Analysis of Beam Splice Results with Square Root
Normalization between VAC and RAC-100124

Table D.21: Parametric Analysis of Beam Splice Results with Fourth Root
Normalization between VAC and RAC-50125

Table D.22: Non-Parametric Analysis of Beam Splice Results with Fourth Root
Normalization between VAC and RAC-50125

Table D.23: Parametric Analysis of Beam Splice Results with Fourth Root
Normalization between VAC and RAC-100126

Table D.24: Non-Parametric Analysis of Beam Splice Results with Fourth Root
Normalization between VAC and RAC-100126

1. INTRODUCTION

1.1. BACKGROUND AND JUSTIFICATION

1.1.1. General. The construction of buildings, bridges, and roadways continues to increase in the twenty-first century, especially in areas with ever-growing populations. Existing structures and highways require repair or replacement as they reach the end of their service life or simply no longer satisfy their intended purpose due to the growing population. As modern construction continues, two pressing issues will become more apparent to societies: an increasing demand for construction materials, especially concrete and asphalt aggregates, and an increasing production of construction and demolition waste. Already, the Federal Highway Administration (FHWA) estimates that two billion tons of new aggregate are produced each year in the United States. This demand is anticipated to increase to two and a half billion tons each year by 2020. With such a high demand for new aggregates, the concern arises of the depletion of the current sources of natural aggregates and the availability of new sources. Similarly, the construction waste produced in the United States is expected to increase. From building demolition alone, the annual production of construction waste is estimated to be 123 million tons (FHWA). Currently, this waste is most commonly disposed of in landfills.

To address both the concern of increasing demand for new aggregates and increasing production of waste, many states have begun to recognize that a more sustainable solution exists in recycling waste concrete for use as aggregate in new concrete, or recycled concrete aggregates (RCA). The solution helps address the question of how to sustain modern construction demands for aggregates as well as helps to reduce the amount of waste that enters already over-burdened landfills.

Based on a survey by FHWA in 2002, many states had begun to implement recycled concrete aggregates in some ways in new construction. As shown in **Figure 1.1**, most states had recognized the many uses of RCA as a raw material, such as for rip-rap, soil stabilization, pipe bedding, and even landscape materials. As shown in **Figure 1.2**, many states had gone a step further in integrating RCA into roadway systems for use as aggregate base course material. However, as shown in **Figure 1.3**, only a small number of states had begun using RCA in Portland cement concrete for pavement construction. However, over the intervening 12 years, the use of RCA has increased significantly, particularly within the last 5 years, and the Missouri Department of Transportation (MoDOT) has instituted a very aggressive program to increase the use of recycled materials in transportation-related construction. However, there are currently no acceptable standards or guidelines in the U.S. for utilizing RCA in structural concrete.

1.1.2. Benefits of Recycled Aggregate Concrete. The use of recycled aggregate concrete (RAC) offers a sustainable solution for the continued growth of modern infrastructure. Primarily, RAC concrete diverts construction and demolition waste from the solid waste stream while easing the demand from non-renewable natural aggregate sources. Much research has been performed that shows up to 100% of the coarse aggregates in new concrete can be replaced with RCA.

1.1.3. Concerns with Recycled Aggregate Concrete. RCAs are composed of both the original, or virgin, aggregate, as well as mortar which remains adhered to the surface of the aggregate. In the production of RCA, the removal of all this residual mortar would prove costly and detrimental to the integrity of the virgin aggregates within the concrete. Therefore, residual mortar is inevitable. Research has shown that this residual

mortar causes high water absorption, low density, low specific gravity, and high porosity in RCAs compared to natural aggregates (Kou et al. 2012). These effects in the recycled aggregate can decrease hardened concrete properties of RAC. According to Abbas et al. (2008), the amount of residual mortar on the RCA can significantly affect the mechanical and durability properties of RAC. To reduce the negative impacts of this residual mortar, new mix design methods such as the equivalent mortar volume method can be used.

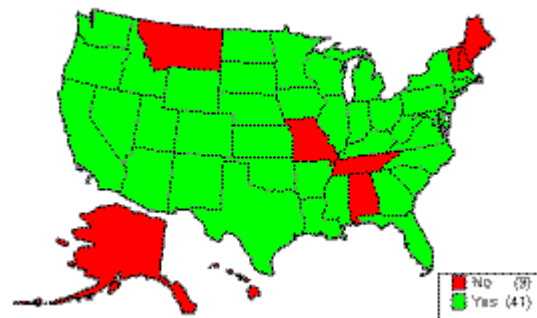


Figure 1.1: States using RCA as Aggregate

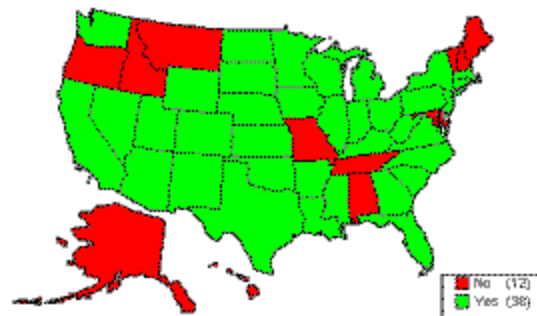


Figure 1.2: States using RCA as Base Aggregate

and construct test fixtures; (4) design and construct test specimens; (5) test specimens to failure and record applicable data; (6) analyze results and conduct comparisons between RAC and control mix designs; (7) develop conclusions and recommendations; (8) prepare this report in order to document the information obtained during this study.

1.3 RESEARCH PLAN

For this experimental program, the bond performance of RCA concrete designed at different replacement levels will be investigated and compared with a standard MoDOT mix design. The RCA mix design procedure to be investigated is the direct replacement method. This design method is a volumetric procedure that replaces a percentage of the virgin coarse aggregate directly with the RCA. For this bond study, the three replacement levels that will be considered are 0%, 50%, and 100%. The 0% replacement mix will serve as the control and will contain only virgin aggregates. For the 50% RCA mix, half of the total volume of coarse virgin aggregates will be substituted with RCA. For the 100% mix, the total volume of coarse virgin aggregates will consist of RCA. For all RCA mixes, the virgin aggregates used to make the RCA will be MoDOT approved 1" Potosi Dolomite. To control the amount of variables in this study, the RCA will be produced from beams that are cast and cured by the researchers in a controlled laboratory environment. The crushing procedure and pre-crushed and post-crushed environmental conditions of the aggregates will be constant.

To investigate the bond performance, two bond test types will be performed: direct pull out tests and large scale beam splice tests. Direct pull out tests will be performed based on the RILEM 7-II-128 *RC6: Bond test for reinforcing steel. 1. Pull-out*

test (RILEM, 1994). While direct pull out tests do not provide a realistic flexural type stress-state response in the specimen, they provide a basis of comparison among other direct pull out results and are commonly used for bond performance comparison. A total of 18 direct pull-out specimens were constructed and tested to bond failure using this test method. The full scale beam splice test will be based on a non-standardized procedure that has been developed in previous bond research. The beam splice test provides the most realistic response for bond performance in flexural stress state. A total of 9 full-scale beam splice specimens were constructed and tested to bond failure.

1.4 OUTLINE

This report consists of six chapters and four appendices. Chapter 1 contains a brief explanation of the current uses, benefits, and concerns of RAC as well as the objective and scope of work of this study.

Chapter 2 provides a discussion of the bond force transfer between concrete and embedded deformed steel bars, bond failure mechanisms, accepted tests for characterizing bond strength, and a review of the literature for RAC bond research.

Chapter 3 details the mix designs that were developed for this study as well as the test methods used to determine fresh and hardened concrete properties that were found at the time of testing the bond specimens.

Chapter 4 details the design, fabrication, test setup, and test procedure for the direct pull-out and full-scale beam splice specimens.

Chapter 5 provides the recorded test data, the methodology used to normalize the data, normalized results, and a comparison among RCA replacement levels and across bar size.

Chapter 6 summarizes the findings, conclusions, and recommendations from this study.

2. LITERATURE REVIEW

2.1. BOND CHARACTERISTICS

In reinforced concrete, the transfer of forces between deformed steel bars and the adjacent concrete occurs by three primary modes: 1) chemical adhesion between the bar and concrete, 2) friction forces, transverse forces, and relative slip, and 3) bearing of the ribs or deformations against the surrounding concrete. For deformed bars, adhesion is lost after the initial slip. This slip initiates bearing of the ribs against the surrounding concrete surface. Frictional forces along the surface of the bar remain small compared to these bearing forces, and bearing plays the biggest role in bond behavior. To balance the forces on the surface of the deformed bar, which are shown in **Figure 2.1**, compressive and shear stresses develop in the contacting concrete surfaces. These stresses develop into tensile stresses which in turn can lead to cracking of the concrete (ACI 408, 2003).

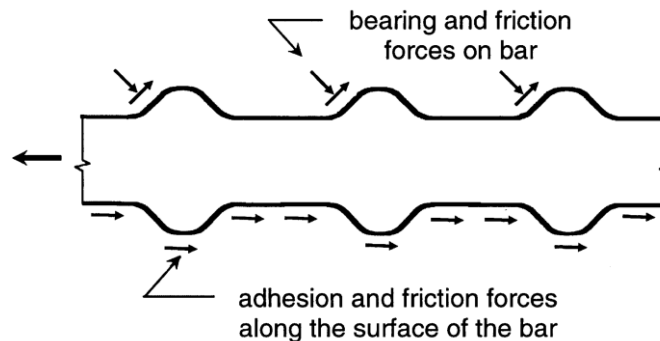


Figure 2.1: Bond Force Transfer Mechanisms (ACI 408, 2003)

Goto cracks can form as a result of the tension stresses induced by the compression forces at the bearing contact surfaces extending from the ribs. The formation of these cracks is shown in **Figure 2.2**. These cracks can result in a conical failure surface

for bars in tension that extend outside of the concrete. However, Goto cracks do not play a significant role in bond anchorage or reinforcement development (ACI 408, 2003).

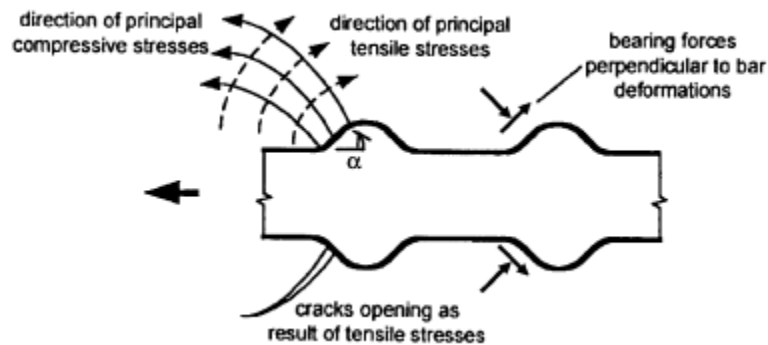


Figure 2.2: Formation of Goto Cracks (ACI 408, 2003)

Transverse cracks, form when the minimum concrete cover or bar spacing is small. The transverse cracks form as a result of hoop tensile stresses in the surrounding concrete induced by the bearing action of the ribs. With small cover, these cracks can reach the outside surface of the concrete and form splitting cracks as shown in **Figure 2.3**.

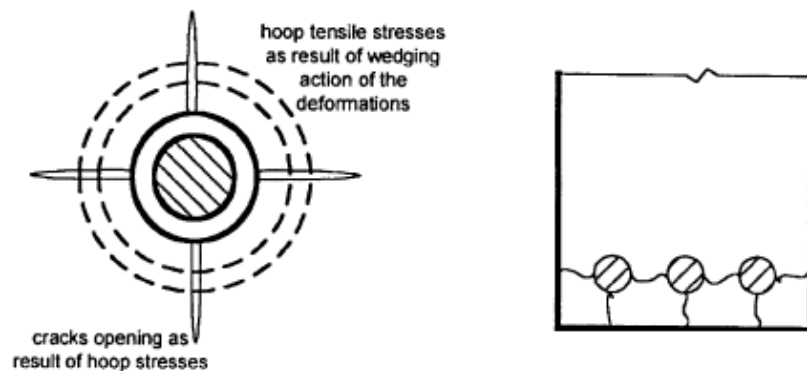


Figure 2.3: Formation of Hoop Stresses and Resulting Splitting Cracks (ACI 408, 2003)

When concrete cover and bar spacing is sufficiently large or enough transverse reinforcement is provided to prevent splitting failure, the bond failure may be a pull out type. This failure results in the shearing along the top surfaces of the reinforcing bar's ribs as shown in **Figure 2.4**. Most bond failures result as a combination of both concrete splitting and pull out type failure modes (ACI 408, 2003). It is also possible that if anchorage of the bar into the concrete is adequate or sufficient confinement is provided to delay crack propagation, the steel bar may yield or strain harden prior to bond failure. Thus, bond failure only occurs when stresses in the steel do not exceed its tensile strength.

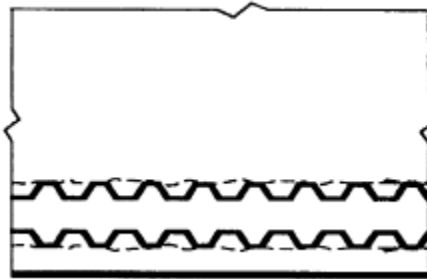


Figure 2.4: Pull-Out Failure (ACI 408, 2003)

Based on the above discussion, it is obvious that bond behavior is largely controlled by the following factors: mechanical properties of the surrounding concrete, concrete cover and bar spacing, presence or absence of confinement, surface condition of the bar, and the geometry of the bar (namely deformation shape, rib height, and bar diameter).

2.2. COMMON BOND TESTS

Many testing methods have been developed to measure bond strength between concrete and reinforcing steel bars. The configuration of each test method has an important role in the bond response. Four of the most common test configurations are pull out specimens, beam-end specimens, beam anchorage specimens, and splice specimens (full beams). The direct pull-out test method is the most commonly used due to the ease of fabricating and testing of these specimens. However, this method produces the least realistic bond response of the four listed. As the bar of a pull-out specimen is loaded in tension, the surrounding concrete is in compression. In most practical applications of reinforced concrete, both the bar and the surrounding concrete experience tension. A concern with pull-out specimens is this additional confinement from the induced compression at the anchorage zone. Due to the unrealistic nature of the stress state produced, pull-out specimens are not recommended as the only means of determining bond strength, but can serve as a useful comparison (ACI 408, 2003). A schematic of the pull-out test is shown in **Figure 2.5**.

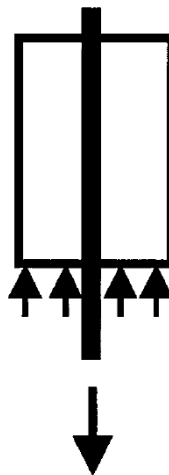


Figure 2.5: Schematic Direct Pull-Out Test (ACI 408, 2003)

The beam-end specimen, also known as the modified cantilever, more accurately represents reinforced concrete behavior. In this method, the bar and the surrounding concrete experience tension. This is achieved by loading the bar in tension and applying a compressive force a distance approximately equal to the embedded length of the bar away from the end of the bar. These specimens are relatively easy to fabricate and test, and offer bond strength measurements more accurate to full-scale tests. A schematic of the beam-end test is shown in **Figure 2.6**.

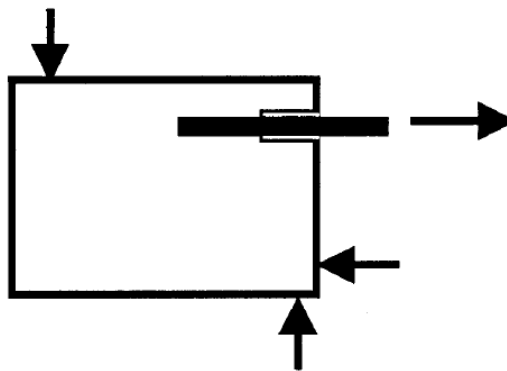


Figure 2.6: Schematic Beam-End Test (ACI 408, 2003)

Beam anchorage specimens are full-scale specimens with a configuration designed to simulate flexural cracks with a known bonded length. While these specimens provide a realistic bond response, they can be challenging to fabricate (ACI 408, 2003). A schematic of the anchorage test is shown in **Figure 2.7**.

Splice specimens are an alternative full-scale bond test. These splice beams are tested under four-point loading such that the splice is located in a constant moment region, similarly to the modulus of rupture test. Splice specimens are much easier to fabricate and will produce similar results as the anchorage specimens. Due to the simplicity of fabricating these specimens and the realistic bond response, splice

specimens have provided the bulk of data used in developing current empirical design equations (ACI 408, 2003). A schematic of the beam splice test is shown in **Figure 2.8**.

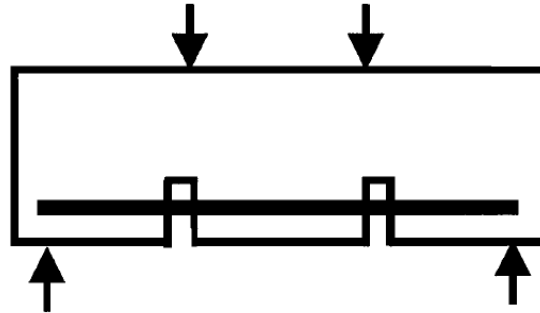


Figure 2.7: Schematic Beam Anchorage Test (ACI 408, 2003)

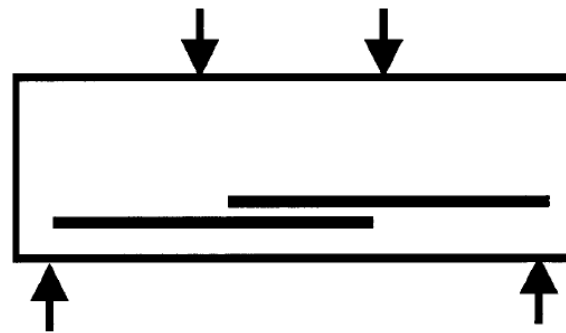


Figure 2.8: Schematic Beam Splice Test (ACI 408, 2003)

2.3. RCA CONCRETE BOND RESEARCH

Much of the existing literature on recycled concrete aggregates (RCA) focuses on the mechanical and durability characteristics of concretes made with RCA. Few studies have been conducted to evaluate the structural performance of RCA concrete, and of those even fewer have concentrated on the bond characteristics of RCA concrete. In a study by Ajdukiewicz and Kliszczewicz (2002), pull-out specimens designed per RILEM recommendations were used to evaluate bond performance of 0% and 100% RCA

replacement. The mix designs used in this study were developed by conventional direct replacement of natural aggregates with RCA. They found that there is no significant difference between bond strength of deformed bars embedded in concrete with coarse RCA replacement and concrete containing only natural coarse aggregates. In this study, the greatest difference in bond strength was observed when smooth bars were used. There was a 20% decrease in bond strength when both coarse and fine aggregates were replaced with RCA, and an 8% decrease when natural sand and coarse RCA was used. (Ajdukiewicz and Kliszczewicz 2002) Typically, though, RCA fines are not recommended for use in new concretes.

Studies have shown that replacing natural sand with fine RCA will drastically increase the water demand and reduce the mix workability. Likewise, the drying shrinkage increases significantly from concrete made with coarse RCA only (20% to 50% more) to concretes made with both fine and coarse RCA (70% to 100% more). Further studies have shown that the mechanical properties are more negatively impacted with the addition of RCA fines. The decrease in compressive strength, tensile strength, and modulus of elasticity are much more pronounced when both fine and coarse RCA are present than when only coarse RCA is present (ACI 555R 2001).

Xiao and Falkner (2005) investigated the bond performance of concretes with 0%, 50%, and 100% replacement of coarse natural aggregates only with RCA using 36 direct pull-out specimens. The conclusions from this study were similar to those by Ajdukiewicz and Kliszczewicz (2002), namely that no difference was observed between the bond strength of deformed bars at 0% RCA replacement and 50% or 100% RCA

replacement. When smooth bars were used, a maximum decrease in bond strength of 12% was observed in the RCA concrete (Xiao and Falkner 2005).

Generally, the mix design method used with RCA concrete has a significant impact on bond strength to mild steel reinforcing bars. Currently, there is no standard procedure for mix design using RCA. The conventional method used in much of the current literature is a direct replacement of coarse aggregate with RCA. However, research has shown that the mortar attached to RCA negatively influences the mechanical and durability properties of RCA concrete (Shayan, 2003). To compensate for this residual mortar on RCA particles, Abbas (2008) has proposed a mix design procedure coined the “Equivalent Mortar Volume” (EMV) method. The key aspect of the EMV method is that the residual mortar of RCA is included in the total mortar volume of the mix, and the amount of new mortar and total amount of coarse aggregate are adjusted to account for this difference (Abbas, 2008).

Existing research has shown that bond strength of RCA designed by the conventional method is lower than bond strength of RCA designed by the EMV method. In 2008, Fathifazl utilized beam-end test specimens to evaluate bond performance under a more realistic stress state response with both conventional and EMV mix designs. Using beam-end specimens with a Canadian standard No. 30 ($d_b = 1.18$ in. or 29.9 mm) deformed reinforcing bars, Fathifazl found that the bond strength (normalized by the square root of compressive strength) of concrete specimens designed using conventional methods of coarse aggregate replacement were 24% lower than their companion natural aggregate specimens. The study showed that bond strength of specimens designed using

the EMV method were only 6% lower than their companion natural aggregate specimens. (Fathifazl, 2008)

In order to investigate the effect of bar size, Fathifazl compared the bond strengths of beam-end specimens containing either a Canadian standard No. 15 ($d_b = 0.63$ in. or 16.0 mm) or No. 30 ($d_b = 1.18$ in. or 29.9 mm) deformed bar. RCA made from two different sources and with different original virgin aggregate material was used. He found that, regardless of the original virgin aggregate material in the RCA and mix design method, the specimens containing No. 15 bars had higher bond strengths than those containing No. 30 bars. These findings are in consensus with ACI 408 that length to develop a reinforcing bar increases as bar diameter increases. This relationship is reflected in the development length equation presented in ACI 318. Furthermore, he found that when designed by the conventional method of direct replacement of natural aggregates for RCA, specimens containing No. 15 bars had 35% higher bond strengths than the specimens containing No. 30 bars. However, when designed by the EMV method, specimens containing No. 15 bars had bond strengths of at least 41% higher than those containing No. 30 bars (Fathifazl 2008).

In 2011, Butler, West, and Tighe evaluated bond performance using 100% direct replacement of coarse aggregates with RCA using 24 beam-end test specimens. This study showed that natural aggregate beam-end specimens had bond strengths 9% to 21% higher than RCA beam-end specimens. Furthermore, they investigated a correlation between the RCA aggregate crushing value (ACV) and bond strength of concretes made with RCA. Using natural aggregates and two different sources of RCA, they found that as ACV increases, the bond strength decreases. For both RCA sources, the ACV of the RCA

was 26% to 43% higher than natural aggregates. Previous research had shown that as the ACV increases, fracture energy of the resulting concrete decreases, and since bond is also related to fracture energy, the researchers reasoned that the ACV would offer a method to predict bond strength when using RCA. Additionally, they observed a strong relationship between ACV and splitting tensile strength, namely that as ACV increases, splitting tensile strength decreases (Butler et al. 2011).

Bond failures where splitting cracks control the peak load is governed by the tensile response of the concrete. The tensile response depends on the splitting tensile capacity and fracture energy, or capacity of the concrete to dissipate energy as a crack opens. As described in ACI 408R (2003), concrete with higher fracture energies provide improved bond capacities even if the concrete has similar tensile strengths.

3. MIX DESIGNS AND CONCRETE PROPERTIES

3.1. INTRODUCTION

The following section contains the procedures used to determine the fresh properties as well as the hardened mechanical properties of the concrete used in this study. A discussion of the mix designs used and their respective properties is also reported in this section.

3.2. CONCRETE PROPERTIES

3.2.1. Fresh Concrete Properties. For all three mixes used in this study the fresh concrete properties that were found were slump, unit weight, and air content. The slump test was performed in accordance with ASTM C 143 (2010) *Standard Test Methods for Slump of Hydraulic Cement Concrete*. The inside of a standard slump cone was wetted and placed on a damp surface. Concrete was added to the cone in three equal lifts and rodded 25 times each lift with the appropriately dimensioned steel rod. Excess concrete was struck off at the top of the cone using the rod, and any superfluous concrete was removed from around the base of the mold. The mold was lifted at a constant rate over five seconds, and the cone was inverted next to the slumped concrete. The slump measurement was taken from the rod placed over the top of the inverted cone to the center of the slumped concrete.

The unit weight of the concrete was determined in accordance with ASTM C 138 (2010) *Standard Test Method for Density (Unit Weight), Yield, and Air Content (Gravimetric) of Concrete*. A steel measure of known volume was weighed then filled with concrete in three equal lifts. Each lift was rodded 25 times and tapped with a rubber

mallet to help consolidate the concrete. Once filled, a steel plate was placed flat on the top of the measure, covering approximately $\frac{3}{4}$ of the open area. The plate was pulled back across the covered area to screed off excess concrete. The plate was then placed flat in the same position and pushed forward to screed the rest of the open area of the measure. Next, the steel plate was tilted at an angle and used to screed the top surface of the measure until it was level and smooth. A wet sponge was used to wipe away excess concrete from the outside of the measure and along the top rim. The measure was then weighed, and the unit weight was determined.

The air content of the fresh concrete was determined in accordance with ASTM C 231 (2010) *Standard Test Method for Air Content of Freshly Mixed Concrete by the Pressure Method* using a type B pressure meter. After the unit weight was determined the same measure filled with concrete was used to determine air content. The pressure meter lid was wetted and secured over the top of the measure. The air chamber positioned on top of this lid was sealed off, and the appropriate initial pressure was added to the chamber. Next, water was gently injected into one petcock until it flowed without air bubbles from the opposite petcock ensuring the space between the lid and the surface of the concrete was filled with water. The stream of water was inspected for the presence of mortar, which would invalidate the test. The petcocks were then closed, and the air from the chamber was injected into the concrete-filled bottom measure while simultaneously tapping the measure with a rubber mallet. The air content was then recorded from the gauge on the pressure meter.

3.2.2. Compressive Strength of Concrete. The compressive strength, f'_c , of the concrete was determined as per ASTM C39 (2011) *Standard Test Method for*

Compressive Strength of Cylindrical Concrete Specimens. For each set of direct pull-out and beam splice specimens, accompanying cylinders were made to determine the compressive strength. The cylindrical molds used had a diameter of 4 in. (10.2 cm) and height of 8 in. (20.3 cm). These cylinders were left to cure in the same condition next to the bond test specimens. The compressive strength of the concrete was tested at 1, 3, 7, 14, 28, and 60 days as well as on the days of testing the bond specimens. Prior to testing, the cylinders were capped with a sulfur compound to give a uniform stress distribution during testing. The load rate was 565lb/sec (2.5kN/sec) as per the ASTM C39 standard. **Figure 3.1** shows a capped cylinder in the loading machine. Three specimens were tested with the average representing one strength data point. The compressive strength of each mix design was determined from companion cylinders to the bond test specimens on the day of testing.



Figure 3.1: Compressive Strength Test

3.2.3. Modulus of Rupture of Concrete. The modulus of rupture, f_r , was determined according to ASTM C 78 (2010) *Standard Test Method for Flexural Strength of Concrete*. Small beams with dimensions 6 in. x 6 in. x 24 in. (15 cm x 15 cm x 60 cm) were cast to find the modulus of rupture. To test these beams, simple third point loading was used with a span length of 18 in. (45 cm). Upon reaching the peak load of the test, the modulus of rupture was calculated by the following equation:

$$f_r = \frac{PL}{bd^2} \quad (3.1)$$

where P is the peak load, L is the beam length, and b and d are the beam width and depth, respectively, measured at the fractured surface of the beam after failure. Three specimens were tested with the average representing one strength data point.

3.2.4. Modulus of Elasticity of Concrete. The modulus of elasticity, E_c , of the concrete was determined according to ASTM C 469 (2010) *Standard Test Method for Static Modulus of Elasticity and Poisson's Ratio of Concrete in Compression*. Cylinders with a 6 in. (15.2 cm) diameter and 12 in. (30.5 cm) height were used to determine the modulus of elasticity. The modulus of elasticity for each mix design was determined from companion cylinders to the bond test specimens on the day of testing.

3.2.5. Splitting Tensile Strength of Concrete. The splitting tensile strength, f_{tsp} , of the concrete was determined according to ASTM C496 (2011) *Standard Test Method for Splitting Tensile Strength of Cylindrical Concrete Specimens*. The splitting tensile strength was found on the day of bond specimen testing for each mix design. To find this strength, 6 in. x 12 in. (15.2 cm x 30.5 cm) cylinders were used. Upon reaching the peak load of this test, the splitting tensile strength was found by the following equation:

$$f_{tsp} = \frac{2P}{\pi LD} \quad (3.2)$$

where P is the peak load, L is the cylinder length, and D is the cylinder diameter. **Figure 3.2** shows the failure mode from the splitting tensile test. Three specimens were tested with the average representing one strength data point. The splitting tensile strength of each mix design was determined from companion cylinders to the bond test specimens on the day of testing.

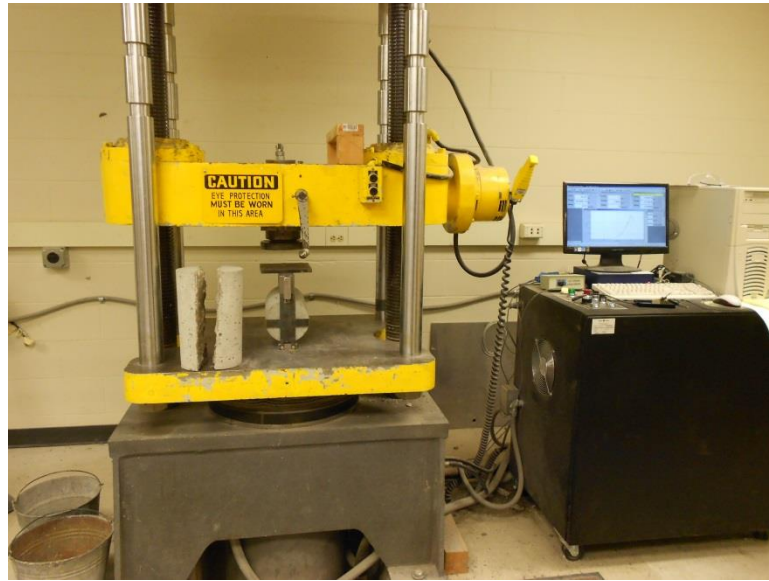


Figure 3.2: Splitting Tensile Failure Mode

3.2.6. Fracture Energy of Concrete. The fracture energy, G_f , was determined according to RILEM TC 50-FMC *Determination of the Fracture Energy of Mortar and Concrete by Means of Three-Point Bend Tests on Notched Beams*. Notched beams with dimensions 6 in. x 6 in. x 24 in. (15 cm x 15 cm x 60 cm) were cast in small batches for each mix design. Under three-point loading, the span was 18 in. (45 cm). The notch was cast into the concrete at midspan with a depth of 1.5 in. (4 cm) and width of 0.25 in. (0.6 cm). A gauge was applied at the notch to measure the crack mouth opening displacement, and displacement was measured at midspan by linear variable differential transformers

(LVDTs). The fracture energy was calculated by dividing the total energy dissipated by the projected surface area of the crack as in the following equation:

$$G_f = \frac{W}{bd-a_o} \quad (3.3)$$

where W is the total energy dissipated, b and d are the beam width and depth respectively, and a_o is the depth of the notch. Three specimens were tested with the average representing one fracture energy data point.

3.3. RAC MIX DESIGNS

For this study, three mix designs were produced and evaluated for bond performance. A MoDOT Class B air-entrained mix design was used as a baseline for reference throughout the study. The specified cement content in this mix was 535 lb., the water-to-cement ratio was 0.40, the target slump was 6 in., and the design air content was 6%. The specified amount of fine aggregate as a volume of total aggregates was 40%. For this mix, the typical dosage range of the MoDOT-approved air entrainment MB-AE 90 was 0.25-4.0 fl.oz./100 lb. of cement (0.16-2.61 mL/kg of cement). The typical dosage of the Type A water reducer Glenium 7500 is 5.0 - 8.0 fl.oz./100 lb of cement (0.33-5.22 mL/kg of cement). Two RAC mixes were produced as modified Class B mix designs. The direct replacement method of RCA for coarse aggregate was used to design the RAC mixes. Two RCA replacement levels were considered: 50% and 100% volumetric replacement.

3.3.1. Pre-Recycled Concrete Mix Design. In order to control the number of variables in this experimental study, the recycled aggregates were produced by the researchers in a controlled laboratory environment. Unreinforced concrete beams were

cast in five separate pours, and fresh and hardened concrete properties were determined from companion small-scale specimens from each pour. An equal volume of concrete was produced in each pour. The mix design used for the RCA production was the same Class B mix design used for the control in this study. MoDOT's specifications for this mix and the oven-dry design batch weights are provided in Section 3.3.2.

To better understand the aggregate properties of the RCA, the concrete properties including air content, unit weight, compressive strength, splitting tensile strength, modulus of rupture, and modulus of elasticity were determined for each pour where the RCA parent beams were cast. The fresh concrete properties are shown below in **Table 3.1**. The hardened concrete properties are shown in **Tables 3.2** through **3.5**. For these hardened properties, an overall average value is presented. This value was assumed to be the average value for all of the concrete used to create the RCA since each pour contributed an equal volume to the total concrete crushed.

Table 3.1: Fresh Concrete Properties of Pre-Recycled Concrete

Pour	Slump (in.)	Air (%)
1	8	5.5
2	7	5.75
3	6	6.5
4	8	7
5	6	5.5

Conversion: 1 in. = 2.54 cm

Table 3.2: Compressive Strength Results of Pre-Recycled Concrete

Pour	Specimen	Compressive Strength, psi	Average Compressive Strength, psi	Overall Average Compressive Strength, psi
1	1	6571	6415	5385
	2	6501		
	3	6173		
2	1	4045	4267	
	2	4363		
	3	4392		
3	1	5472	5353	
	2	5311		
	3	5277		
4	1	4780	5293	
	2	5553		
	3	5547		
5	1	5690	5598	
	2	5619		
	3	5484		

Conversion: 1 psi = 6.9 kPa

Table 3.3: Splitting Tensile Strength Results of Pre-Recycled Concrete

Pour	Specimen	Tensile Strength (psi)	Average Tensile Strength (psi)	Overall Average Tensile Strength (psi)
1	1	564	587	522
	2	611		
2	1	554	516	
	2	478		
3	1	555	525	
	2	494		
4	1	520	513	
	2	507		
5	1	592	467	
	2	342		

Conversion: 1 psi = 6.9 kPa

Table 3.4: Modulus of Rupture Results of Pre-Recycled Concrete

Pour	Specimen	MOR (psi)	Average MOR (psi)	Overall Average MOR (psi)
1	1	716	745	570
	2	775		
2	1	572	505	
	2	438		
3	1	538	565	
	2	593		
4	1	532	501	
	2	471		
5	1	582	535	
	2	488		

Conversion: 1 psi = 6.9 kPa

Table 3.5: Modulus of Elasticity Results of Pre-Recycled Concrete

Pour	MOE (psi)	Overall Average MOE (psi)
1	6,000,000	5,520,000
2	5,100,000	
3	5,700,000	
4	5,150,000	
5	5,650,000	

Conversion: 1 psi = 6.9 kPa

3.3.2. VAC Control Mix Design and Concrete Properties. A MoDOT Class B air-entrained mix was used for the control mix in this study. The target strength was 4000 psi (27.58 MPa). The MoDOT mix specifications are summarized in **Table 3.6**, and the oven-dry design batch weights are shown in **Table 3.7**. The fresh properties of the concrete were determined after the addition of the chemical admixtures on the day of casting the bond test specimens. The slump was 8 in. (20.3 cm), the air content was 13%, and the unit weight was 144.4 lb/yd³ (2313 kg/m³). However, the 13% air content value was believed to be incorrect due to a faulty air meter as the mix design and remaining

fresh properties were identical to the Class B mix design used as the parent material for the RAC. As a result, an air content of 6% was assumed for the control concrete.

The compressive strength, splitting tensile strength, and modulus of elasticity of the mix were determined from companion cylinders that were cast from the same concrete batch as the bond test specimens. **Figure 3.3** shows the compressive strength gain over time. At 90 days, the compressive strength was found to be 4650 psi (32.06 MPa), just over the target strength. On the day of testing, the compressive strength was 4000 psi (27.58 MPa). The splitting tensile strength on the day of testing the bond specimens was 397 psi (2.74 MPa). The results are shown in **Table 3.8**. Likewise, the modulus of elasticity of the concrete found on the day of testing the bond specimens was 4,300,000 psi (29.65 GPa).

Table 3.6: Control Mix Design Specifications

Cementitious Amount, lb/yd ³	535
w/c Ratio	0.4
Amount of Fine Aggregate (by volume), %	40
Design Air Content, %	6.0
Target Slump, in.	6.0

Conversion: 1 lb./yd³ = 0.59 kg/m³
1 in. = 2.54 cm

Table 3.7: Control Design Mix Proportions, Oven-Dry Basis

Cement	535 lb/yd ³
Water	214.0 lb/yd ³
Coarse Aggregate	1958.2 lb/yd ³
Fine Aggregate	1252.7 lb/yd ³
Air Entrainment MB-AE 90	1 fl.ozs/cwt
Water Reducer Glenium 7500	6 fl.ozs/cwt

Conversion: 1 lb./yd³ = 0.59 kg/m³
1 oz. = 29.6 ml

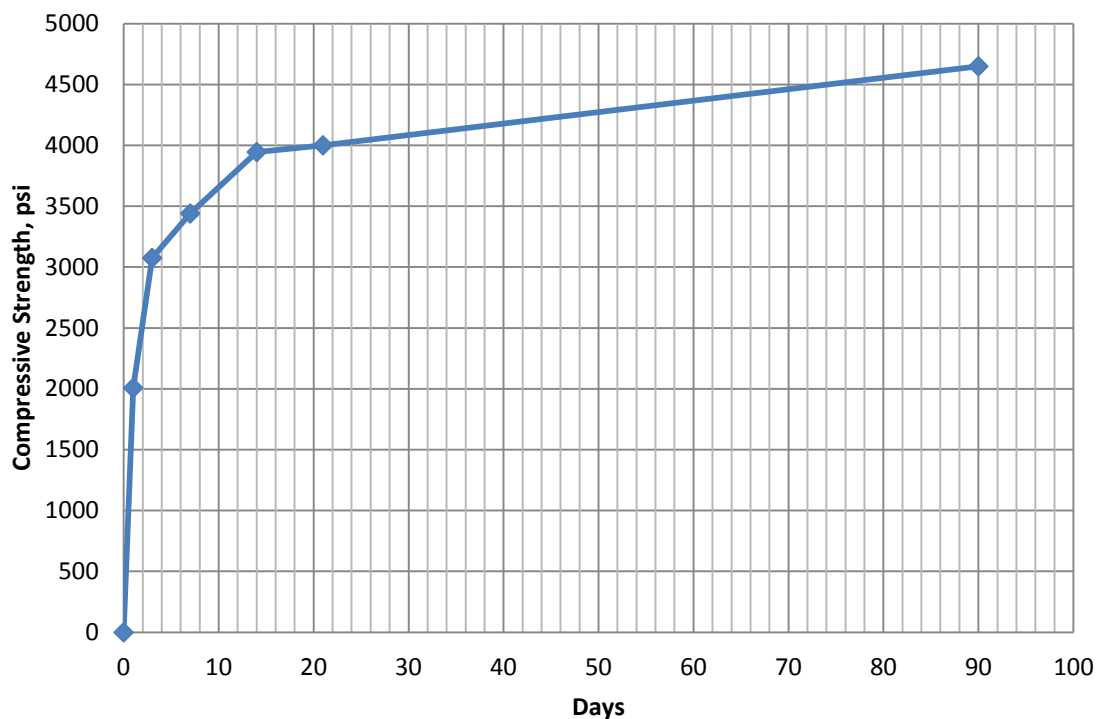


Figure 3.3: Control Mix Strength Gain with Time
Conversion: 1 psi = 6.9 kPa

Table 3.8: Control Splitting Tensile Strength Results

Specimen	Splitting Tensile Strength (psi)	Average Splitting Tensile Strength (psi)
Control-1	369	397
Control-2	423	
Control-3	397	

Conversion: 1 psi = 6.9 kPa

3.3.3. RAC-50% Mix Design and Concrete Properties. The first mix incorporating RCA was a 50% direct replacement design, subsequently referred to as RAC-50. Half of the total volume of coarse aggregate in the control MoDOT Class B mix was directly substituted with the laboratory-produced RCA. In order to maintain consistency with the control specimens, the MoDOT Class B mix specifications were

used to design the 50% direct replacement mix. The achieved 28-day strength of this mix during trial batching was 5500 psi (37.92 MPa), so this was used for the design of bond test specimens.

The mix specifications are summarized in **Table 3.9**, and the oven-dry design batch weights are shown in **Table 3.10**. The fresh properties of the concrete were determined after the addition of the chemical admixtures on the day of casting the bond test specimens. The slump was 6.5 in. (16.5 cm), the air content was 8%, and the unit weight was 139.8 lb/yd³ (2239 kg/m³).

The compressive strength, splitting tensile strength, and modulus of elasticity of the mix were determined from companion cylinders that were cast from the same concrete batch as the bond test specimens. **Figure 3.4** shows the compressive strength gain over time. At 60 days, the compressive strength was 3800 psi (26.20 MPa). On the day of testing, the compressive strength was 3560 psi (24.54 MPa). The splitting tensile strength on the day of testing the bond specimens was 344 psi (2.37 MPa). The results are shown in **Table 3.11**. Likewise, the modulus of elasticity of the concrete on the day of testing the bond specimens was 3,750,000 psi (25.86 GPa).

Table 3.9: RAC-50 Mix Design Specifications

Cementitious Amount, lb/yd ³	535
w/c Ratio	0.4
Amount of Fine Aggregate (by volume), %	40
Design Air Content, %	6.0
Target Slump, in.	6.0

Conversion: 1 lb./yd³ = 0.59 kg/m³

1 in. = 2.54 cm

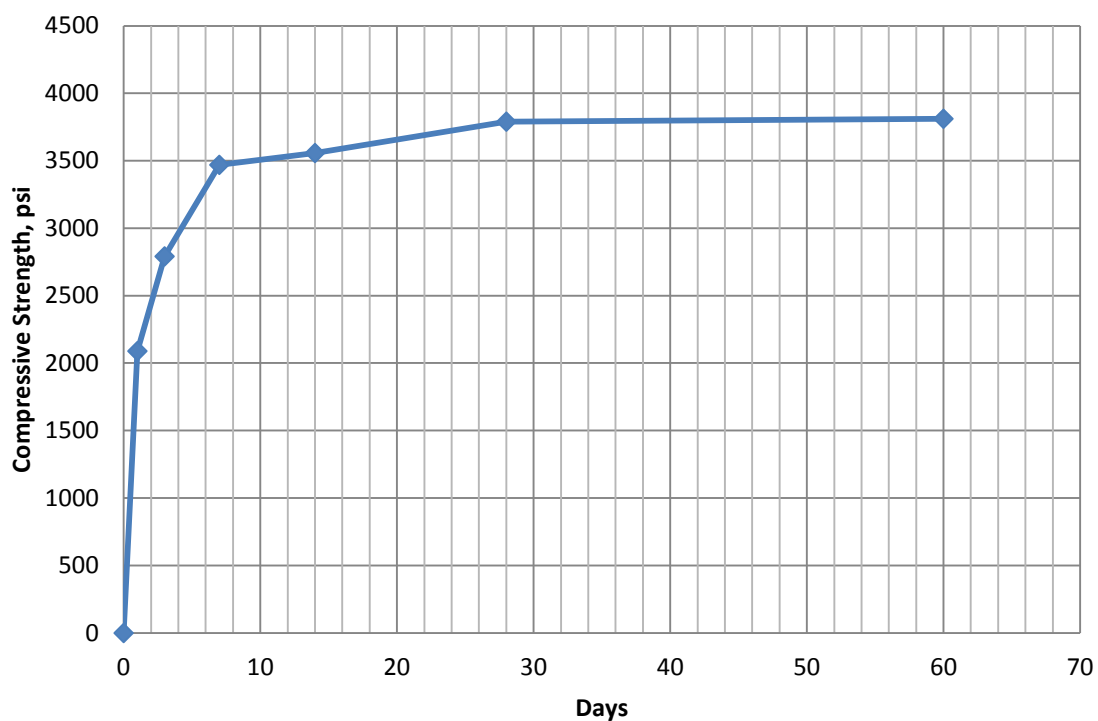
Table 3.10: RAC-50 Design Mix Proportions, Oven-Dry Basis

Cement	535 lb/yd ³
Water	214.0 lb/yd ³
Coarse Natural Aggregate	979.1 lb/yd ³
Coarse Recycled Aggregate	845.9 lb/yd ³
Fine Aggregate	1252.7 lb/yd ³
Air Entrainer MB-AE 90	1 fl.ozs/cwt
Water Reducer Glenium 7500	4 fl.ozs/cwt

Conversion: 1 lb./yd³ = 0.59 kg/m³

1 oz. = 29.6 ml

1 lb. = 0.45 kg

**Figure 3.4: RAC-50 Mix Strength Gain with Time**

Conversion: 1 psi = 6.9 kPa

3.3.4. RAC-100% Mix Design and Concrete Properties. The second mix incorporating RCA was a 100% direct replacement design, subsequently referred to as RAC-100. The total volume of coarse aggregate in the control MoDOT Class B mix was

directly substituted with the laboratory-produced RCA. In order to maintain consistency with the control specimens, the MoDOT Class B mix specifications were used to design the 100% direct replacement mix. However, during laboratory trial batching, it was noticed from the slump test that the mixes lacked cohesion. To remediate this lack of cohesion, the mix was modified by increasing the amount of fine aggregate volume by 5% of total aggregates. This change notably improved the cohesion of the mix. The achieved 28-day strength of this mix during trial batching was 5500 psi (37.92 MPa), so this was used for the design of bond test specimens.

Table 3.11: RAC-50 Splitting Tensile Strength Results

Specimen	Splitting Tensile Strength (psi)	Average Splitting Tensile Strength (psi)
RAC-50-1	341	344
RAC-50-2	347	

Conversion: 1 psi = 6.9 kPa

The mix specifications are summarized in **Table 3.12**, and the oven-dry design batch weights are shown in **Table 3.13**. The fresh properties of the concrete were determined after the addition of the chemical admixtures on the day of casting the bond test specimens. The slump was 8.5 in. (21.6 cm), the air content was 7%, and the unit weight was 137.2 lb/yd³ (2198 kg/m³).

The compressive strength, splitting tensile strength, and modulus of elasticity of the mix were determined from companion cylinders that were cast from the same concrete batch as the bond test specimens. **Figure 3.5** shows the compressive strength gain over time. At 60 days, the compressive strength was 5300 psi (36.54 MPa). On the day of testing, the compressive strength was 4840 psi (33.37 MPa). The splitting tensile

strength found on the day of testing the bond specimens was 320 psi (2.21 MPa). The results are shown in **Table 3.14**. Likewise, the modulus of elasticity of the concrete found on the day of testing the bond specimens was 4,000,000 psi (27.58 GPa).

Table 3.12: RAC-100 Mix Design Specifications

Cementitious Amount, lb/yd ³	535
w/c Ratio	0.36
Amount of Fine Aggregate (by volume), %	45
Design Air Content, %	6.0
Target Slump, in.	6.0

Conversion: 1 lb./yd³ = 0.59 kg/m³
1 in. = 2.54 cm

Table 3.13: RAC-100 Design Mix Proportions, Oven-Dry Basis

Cement	535 lb/yd ³
Water	192.6 lb/yd ³
Coarse Aggregate	1650.5 lb/yd ³
Fine Aggregate	1441.6 lb/yd ³
Air Entrainer MB-AE 90	1 fl.ozs/cwt
Water Reducer Glenium 7500	6 fl.ozs/cwt

Conversion: 1 lb./yd³ = 0.59 kg/m³
1 oz. = 29.6 ml
1 lb. = 0.45 kg

Table 3.14: RAC-100 Splitting Tensile Strength Results

Specimen	Splitting Tensile Strength (psi)	Average Splitting Tensile Strength (psi)
RAC-100-1	320	320
RAC-100-2	320	
RAC-100-3	319	

Conversion: 1 psi = 6.9 kPa

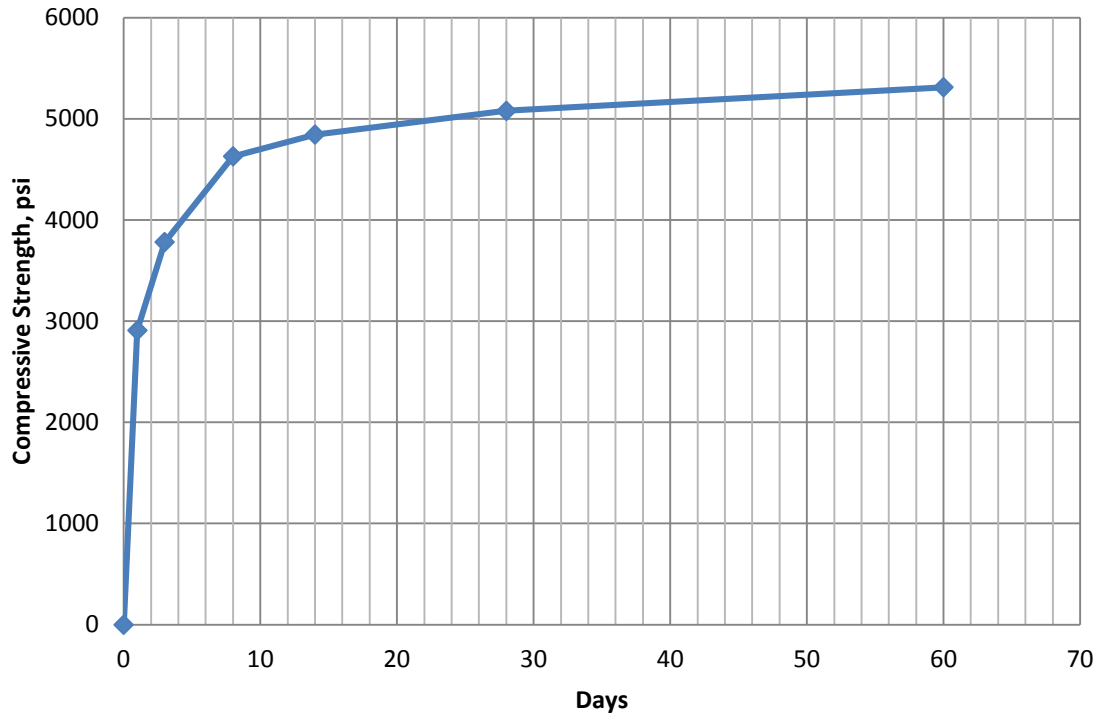


Figure 3.5: RAC-100 Mix Strength Gain with Time
Conversion: 1 psi = 6.9 kPa

3.4. CONCRETE MECHANICAL PROPERTIES

3.4.1. Modulus of Rupture Results. The modulus of rupture, f_r , of the VAC and 100% RCA mixes is shown in **Table 3.15** along with the corresponding compressive strengths on the day of testing. The modulus of rupture for each mix was determined from small batches, and companion cylinders were cast to find the compressive strength. In order to compare the test results across mix designs, the moduli of rupture were normalized by dividing the test value by the square root of the concrete compressive strength. This method of normalization is based on the accepted relationship between modulus of rupture and compressive strength as presented in ACI 318R (2011):

$$f_r = 7.5\lambda\sqrt{f'_c} \quad (3.4)$$

where λ is a correction factor for lightweight concrete.

Table 3.15: Modulus of Rupture Results

Mix	f_c (psi)	f_r (psi)	Normalized f_r	COV	Average Normalized f_r
VAC	5416	501	6.81	9.3%	6.39
	4959	420	5.96		
RAC-100	4546	339	5.03	8.5%	5.69
	4417	391	5.88		
	4944	400	5.69		
	4350	407	6.17		

Conversion: 1 psi = 6.9 kPa

3.4.2. Modulus of Elasticity Results. The average modulus of elasticity, E_c , of the VAC, 50% RCA, and 100% RCA mixes is shown in **Table 3.16** along with the corresponding compressive strengths on the day of testing. The modulus of elasticity of each mix was determined from companion cylinders cast on the same day as the beam splice specimens. To compare the results across mix designs, the moduli of elasticity were normalized by dividing the test value by the square root of the concrete compressive strength. This method of normalization is based on the accepted relationship between modulus of elasticity and compressive strength as presented in ACI 318R (2011):

$$E_c = w_c^{1.5} 33 \sqrt{f'_c} \quad (3.5)$$

where w_c is the unit weight of the concrete.

3.4.3. Splitting Tensile Strength Results. The average splitting tensile strength, f_{tsp} , of the VAC, 50% RCA, and 100% RCA mixes is shown in **Table 3.17** along with corresponding compressive strengths on the day of testing. The splitting tensile strength of each mix was determined from companion cylinders cast on the same day as the beam splice specimens. To compare the results across mix designs, the splitting tensile strengths were normalized by dividing the test value by $f'_c^{2/3}$. This method of

normalization is based on the relationship between splitting tensile strength and compressive strength as presented in CEB-FIP (1990):

$$f_{tsp} = 1.57f_c^{2/3} \quad (3.6)$$

Table 3.16: Modulus of Elasticity Results

Mix	f_c (psi)	Average MOE (ksi)	Average Normalized MOE
VAC	4000	4300	67.99
RAC-50	3560	3750	62.85
RAC-100	4840	4000	57.50

Conversion: 1 psi = 6.9 kPa

Table 3.17: Splitting Tensile Strength Results

Mix	f_c (psi)	Average f_{tsp} (psi)	Average Normalized f_{tsp}
VAC	4000	397	1.58
RAC-50	3560	325	1.39
RAC-100	4840	320	1.12

Conversion: 1 psi = 6.9 kPa

3.4.4. Fracture Energy Results. The average fracture energy, G_f , of the VAC, 50% RCA, and 100% RCA mixes is shown in **Table 3.18** along with the corresponding compressive strengths on the day of testing. The fracture energy for each mix was determined from small batches, and companion cylinders were cast to find the compressive strength. To compare the results across mix designs, the fracture energies were normalized by dividing the test value by $f_c^{0.7}$. This method of normalization is based on the relationship between fracture energy and compressive strength as presented in CEB-FIP (1990):

$$G_f = G_{fo} \left(\frac{f_c}{f_{cmo}} \right)^{0.7} \quad (3.7)$$

where G_{fo} is a constant base value fracture energy dependent on the maximum aggregate size and f_{cmo} is a constant equal to 1450 psi (10 MPa).

Table 3.18: Fracture Energy Results

Mix	f_c (psi)	Average G_f (lbf/ft)	Average Normalized G_f
VAC	5394	20.9	0.0510
RAC-50	6598	20.8	0.0440
RAC-100	4945	15.3	0.0397

Conversion: 1 psi = 6.9 kPa
1 lbf/ft = 6.9 N/m

3.4.5. Comparison of Mechanical Properties. Figure 3.6 shows a graphical comparison of the mechanical properties of the three mixes. All properties are negatively impacted with increasing replacement of coarse natural aggregates with RCA. The most drastic decreases were seen in splitting tensile strength and fracture energy. The splitting tensile strength decreased 12% and 29% for 50% RCA replacement and 100% RCA replacement, respectively. The fracture energy decreased 14% and 22% for 50% RCA replacement and 100% RCA replacement, respectively. In bond failures where splitting cracks control, the peak load is governed by the tensile response of the concrete, which depends on the splitting tensile capacity and fracture energy. Thus, as shown in the reduced splitting tensile strength and fracture energy of high volume RCA concrete, it is expected that the bond carrying capacity will be negatively impacted as well.

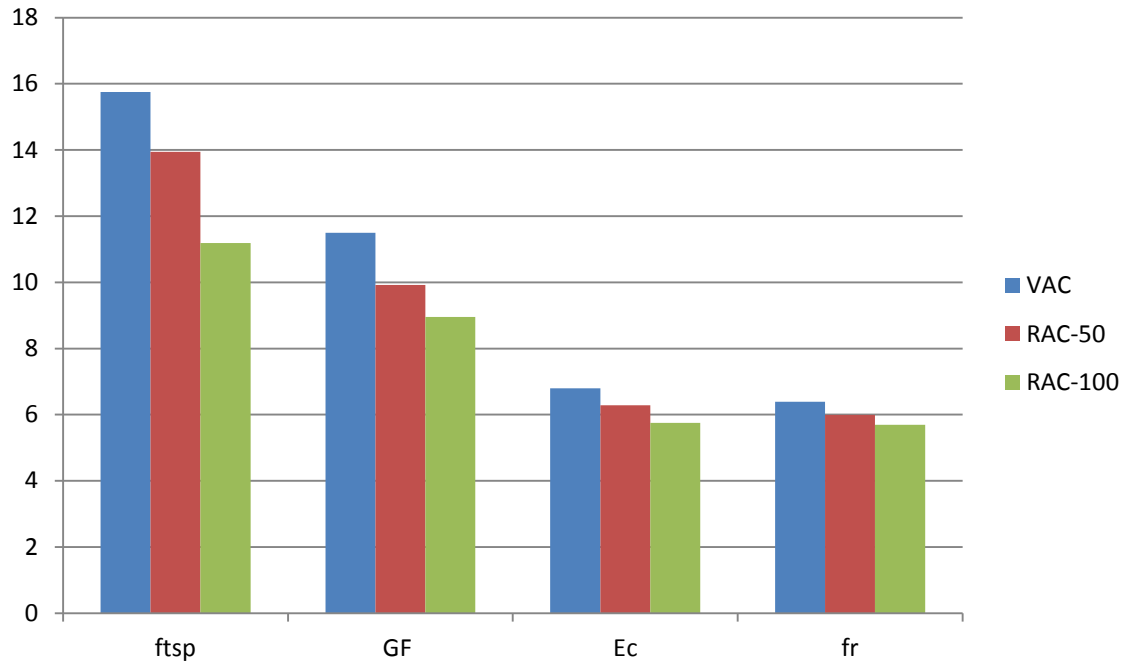


Figure 3.6: Comparison of Normalized Mechanical Properties

Note: Normalized values of $f_{tsp} * 10$ and $E_c * 10^{-1}$

4. EXPERIMENTAL PROGRAM

4.1. INTRODUCTION

To evaluate the bond performance of RAC, both direct pull-out and full-scale beam splice specimens were used. RILEM 7-II-128 *RC6: Bond test for reinforcing steel* was used to develop the direct pull-out type specimens and test method. Likewise, recommendations from ACI 408R-03 *Bond and Development of Straight Reinforcing Bars in Tension* as well as procedures reported in previous research of bond performance were used to develop the full-scale beam splice specimens and test method.

4.2. RCA PRODUCTION

The RCA used throughout the study was produced in the laboratory environment. This step precluded variables such as varying levels of chloride and organic contamination, varying and/or unknown sources of virgin aggregates, and different levels of residual mortar deterioration of the recycled aggregates. By using this laboratory-produced RCA, the amount of residual mortar on the aggregates was a “worst-case” condition with a very high content by volume.

In order to make the RCA, the parent concrete beams were cast and cured in the laboratory. Thirty 1 ft. x 1.5 ft. x 5 ft. (0.30 m x 0.46 m x 1.52 m) and twenty 1 ft. x 1.5 ft. x 7 ft. (0.30 m x 0.46 m x 2.13 m) un-reinforced beams were cast in a total of five separate pours. Short beams were produced to improve the ease of transportation to the crushing site. To build the formwork for these beams, 10 ft. (3.05 m) and 14 ft. (4.27 m) steel and wood forms were used with a plywood divider in the middle to create the smaller beams. Polyvinyl chloride (PVC) tubes were inserted at two locations through the

middle of each formwork such that a steel rod could be temporarily placed through the beams after the formwork was removed and used to lift the beams onto a truck bed. This step was done to eliminate the need to use steel hooks which might have damaged the crushing equipment. **Figure 4.1** shows the prepared formwork for the parent concrete beams.



Figure 4.1: Formwork for Casting Pre-Recycled Concrete

Once all these beams were cast and allowed to reach a minimum compressive strength of 4000 psi (27.58MPa), they were transported to the crushing site. For this study, rock crushers at the Rolla, Missouri quarry of Capitol Quarries (Jefferson City, Missouri) were used to crush down the parent concrete beams to the desired MoDOT Gradation D distribution. A mobile crushing plant with both primary and secondary steel jaw crushers was used to process the material.

4.3. DIRECT PULL-OUT SPECIMENS

4.3.1. Direct Pull-Out Specimen Design. RILEM 7-II-128 RC6: *Bond test for reinforcing steel* describes the pull-out specimen as a steel reinforcing bar embedded in a concrete cube with a volume of $10d_s$ by $10d_s$ by $10d_s$, where d_s is the bar diameter. A direct tensile load is applied to the end of the steel bar until the bonded region fails. During testing, both the slip of the embedded bar and applied load are measured. The test specification calls for a bonded length of $5d_s$ and an un-bonded length of $5d_s$ at the end closest to the applied load. Some changes were made to RILEM recommended test specimen design based on results from previous research (Wolfe, 2011).

The direct pull out specimen used in this experimental program was a reinforcing steel bar embedded in a cylindrical volume of concrete with a diameter of 12 in. (30.5 cm). This deviation from the RILEM standard was made to reduce the potential for a splitting failure by maintaining a constant, large concrete cover for the reinforcing bar. The bonded length was $5d_s$ and the un-bonded length was $5d_s$ as per the RILEM testing standard. This un-bonded length is necessary in the design of the direct pull-out specimens to prevent a conical failure surface from forming within the concrete volume at the location of bearing (ACI 408, 2003).

In this testing program, both ASTM A615-09, Grade 60 #4 (No. 13) and #6 (No. 19) deformed steel bars were used in direct pull out specimens. The total length of each bar measured 40 in. (101.6 cm). A length of $3/8$ in. (.95 cm) remained exposed at the end of the bonded portion to facilitate the measure of slip during testing using a linear voltage differential transformer (LVDT). The bonded and un-bonded lengths were 2.5 in. (6.4 cm) for the #4 (No.13) direct pull-out specimens and 3.75 in. (9.5 cm) for the #6 (No. 19)

direct pull out specimens. A schematic of the #4 (No. 13) and #6 (No. 19) specimens are shown in **Figures 4.2** and **4.3**, respectively.

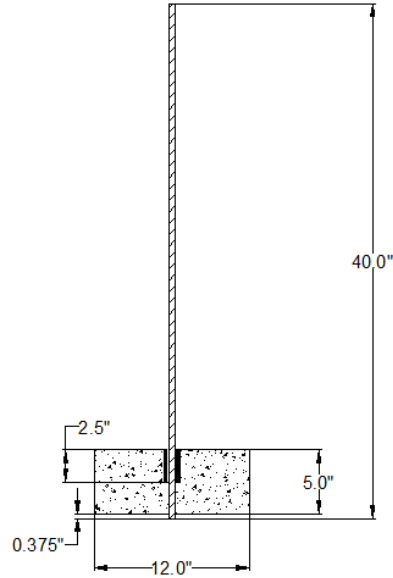


Figure 4.2: Schematic of #4 (No. 13) Bar Direct Pull-Out Specimen

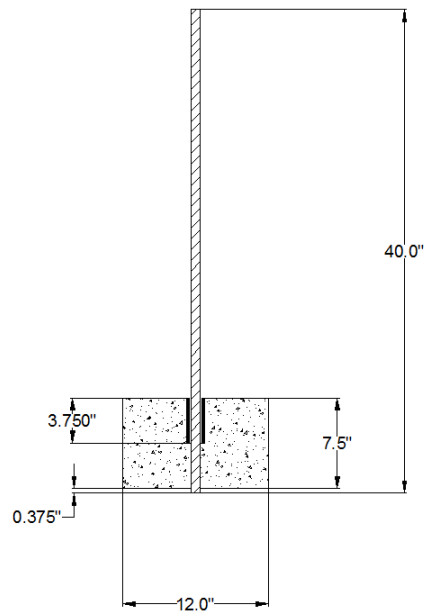


Figure 4.3: Schematic of #6 (No. 19) Bar Direct Pull-Out Specimen

4.3.2. Direct Pull-Out Specimen Fabrication. The molds for the direct pull out specimens were constructed from segments of 12 in. (30.5 cm) diameter cardboard tube concrete forms (QuickTube). Strips measuring 5 in. (12.7 cm) and 7.5 in. (19.1 cm) in length were cut for the #4 (No. 13) bar and #6 (No. 19) bar specimens, respectively. The bases of the molds were constructed from 3/8 in. (.95 cm) plywood cut to 14 in. x 14 in. (35.6 cm x 35.6 cm) squares. The 3/8 in. (0.95 cm) base thickness was chosen to allow a 3/8 in. (0.95 cm) length exposed at the end of the bonded portion to facilitate the measure of slip during testing. A hole was drilled in the center of the base pieces 1/16 in. (0.16 cm) larger than the nominal diameter of the bar in order for the 3/8 in. (0.95 cm) length of the bar to remain exposed. The cardboard segments of QuickTube were then aligned along the base pieces with the drilled-out hole at the center. A bead of waterproof, adhesive silicon was applied at the junction of the plywood base and cardboard segment in order to attach the pieces of the mold and to prevent cement paste from leaking during the casting and curing of the specimens.

Both the #4 (No.13) and #6 (No. 19) steel reinforcing bars were sectioned into 40 in. (101.6cm) long segments for the pull out specimens. PVC pipes were used to form the bond breaker within the concrete cylinder. For the #4 (No. 13) bars, PVC pipe with an inner diameter of 3/4 in. (1.91cm) was used, and for the #6 (No. 19) bars, PVC pipe with an inner diameter of 1 in. (2.54 cm) was used. The PVC pipe segments were cut 1/4 in. (0.64 cm) longer than the required un-bonded length. This step was done so that this 1/4 in. (0.64 cm) length would remain beyond the concrete cylinder on the bearing surface. This extra length was used to help ensure that concrete did not inadvertently fall between the PVC bond breaker and steel bar during casting and finishing of the specimens.

To attach the bond breaker to the bars, a single layer of bubble wrap was taped around the portion to remain un-bonded. This wrap helped to align the PVC concentrically with the steel bar and to also help keep concrete from filling the space within the bond breaker. The segments of PVC were slid over the bubble wrap, and a small bead of waterproof silicone was carefully applied around the top and bottom of the bond breaker to prevent concrete infiltration.

The top pieces of the direct pull out molds were made from 3/8 in. plywood cut to 14 in. x 14 in. (35.6 cm x 35.6 cm) squares. A hole measuring 1/16 in. (0.16 cm) larger than the outside diameter of the PVC pipe was drilled at the center of each top piece. Prior to casting the specimens, the reinforcing bars were placed into the completed forms and leveled to ensure they were plumb with the cylindrical mold base. An outline of the cylindrical base was sketched on the bottom side of the top piece when the steel bar was shown to be plumb through the use of levels. Three wood blocks were then screwed onto the bottom of the top piece of plywood tangentially along the outline of the cardboard tubing to snugly secure the top in place.

To cast the specimens, the steel bar was first inserted into the hole in the bottom of the mold. The bar was held perpendicular as concrete was filled to the top of the mold. A vibrator was used to lightly consolidate the concrete as needed, and the surface of the concrete was finished with a trowel. Once finished, the top piece of the mold was gently slid down over the bar and fitted around the extruded PVC bond breaker. The pull out specimens and the companion compression and splitting tensile specimens were left to cure until the specified peak strength was reached prior to testing. The cardboard and

plywood components of the molds were removed on the day of testing. The completed pull-out specimens curing in their molds are shown in **Figure 4.4**.



Figure 4.4: Completed Direct Pull-Out Specimens in Molds

4.3.3. Direct Pull-Out Specimen Test Set-Up. A 200 kip-capacity (890kN) loading frame manufactured by Tinius Olson was used to test the direct pull out specimens. After the specimens were de-molded, they were inverted and positioned through the top platform of the load frame as shown in **Figure 4.5**. A steel bearing plate was used, and a neoprene pad was placed directly between the concrete surface and steel plate to ensure uniform bearing on the concrete. The steel bar was fed through grips on the middle platform of the testing frame. A smaller steel plate was placed on the top of the concrete cylinder and an LVDT was clamped to a magnetic stand at the top of the specimen. The head of the LVDT was placed on the 3/8 in. (0.95 cm) exposed end of the steel bar to measure the slip during testing. The LVDT set-up is shown in **Figure 4.6**.

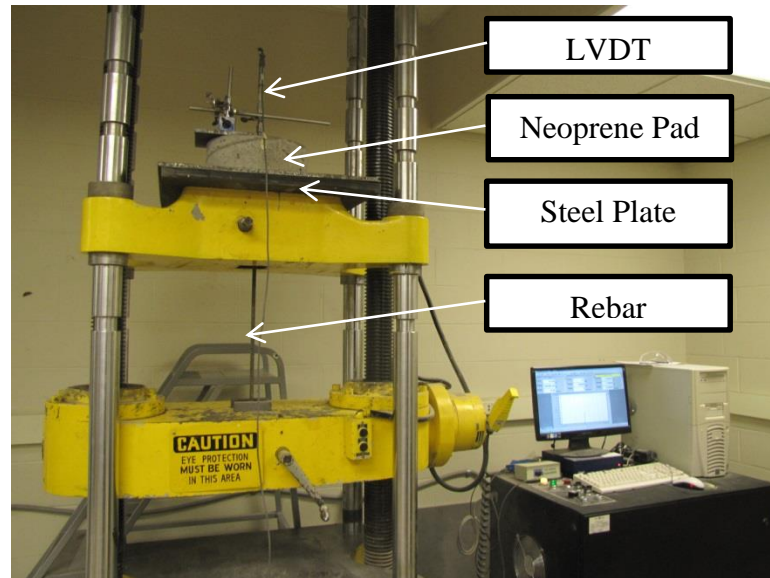


Figure 4.5: Test Set-Up for Direct Pull-Out Specimen



Figure 4.6: LVDT Set-Up for Direct Pull-Out Specimen

4.3.4. Direct Pull-Out Specimen Test Procedure. The computer software controlling the Tinius Olson was programmed to apply a displacement controlled load rate of 0.10 in. (0.3 cm) per minute. A preload of approximately 100 lb. (0.44kN) was applied to the rebar by manually moving the middle platform. This was done to help the

middle fixture properly grip the steel bar. After this preload was applied, the test was initiated. A distinct peak in the load versus slip output plot was watched for during testing. After this peak was detected, the test was continued while the load began to decrease with increasing slip. The test was allowed to run this way in order to determine if there was any additional bond capacity and to be sure that the captured peak load was a true bond failure.

4.4. BEAM SPLICE SPECIMENS

4.4.1. Beam Splice Specimen Design. The beam splice test used in this experimental program is a non-ASTM testing procedure for full scale beams. The design and fabrication of the specimens was based on previous research of bond performance (Looney, 2012 and Wolfe, 2011). The beams used in this study were 10 ft. (3.05m) long with a cross section of 12 in. x 18 in. (0.30m x 0.46m). The longitudinal reinforcement consisted of three ASTM A615-09, Grade 60 #6 (No. 19) deformed steel bars, which were contact lap-spliced at the midspan of the beams. The splice length used for these beams was a reduced value of the development length equation recommended in ACI 318-11 “Building Code Requirements for Structural Concrete”, shown as **Equation 4.1**. Based on previous research by Looney (2012), 70% of this calculated development length was used for the beam splice specimen design. Looney found that this reduction was sufficient to avoid yielding of the bar in a flexural failure mode and to ensure a bond failure mechanism. The equation for development length is:

$$l_d = \left[\frac{3}{40} \frac{f_y}{\lambda \sqrt{f'_c}} \frac{\psi_t \psi_e \psi_s}{\left(\frac{c_b + K_{tr}}{d_b} \right)} \right] * d_b \quad 4.1$$

where, l_d = development length
 f_y = specified yield strength of reinforcement
 λ = lightweight concrete modification factor
 f'_c = specified compressive strength of concrete
 Ψ_t = reinforcement location modification factor
 Ψ_e = reinforcement coating modification factor
 Ψ_s = reinforcement size modification factor
 c_b = smallest of distance from center of a bar to nearest concrete surface or one-half the center-to-center bar spacing
 K_{tr} = transverse reinforcement index
 d_b = nominal diameter of the reinforcing bar

A standard hook was specified at the ends of each longitudinal reinforcing bar to achieve sufficient development. As per ACI 318-11, this hook included a 90-degree bend with the minimum recommended bend diameter of 4.5 in.(11.4cm) and an extension of $12d_b$ at the free end of the bar (ACI 318, 2011).

Transverse reinforcement against shear failure consisted of #3 (No. 10), ASTM A615-09, Grade 60, U-shaped stirrups. To ensure that a shear failure would not occur before bond failure, a stirrup spacing less than the ACI 318-11 maximum stirrup spacing was used. The stirrups were not placed within the lap spliced region in order to avoid the interaction of confinement of the concrete within the splice zone. **Figures 4.7 and 4.8** detail the cross-sectional and plan views of the beam splice specimens, respectively. As shown in the schematic below, 180-degree hooks were used at the free ends of the U-stirrups. To help stabilize and align the cages, #4 (No. 13) bars were used as top bars and placed inside of these hooks.

4.4.2. Beam Splice Specimen Fabrication. The reinforcing bars were sectioned and bent to the appropriate lengths. Before the cages were assembled, a wire brush was used to clear the rust and mill scale at the ends of the longitudinal bars that were to be spliced. This was done to reduce test variability by reducing the influence of the rust and

mill scale on the bond performance. Saw-horses were then used to lay out the bottom reinforcement. Stirrups were placed along the longitudinal bars at the appropriate locations and the top bars were laid in the stirrup hooks. Levels were used to ensure that the stirrups were plumb with the longitudinal reinforcement, and then wire ties were used to connect every joint of the cages. To ensure appropriate concrete cover on the sides of the cages, two very short pieces of #8 (No. 25) bars, about 1in. (2.54 cm) in diameter, were tied to the outside to serve as spacers. Likewise, 1.5 in (3.81 cm) steel chairs were tied to the bottom of the cages in order to provide sufficient cover.

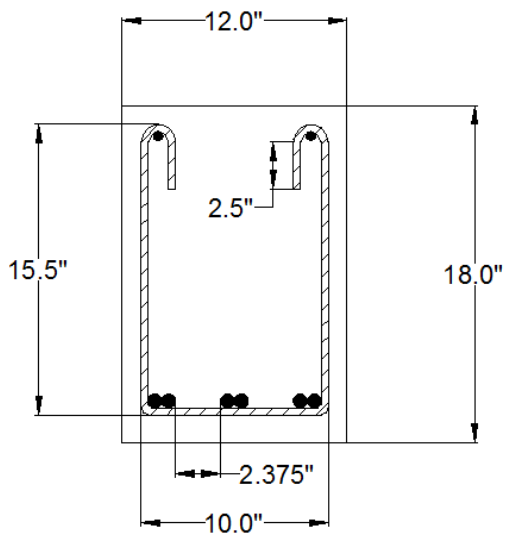


Figure 4.7: Schematic of Beam Splice Specimen Profile
Note: Stirrups omitted from within splice length.

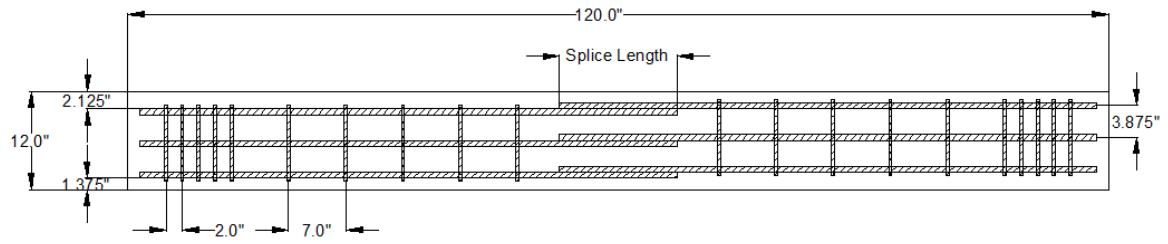


Figure 4.8: Schematic of Beam Splice Specimen Plan

Upon completion of the steel cages, strain gauges were installed at both ends of the contact lap splice to measure strain in the steel during testing. Before the strain gages were attached to the steel, the location along the bar was prepared by grinding a smooth surface, cleaning the area with an acid, and then neutralizing the area. **Figure 4.9** shows the spliced region with installed strain gauges, and **Figure 4.10** shows the finished cages.



Figure 4.9: Spliced Length with Attached Strain Gauges



Figure 4.10: Completed Cage for Beam Splice Specimen

Steel-framed forms were used to construct the beam splice specimens. The walls of these forms were constructed of wood and were held together by steel pins and wire ties. The forms measured 14ft. (4.27m) in length, but in order to reduce this length to the required 10ft. (3.05m) wood block-outs were constructed. After the forms were assembled, form release oil was applied to the walls of the forms to facilitate de-molding of the beams. The finished cages were then placed inside of the forms, and hooks were welded onto the top bars to allow for ease of transportation of the beams after curing.

Figure 4.11 shows the completed cages inside the concrete forms.



Figure 4.11: Steel Cages in Forms

The mix design was sent to the local Rolla Ready Mix plant, and the concrete was delivered to the lab. A small amount of the water was withheld from each mix design during delivery so that the water content could be slightly adjusted at the lab. Upon arrival of the truck, the slump of the concrete was performed in order to verify that the mix was correct prior to the addition of the chemical admixtures. Once this check was

performed, the air entraining dose and high range water reducer were added along with the additional water required to bring the water-to-cement ratio up to the required mix design. The concrete was allowed to mix at higher speed to produce the desired mix. Once this mixing was complete, the slump and air content were measured to ensure the mix behaved as anticipated. Once this was verified, fresh concrete was placed into an overhead crane bucket which was used to fill the concrete forms. The filling of the forms is shown in **Figure 4.12**. Simultaneously, a wheelbarrow was filled with fresh concrete and used to cast the companion splitting tensile and compression cylinders.



Figure 4.12: Casting of Beam Splice Specimens

The concrete was consolidated in layers in the beam forms. Once the forms were filled, wood blocks were used to screed the surface of the beams. Finishing towels were then used to smooth and level the beam top surface. Care was taken to avoid damage to the strain gauge wires that extended from the middle edge of the concrete beams.

The following day, the beams were removed from their forms after a compression test confirmed that the concrete had developed sufficient strength after 24 hours. Before the day of testing, the beams were prepared by lines being drawn at the locations of the supports and load points. Additionally, an aluminum angle was anchored into the concrete on the side of the beam at the midspan so that the deflection there could be monitored.

4.4.3. Beam Splice Specimen Test Set-Up. Third-point loading was used in order to create a constant, maximum moment in the middle third of the beam, helping to induce bond failure at the splice location at midspan. **Figure 4.13** shows a schematic of the third-point loading condition used to test the beam splice specimens. Through the use of jacks and wheeled-platforms, the beam was positioned onto roller supports beneath two 140 kip-capacity (623kN) hydraulic actuators in the load test frame shown below in **Figure 4.14**. Care was taken to ensure that the beam was positioned along the center line of the test frame. Spreader beams were used to transfer the applied load from the actuators to the concrete test beam. Rollers were placed on top of the beam at the location of the third points. Well sorted masonry sand was placed beneath these rollers and leveled to prevent any roughness along the top of the concrete beam from causing gaps beneath the base of the rollers. The actuators were lowered, and the bottom spreader beam was lined up along the center of the test specimen through the use of levels and T-squares. A 4 ft. (1.22 m) long mirror was kept nearby so that the rupture at the bottom of the beam could be safely inspected upon failure.

The LVDT was attached to a stand next to the beam. The pin of the LVDT was placed on the aluminum angle that had been previously anchored at the midspan of the

beam so that midspan deflection could be measured and recorded. This set-up is shown in **Figure 4.15**. The LVDT along with all six strain gauges were connected to data acquisition channels.

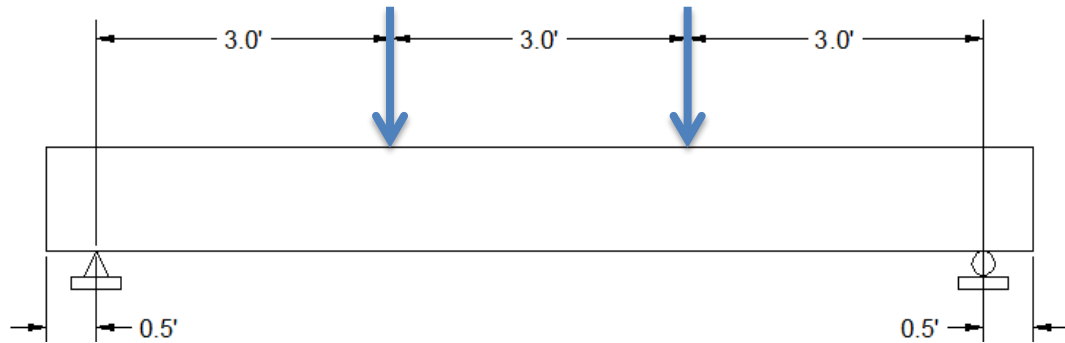


Figure 4.13: Schematic of Beam Splice Loading



Figure 4.14: Beam Splice Specimens in Load Test Frame



Figure 4.15: LVDT Set-Up for Beam Splice Test

4.4.4. Beam Splice Specimen Test Procedure. The data acquisition system was initiated to record data from the strain gauges and LVDT as well as the applied load from the actuators. The test was performed on a displacement-controlled basis; the load was applied in a series of loading steps where each step corresponded to a midspan deflection of 0.02 in. (0.05 cm). After each applied step, the crack patterns were traced in order to track the crack propagation.

The beam was loaded until failure occurred. This bond failure was marked by a very sudden rupture in the concrete along the bottom of the beam in the spliced region. Often, pieces of the concrete cover in the spliced region fell from the beam. This rupture was accompanied by a rapid and drastic drop-off in the load and increase in midspan deflection. Once this failure occurred, testing was completed and data collection was terminated.

5. TEST RESULTS AND EVALUATIONS

5.1. DIRECT PULL-OUT TEST RESULTS

The direct pull-out specimens were constructed to provide a relative measure of performance among the three mix designs. Both RAC mix designs were compared with the MoDOT Class B control mix. For this experimental program, a total of 18 pull-out specimens were tested. To investigate the effect of bar size on the relative bond performance, three specimens were constructed with #4 (No. 13) bars and three with #6 (No. 19) bars for each mix design. The testing matrix is shown below in **Table 5.1**.

Table 5.1: Testing Matrix for Direct Pull-Out Specimens

Mix	Reinforcing Bar Size	Number of Specimens
VAC	#4 (No. 13)	3
	#6 (No. 19)	3
RAC-50	#4 (No. 13)	3
	#6 (No. 19)	3
RAC-100	#4 (No. 13)	3
	#6 (No. 19)	3

Throughout the testing of these specimens, the slip of the bar and the applied load were recorded. When all testing was completed, the maximum applied load was determined for each pull-out specimen, and an average maximum value was found. The maximum bond stress was found by dividing the peak load carried by the bonded surface area of the bar. **Table 5.2** shows the results from the testing. Within each of the specimen names, VAC represents virgin aggregate concrete (the control), RAC50 represents recycled aggregate concrete designed with 50% RCA replacement, and RAC100

represents recycled aggregate concrete designed with 100% RCA replacement. The letters PO signify that these were pull-out specimens, and the number 4 or 6 indicates what bar size was used in the specimen. The final number in the specimen name indicates which of the three tests that specimen was identified as.

The coefficient of variation (COV) of each set of data is also given in **Table 5.2**. For each test set, the variation is relatively low; the maximum within all of the collected test data is 7.3%. These low COV values indicate consistency in the results and reliability in the test as a measure of relative bond performance. Plots of the peak bond stresses for VAC, RAC-50, and RAC-100 specimens are shown in **Figures 5.1, 5.2, and 5.3**, respectively.

Table 5.2: Pull-Out Test Results

Mix	Bar Size	Specimen	Max. Applied Load (lb)	Bond Stress (psi)	Average Bond Stress (psi)	Bond Stress COV
VAC	#4(No. 13)	VAC-PO4-1	10344	2634	2730	5.3%
		VAC-PO4-2	10435	2657		
		VAC-PO4-3	11379	2898		
	#6 (No. 19)	VAC-PO6-1	27172	3075	2965	3.3%
		VAC-PO6-2	25869	2928		
		VAC-PO6-3	25563	2893		
RAC-50	#4(No. 13)	RAC50-PO4-1	12760	3249	3183	6.0%
		RAC50-PO4-2	13083	3332		
		RAC50-PO4-3	11657	2968		
	#6 (No. 19)	RAC50-PO6-1	31109	3521	3432	5.4%
		RAC50-PO6-2	28430	3218		
		RAC50-PO6-3	31440	3558		
RAC-100	#4(No. 13)	RAC100-PO4-1	13968	3557	3281	7.3%
		RAC100-PO4-2	12236	3116		
		RAC100-PO4-3	12451	3171		
	#6 (No. 19)	RAC100-PO6-1	30302	3429	3384	1.2%
		RAC100-PO6-2	29597	3350		
		RAC100-PO6-3	29804	3373		

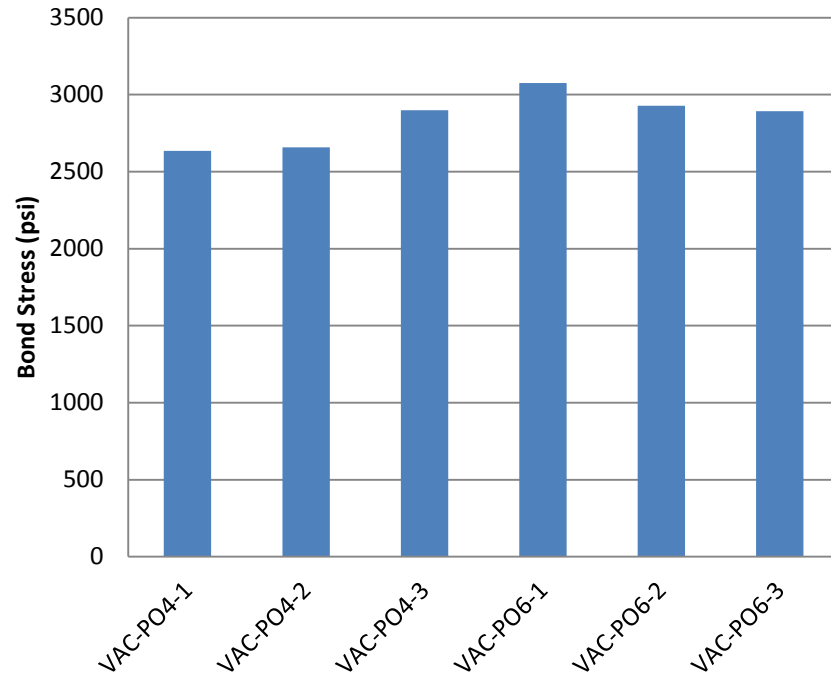


Figure 5.1: Peak Bond Stresses for VAC Pull-Out Specimens
Conversion: 1 psi = 6.9 kPa

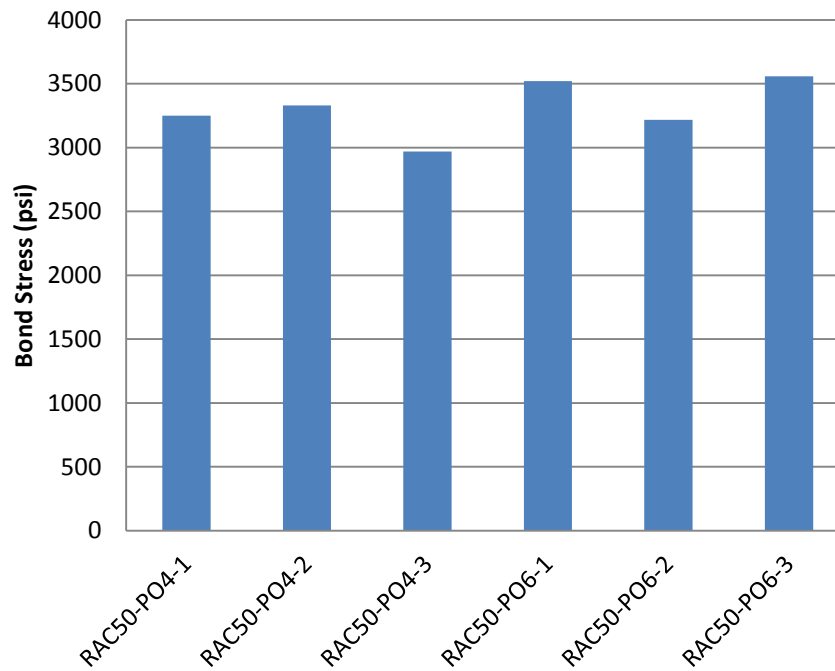


Figure 5.2: Peak Bond Stresses for RAC-50 Pull-Out Specimens
Conversion: 1 psi = 6.9 kPa

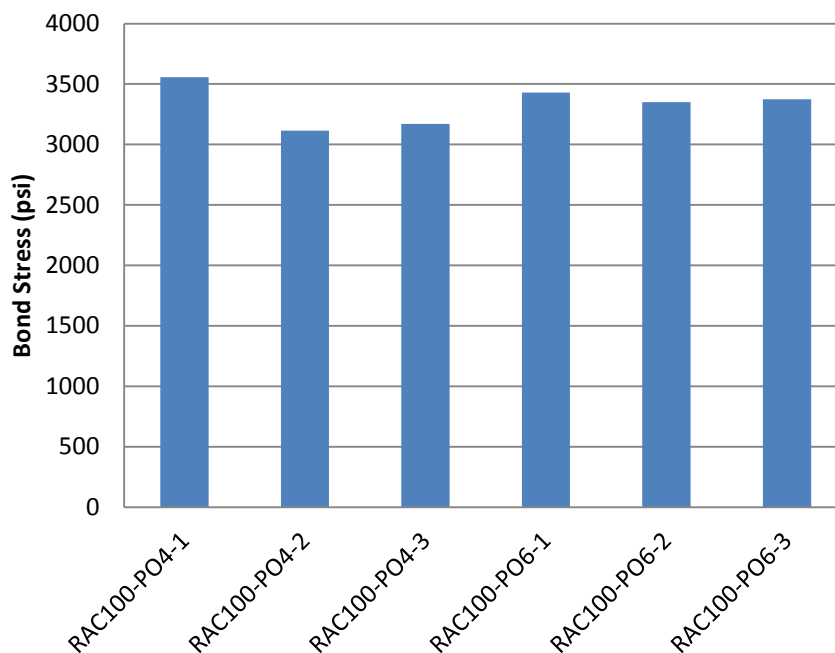


Figure 5.3: Peak Bond Stresses for RAC-100 Pull-Out Specimens
Conversion: 1 psi = 6.9 kPa

For each tested specimen, the bar slip was plotted against the applied load. The plots for most of these specimens indicated that a pull-out failure did occur, as evidenced in the gradual shedding of load after the peak. A typical load-slip plot is shown in **Figure 5.4** from specimen RAC50-PO4-2. The load-slip plots for all tested direct pull-out specimens are included in Appendix A.

5.2. BEAM SPLICE TEST RESULTS

Beam splice specimens were included in this experimental program to provide a test method to evaluate bond performance under a realistic flexural stress-state response. Three beam splice specimens were constructed for each mix design in this study as shown in the test matrix in **Table 5.3**. Both RCA mixes were compared to the

performance of the control specimens. The beams were all constructed with a splice in the longitudinal reinforcement located at midspan.

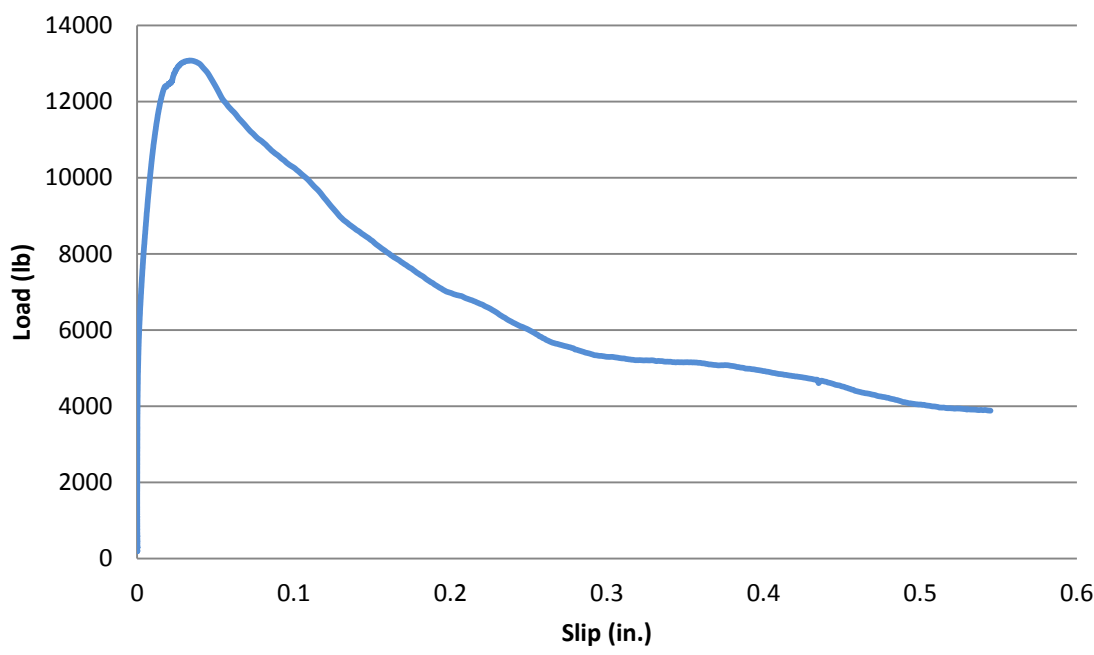


Figure 5.4: Typical Plot of Slip versus Applied Load
Conversion: 1 in. = 25.4 mm
1 lb. = 4.45 N

Table 5.3: Testing Matrix for Beam Splice Specimens

Mix	Bottom Reinforcement	Top Reinforcement	Number of Beams
Control	3 #6	2 #4	3
RAC-50	3 #6	2 #4	3
RAC-100	3 #6	2 #4	3

Throughout the testing of the beam splice specimens, the midspan deflection, applied total load, and strain in the steel were recorded. When all testing was complete, the maximum applied load (peak load) of each beam was determined. Additionally, the

maximum strain in the steel was taken as the average of the maximum strains in each of the strain gauges. Then, using the modulus of elasticity of the steel as determined in the tension testing of the reinforcing bars, the average maximum stress in the steel was determined. This value was compared with the yield stress of the steel found in the tension testing of the bars to ensure that the steel did not yield during beam splice testing. The experimentally determined yield stress of the steel was found to be 74.9 ksi. Upon comparing the maximum stress in the steel to the yield stress, it was observed that none of the specimens experienced steel yield prior to bond rupture failure.

Table 5.4 shows the results from the beam splice testing. Within each of the specimen names, VAC represents virgin aggregate concrete (the control), RAC50 represents recycled aggregate concrete designed with 50% RCA replacement, and RAC100 represents recycled aggregate concrete designed with 100% RCA replacement. The final number in the specimen name indicates which of the three tests that specimen was identified as. The coefficient of variation (COV) of both the peak load carried and the peak stress developed in the longitudinal reinforcement of each set of data is also given in **Table 5.4**. For each test set, the variation is relatively low; the maximum within all of the collected test data is 7.8%. These low COV values indicate consistency in the results and reliability in the test as a measure of bond performance. Plots of the maximum applied loads for VAC, RAC-50, and RAC-100 specimens are shown in **Figures 5.5, 5.6, and 5.7**, respectively. Likewise, plots of the maximum developed stresses for VAC, RAC-50, and RAC-100 specimens are shown in **Figures 5.8, 5.9, and 5.10**, respectively.

Table 5.4: Beam Splice Test Results

Mix	Specimen	Peak Load (kips)	Peak Load COV	Steel Stress at Failure (ksi)	Peak Stress COV
VAC	VAC-1	62.0	4.2%	63.0	7.6%
	VAC-2	67.3		70.8	
	VAC-3	65.9		61.6	
RAC-50	RAC50-1	54.4	5.7%	56.5	1.7%
	RAC50-2	48.8		55.2	
	RAC50-3	50.1		54.8	
RAC-100	RAC100-1	48.8	7.3%	47.3	7.8%
	RAC100-2	50.7		49.9	
	RAC100-3	56.1		55.1	

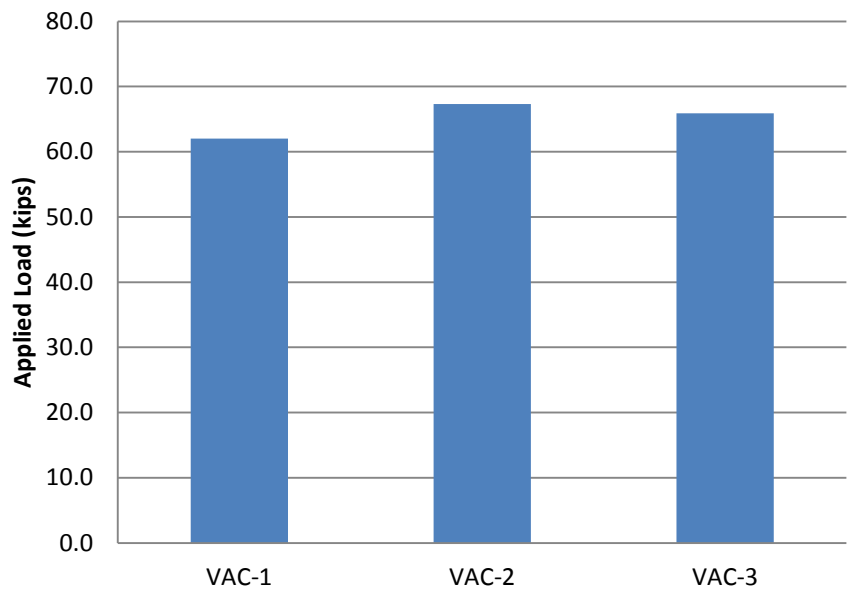


Figure 5.5: Peak Loads for VAC Beam Splice Specimens
 Conversion: 1 kip = 4.45 kN

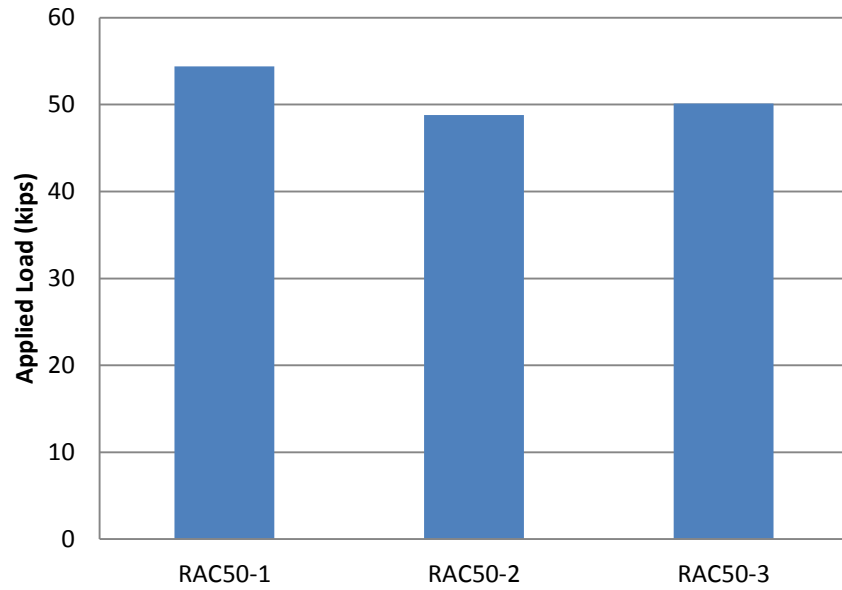


Figure 5.6: Peak Loads for RAC-50 Beam Splice Specimens
Conversion: 1 kip = 4.45 kN

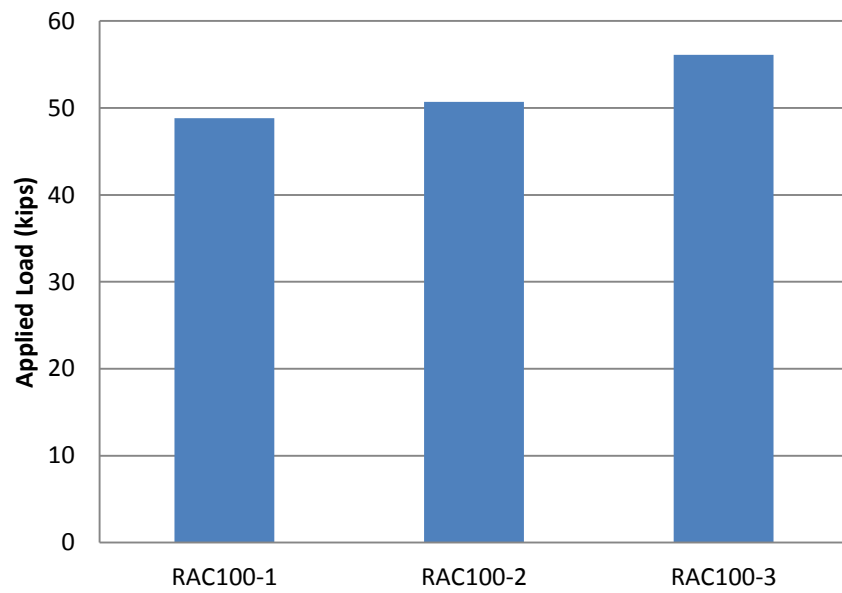


Figure 5.7: Peak Loads for RAC-100 Beam Splice Specimens
Conversion: 1 kip = 4.45 kN

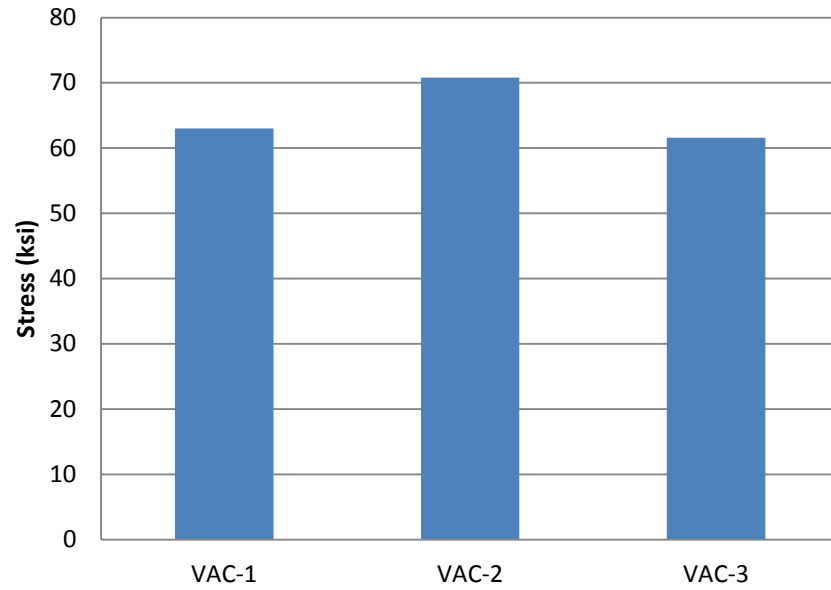


Figure 5.8: Peak Stresses for VAC Beam Splice Specimens
Conversion: 1 ksi = 6.9 MPa

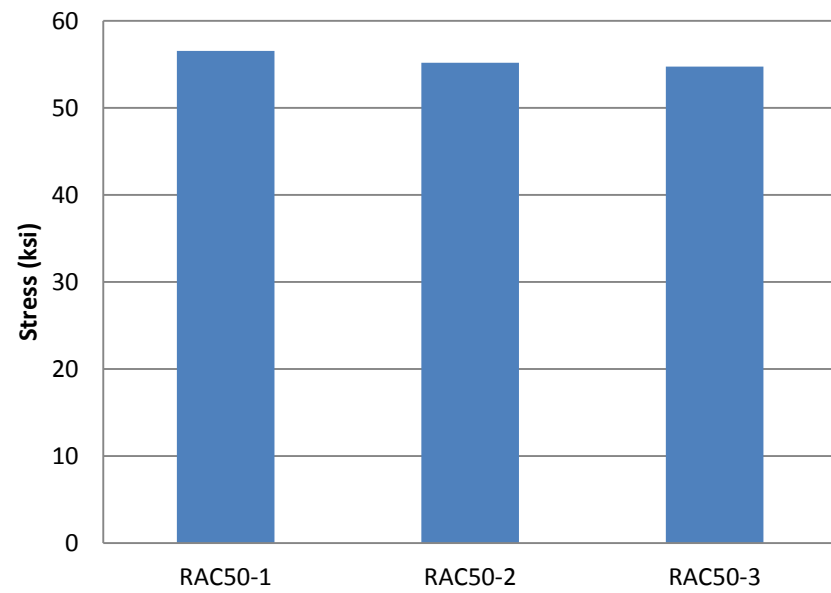


Figure 5.9: Peak Stresses for RAC-50 Beam Splice Specimens
Conversion: 1 ksi = 6.9 MPa

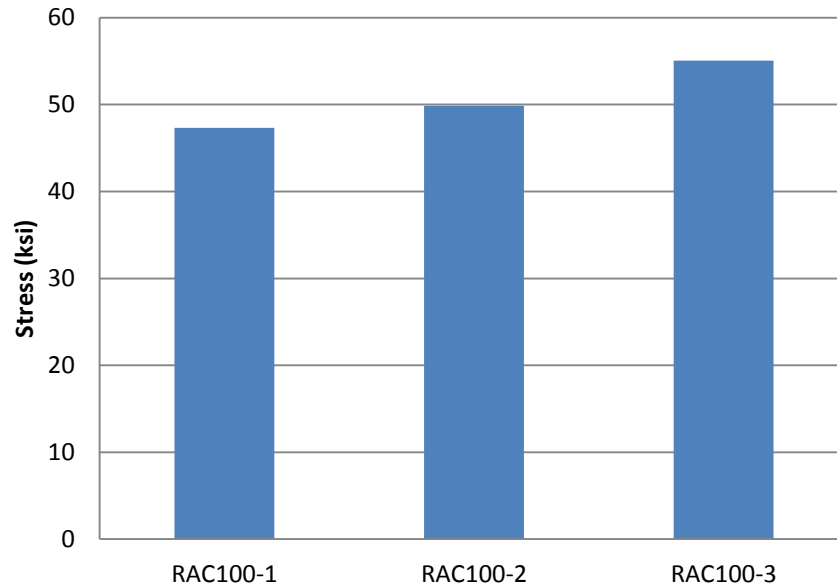


Figure 5.10: Peak Stresses for RAC-100 Beam Splice Specimens
Conversion: 1 ksi = 6.9 MPa

In order to better evaluate and compare the response of the beam splice specimens, the deflection and steel strain data were plotted against the total applied load for each beam. A typical plot of load versus deflection is shown in **Figure 5.11**, and a typical plot of load versus strain is shown in **Figure 5.12**. The plots shown are from specimen VAC-3. Both plots indicate that flexural cracking began to occur in specimen VAC-3 around 15 kips (66.7 kN), as evidenced by the change in slope of the plots at this load. From the constant linear-elastic nature of the load versus strain and load versus deflection plots of the specimens, it was again verified that the steel did not reach yield in any of the test specimens. The load versus deflection and load versus strain plots for each of the tested specimens are included in Appendix B.

At their failure loads, all specimens experienced a bond rupture type of failure. This failure type was indicated by the abrupt audible and visible signs of splitting crack development at the peak load. A typical crack pattern at failure is shown from specimen

RAC50-1 in **Figure 5.13**. The corresponding bottom view at midspan of specimen RAC50-1 is shown in **Figure 5.14**. In both pictures, the splitting cracks at the spliced longitudinal reinforcement are evident. In some beam splice tests, the splitting cracks were so pronounced that the concrete cover within the spliced region spalled off of the specimen. Images of crack patterns of all tested specimens at failure are shown in Appendix C.

5.3. REINFORCING BAR TENSION TEST RESULTS

In order to determine the ultimate stress, yield stress, and modulus of elasticity of the reinforcing bars used in the beam splice specimens, tension tests were performed in accordance with ASTM E8-09 *Standard Test Methods for Tension Testing of Metallic Materials* (ASTM E9-09). This test was performed on three 30 in. (76.2 cm) lengths of #6 reinforcing bars. Each specimen was clamped at each end in a 200 kip (890kN) capacity load frame and loaded until rupture. Throughout testing, both strain and load were recorded. For each specimen, the yield stress of the bar was determined from the 0.5% strain offset of the stress versus strain plot. The modulus of elasticity was also determined for each bar using both the 0.5% offset stress and strain value and the stress and strain value at 40% of the yield stress. **Table 5.5** shows the results of the #6 reinforcing bar tension test.

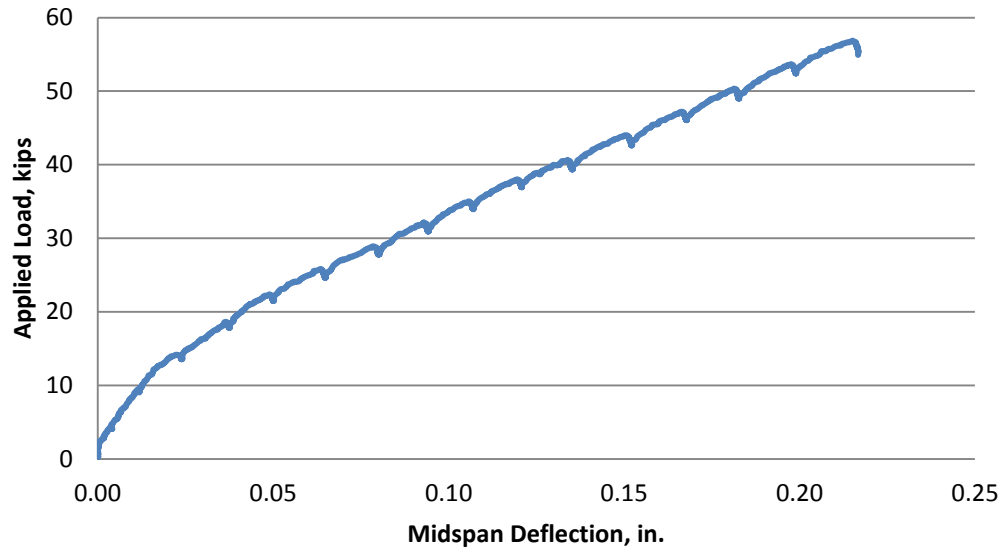


Figure 5.11: Typical Load versus Deflection Plot (VAC-3)

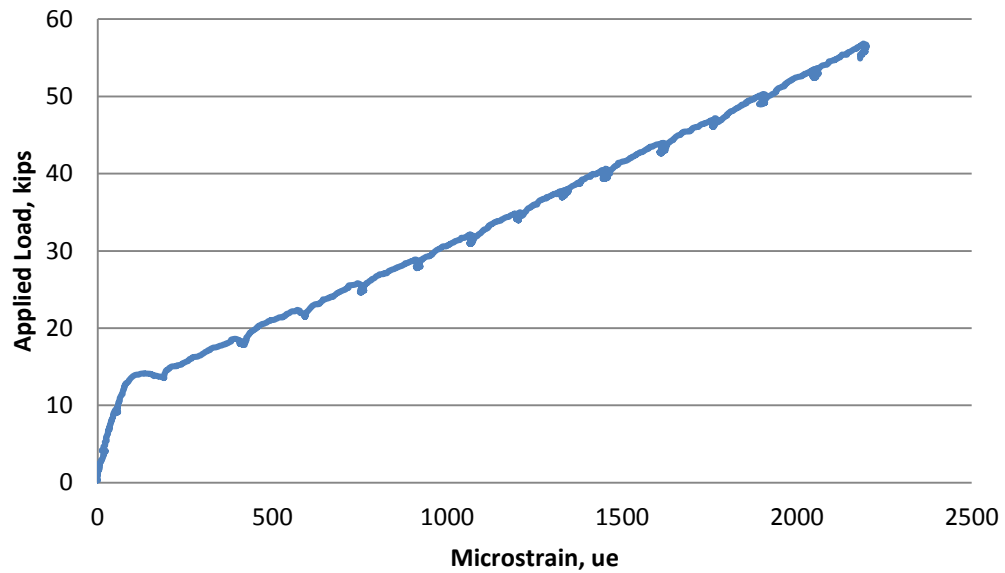


Figure 5.12: Typical Load versus Strain Plot (VAC-3)



Figure 5.13: Beam Splice Crack Propagation at Failure (RAC50-1)



Figure 5.14: Beam Splice Specimen Bottom View at Failure (RAC50-1)

Table 5.5: #6 Reinforcing Bar Tension Test Results

Specimen	Yield Stress (ksi)	Average Yield Stress (ksi)	Modulus of Elasticity (ksi)	Average Modulus of Elasticity (ksi)
1	74.84	74.85	28,114	27,992
2	75.14		29,814	
3	74.58		26,048	

Conversion: 1 ksi = 6.9 MPa

5.4. ANALYSIS OF RESULTS

5.4.1. Methodology. In order to directly compare the test results across mix designs, the data was normalized to account for the different test day strengths of the concrete. For the beam splice specimens, the data was also normalized to account for the design strength of the beams. Two different normalization techniques were used to compare the results. The first normalization technique was based on the development length equations provided in ACI 318-11 (ACI 318, 2011), shown in **Equation 5.1**, and AASHTO LRFD-07 (AASHTO, 2007), shown in **Equation 5.2**. Both development length equations are indirectly proportional to the square root of the concrete compressive strength. Thus, in order to normalize the results with varying compressive strengths, peak bond stresses in the direct pull-out tests were divided by the square root of the corresponding compressive strength as shown in **Equation 5.3**. Furthermore, to account for the different design strengths of the concrete used in developing the splice length of the beam splice specimens, the results from these tests were normalized by multiplying the peak stresses by the square root of the design concrete strength. Thus, the developed stress in the steel was multiplied by the square root of the ratio of design strength to actual test-day strength as shown in **Equation 5.4**.

$$l_d = \left[\frac{3}{40} \frac{f_y}{\lambda \sqrt{f'_c}} \frac{\Psi_t \Psi_e \Psi_s}{\left(\frac{c_b + K_{tr}}{d_b} \right)} \right] * d_b \quad (5.1)$$

where,

- l_d = development length
- f_y = specified yield strength of reinforcement
- λ = lightweight concrete modification factor
- f'_c = specified compressive strength of concrete
- Ψ_t = reinforcement location modification factor
- Ψ_e = reinforcement coating modification factor
- Ψ_s = reinforcement size modification factor

c_b = smallest of distance from center of a bar to nearest concrete surface or one-half the center-to-center bar spacing
 K_{tr} = transverse reinforcement index
 d_b = nominal diameter of the reinforcing bar

$$l_{db} = \frac{1.25 A_b f_y}{\sqrt{f'_c}} \geq 0.4 d_b f_y \quad (5.2)$$

where, l_{db} = tension development length
 A_b = area of the reinforcing bar
 f_y = specified yield strength of reinforcement
 f'_c = specified compressive strength of concrete
 d_b = the nominal diameter of the reinforcing bar

$$\text{Normalized Stress} = \frac{\text{Failure Stress}}{\sqrt{\text{Test-Day Concrete Strength}}} \quad (5.3)$$

$$\text{Normalized Stress} = \text{Failure Stress} * \sqrt{\frac{\text{Design Concrete Strength}}{\text{Test-Day Concrete Strength}}} \quad (5.4)$$

The second normalization technique is a fourth root normalization as recommended by ACI 408R (2003) and Zuo and Darwin (2000). Zuo and Darwin observed from a large international database of beam splice specimens that $f'_c^{1/4}$ best represents the effect of concrete strength on development and splice length. This observation was based on 171 beam specimens with bottom-cast bars not confined by transverse reinforcement (Zuo and Darwin 2000). Using this relationship with bond strength and concrete compressive strength, the peak bond stresses of direct pull-out specimens were divided by the fourth root of the test-day concrete compressive strength as shown in **Equation 5.5**. Similarly, the peak stress developed in the beam splice specimens was normalized by the fourth root of the ratio of the design concrete compressive strength and the actual test-day strength as shown in **Equation 5.6**.

$$\text{Normalized Stress} = \frac{\text{Failure Stress}}{\sqrt[4]{\text{Test-Day Concrete Strength}}} \quad (5.5)$$

$$\text{Normalized Stress} = \text{Failure Stress} * \sqrt[4]{\frac{\text{Design Concrete Strength}}{\text{Test-Day Concrete Strength}}} \quad (5.6)$$

For the VAC control beam splice specimens, the design strength used was 4000 psi (27.58 MPa). For the RCA-50 and RCA-100 beam splice specimens, the design strength was 5500 psi (37.92 MPa). These design strengths were determined from trial batching of the mix designs prior to beam splice specimen construction. On test day, the actual concrete compressive strengths were determined from companion cylinder specimens, and the resulting values are shown in **Tables 5.6**.

Table 5.6: Beam Splice Test Day Compressive Strengths

Cylinder Break	VAC	RAC-50	RAC-100
1	4012	3666	4861
2	4166	3436	4750
3	3823	3571	4919
Average	4000	3558	4843
COV	4.3%	3.2%	1.8%

Conversion: 1 psi = 6.9 kPa

5.4.2. Analysis and Interpretation of Direct Pull-Out Results. The normalized results from the direct pull-out tests are shown in **Table 5.7** below. The table shows the test-day compressive strength used to normalize the peak bond stress prior to pull-out failure for each set of specimens. For the #4 (No. 13) specimens, the average square root and fourth root normalized results for each RCA replacement level are shown in **Figures 5.15** and **5.17**, respectively. For the #6 (No. 19) specimens, the average square root and fourth root normalized results for each RCA replacement level are shown in **Figures 5.19**

and **5.21**, respectively. Boxplots indicating the spread of the data for each normalization technique are shown in **Figures 5.16** and **5.18** for the #4 (No.13) specimens and **Figures 5.20** and **5.22** for the #6 (No.19) specimens.

A comparison of the average square root normalized data for the #4 (No.13) specimens indicates that there was essentially no change in peak bond stress between the VAC and RAC-50 specimens. However, there was a 6.0% increase in the RAC-100 over the VAC specimens. Using the average fourth root normalized data for the #4 (No.13) specimens, there was a slight increase in peak bond stress between the control and both RCA replacement levels. The bond stress increased 7.9% in RAC-50 specimens and 12.9% in the RAC-100 specimens.

A comparison of the average square root normalized data for the #6 (No.19) specimens indicates that there was a 1% decrease in peak bond stress in the RAC-50 specimens over the controls. However, there was a very slight increase in peak bond stress of 0.5% in the RAC-100 specimens over the VAC specimens. Using the average fourth root normalized data for the #6 (No. 19) specimens, there was a slight increase in peak bond stress between the control and both RCA replacement levels. In both RAC-50 and RAC-100 specimens, the average peak bond stress was 7.1% higher than the control.

A parametric statistical analysis was performed on the normalized peak bond stresses between both RCA replacement levels and the control specimens for both normalization techniques. The analysis used an independent, two-sample, student's t-test assuming unequal variances and a 95% confidence interval. An analysis of the square root normalized bond stresses in the #4 (No. 13) pull-out specimens showed that both the 50% and 100% RCA specimens were statistically the same as the control #4 (No.13)

specimens. Likewise, an analysis of the fourth root normalized bond stresses in the #4 (No. 13) pull-out specimens showed that both the 50% and 100% RCA specimens were statistically the same as the control #4 (No.13) specimens. This analysis helps verify that the slight percent increase in bond stress was within the test variability. An analysis of the square root normalized bond stresses in the #6 (No. 19) pull-out specimens showed that both the 50% and 100% RCA specimens were statistically the same as the control #6 (No.13) specimens. Likewise, an analysis of the fourth root normalized bond stresses in the #6 (No. 13) pull-out specimens showed that the 50% RCA specimens were statistically the same as the control #6 (No.13) specimens. However, the student's t-test shows that the percent increase between the 100% RCA specimens and the controls is statistically significant.

Because the data sets are small, a non-parametric analysis was also performed to verify the student's t-test. The Mann-Whitney test was utilized to compare the normalized peak bond stresses between both RCA pull-out sets and the control set with a 95% confidence interval. Analyzing the square root normalized peak bond stresses, this test showed that there was no significant difference from the control in either the 50% RCA specimens or 100% RCA specimens for both #4 (No.13) and #6 (No.19) bars. Likewise, analyzing the fourth root normalized peak bond stresses, this test showed that there was no significant difference from the control in either the 50% RCA specimens or 100% RCA specimens for both #4 (No.13) and #6 (No.19) bars. This analysis reveals that while there was a slight increase in peak bond stress, this increase was not significantly large. A summary of these statistical analyses are provided in Appendix D.

Table 5.7: Normalized Bond Stresses for Pull-Out Specimens

Mix	Bar Size	Specimen	Max. Applied Load (lb)	Bond Stress (psi)	Test Day Strength (psi)	Normalized Bond Stress (Square Root)	Average of Normalized Bond Stress (Square Root)	Normalized Bond Stress (Fourth Root)	Average of Normalized Bond Stress (Fourth Root)
VAC	#4 (No. 13)	VAC-PO4-1	10344	2634	4000	42	43	331	343
		VAC-PO4-2	10435	2657		42		334	
		VAC-PO4-3	11379	2898		46		364	
	#6 (No. 19)	VAC-PO6-1	27172	3075		49	47	387	373
		VAC-PO6-2	25869	2928		46		368	
		VAC-PO6-3	25563	2893		46		364	
RAC-50	#4 (No. 13)	RAC50-PO4-1	12760	3249	5460	44	43	378	370
		RAC50-PO4-2	13083	3332		45		388	
		RAC50-PO4-3	11657	2968		40		345	
	#6 (No. 19)	RAC50-PO6-1	31109	3521		48	46	410	399
		RAC50-PO6-2	28430	3218		44		374	
		RAC50-PO6-3	31440	3558		48		414	
RAC-100	#4 (No. 13)	RAC100-PO4-1	13968	3557	5147	50	46	420	387
		RAC100-PO4-2	12236	3116		43		368	
		RAC100-PO4-3	12451	3171		44		374	
	#6 (No. 19)	RAC100-PO6-1	30302	3429		48	47	405	400
		RAC100-PO6-2	29597	3350		47		395	
		RAC100-PO6-3	29804	3373		47		398	

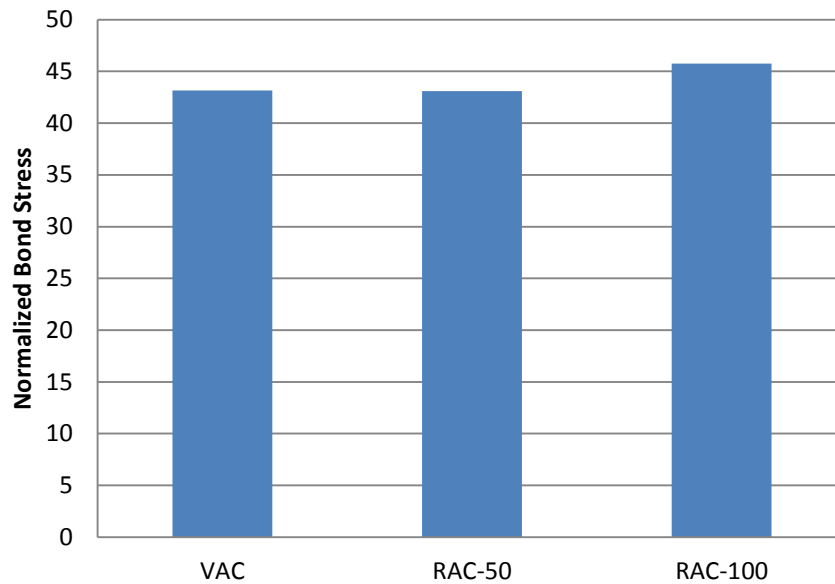


Figure 5.15: Average #4 Pull-Out Bond Stresses by Square Root Normalization

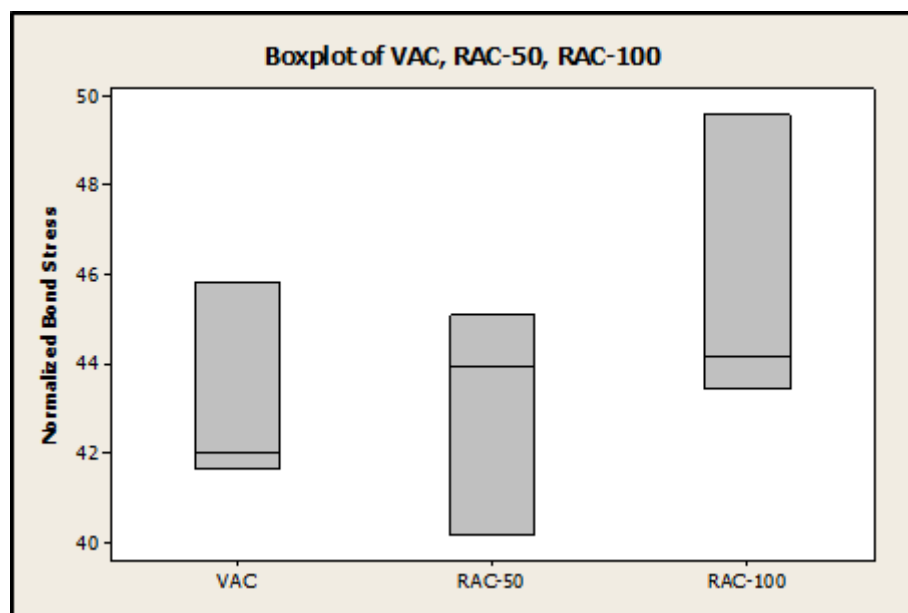


Figure 5.16: Boxplot of #4 Pull-Out Bond Stresses by Square Root Normalization

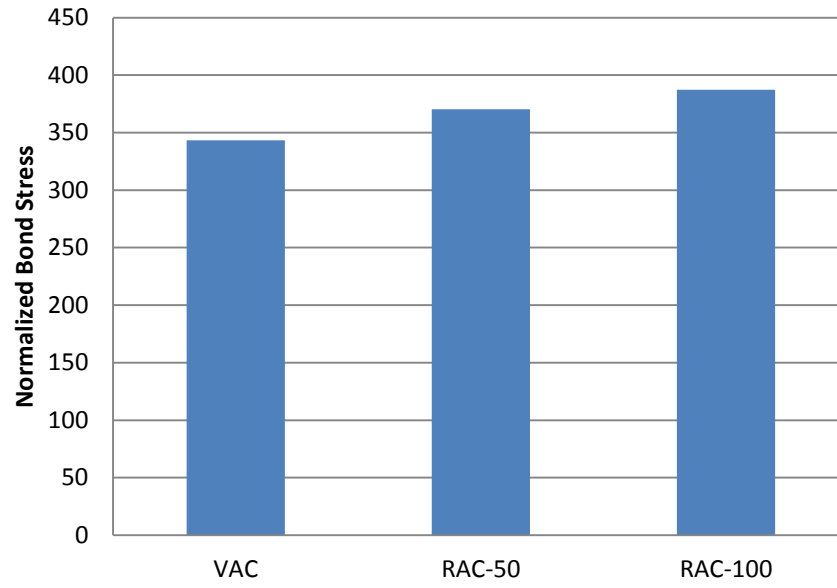


Figure 5.17: Average #4 Pull-Out Bond Stresses by Fourth Root Normalization

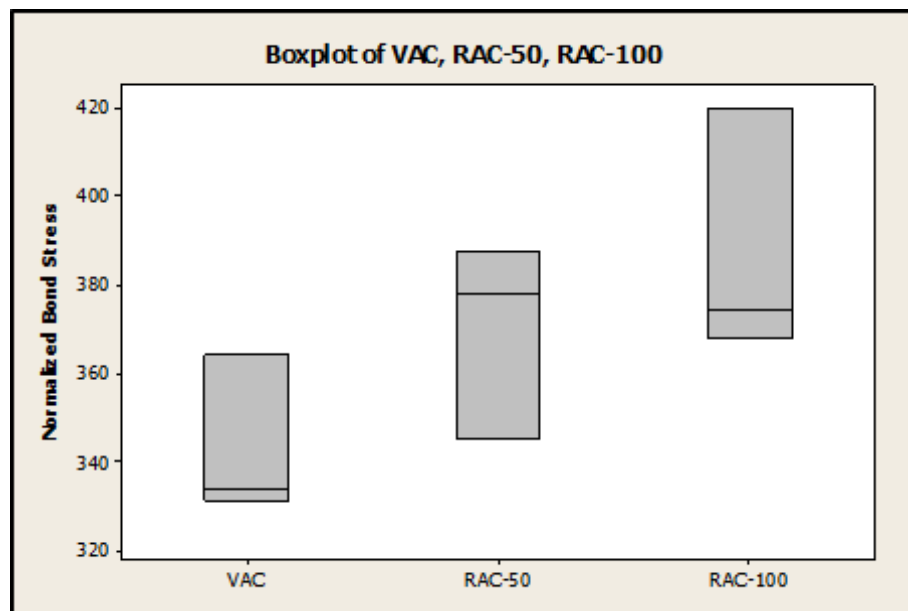


Figure 5.18: Boxplot of #4 Pull-Out Bond Stresses by Fourth Root Normalization

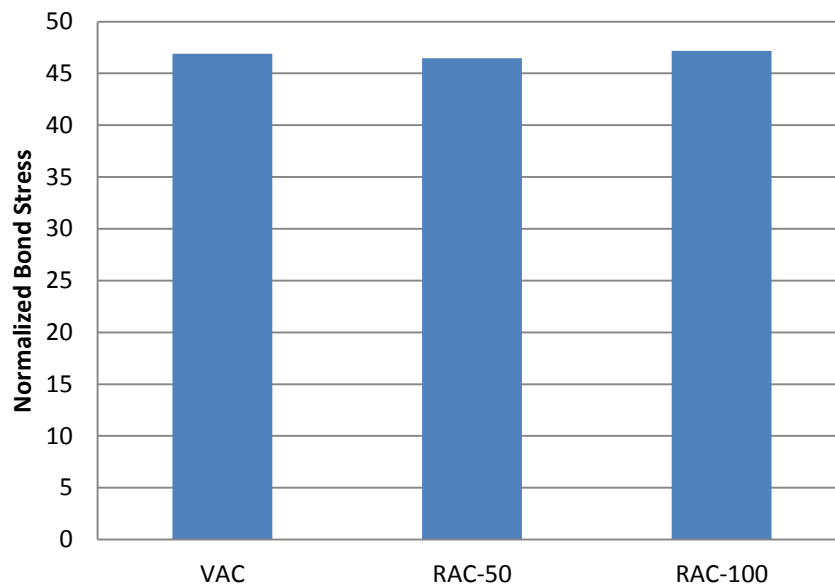


Figure 5.19: Average #6 Pull-Out Bond Stresses by Square Root Normalization

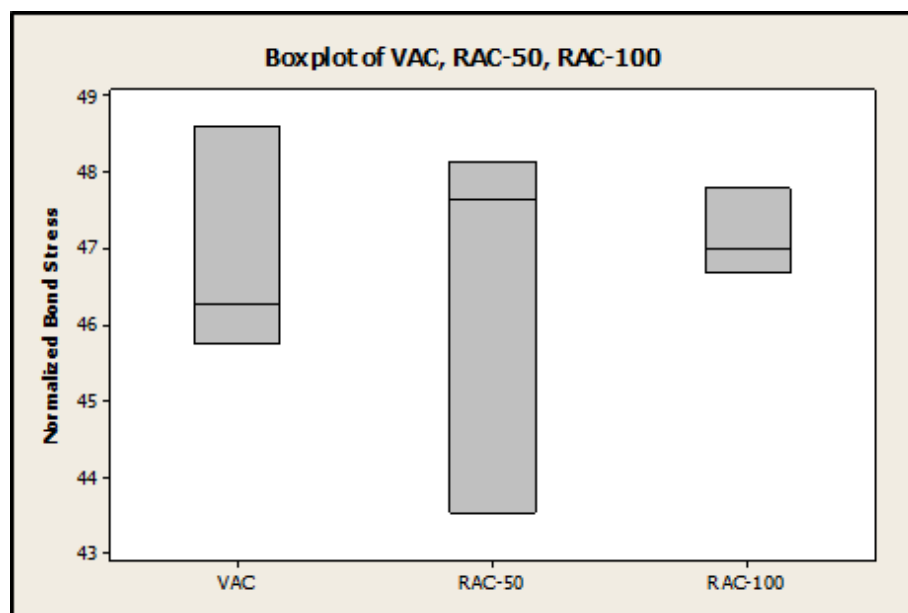


Figure 5.20: Boxplot of #6 Pull-Out Bond Stresses by Square Root Normalization

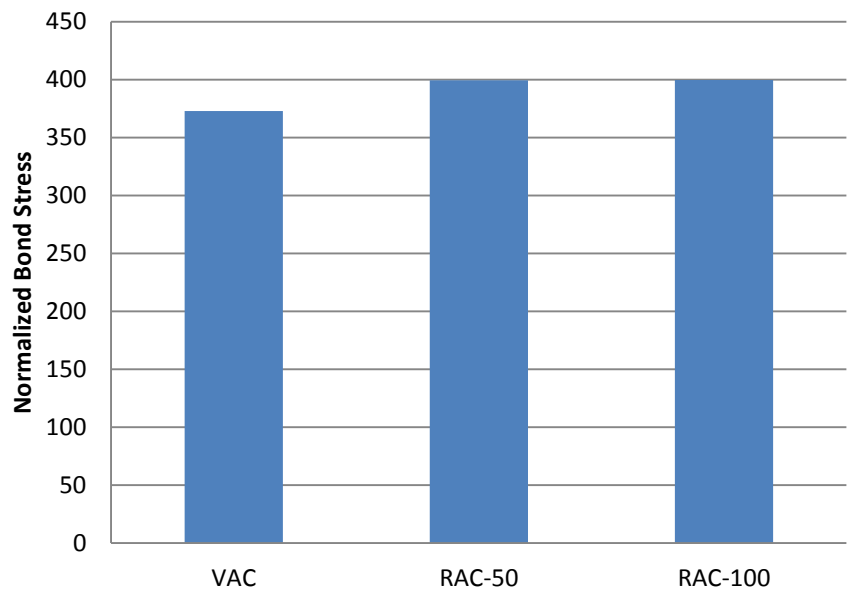


Figure 5.21: Average #6 Pull-Out Bond Stresses by Fourth Root Normalization

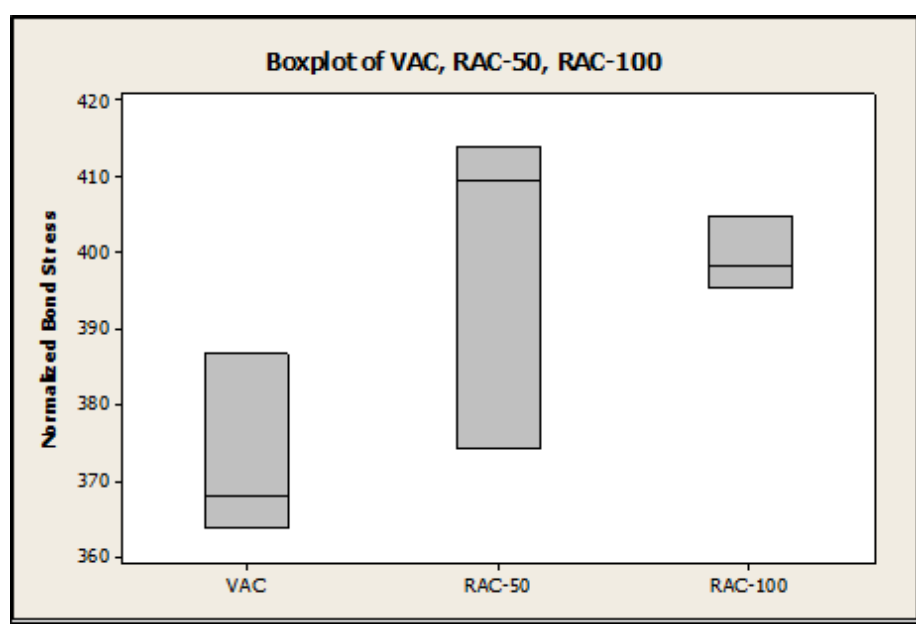


Figure 5.22: Boxplot of #6 Pull-Out Bond Stresses by Fourth Root Normalization

To evaluate the effect of bar size, the average normalized peak bond stresses were compared between the #4 (No. 13) and #6 (No. 19) specimens. In all RCA replacement levels, the #6 (No. 19) specimens exhibited higher bond stresses than the #4 specimens. However, as RCA replacement increases, the percent difference between decreased. The percent difference between #4 (No. 13) and #6 (No. 19) was 8.6%, 7.8%, and 3.1% for the VAC, RAC-50, and RAC-100, respectively. This comparison is shown in **Figure 5.23** for the square root normalized bond stresses and in **Figure 5.24** for the fourth root normalized bond stresses.

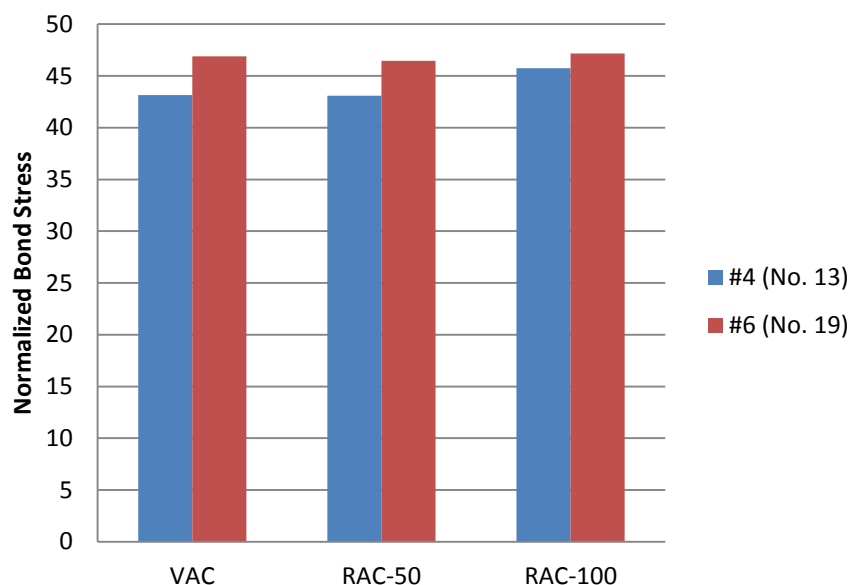


Figure 5.23: Comparison of #4 (No.13) and #6 (No. 19) Square Root Normalized Pull-out Results

5.4.3. Analysis and Interpretation of Beam Splice Results. The normalized results from the beam splice tests are shown in **Table 5.8**. The table shows the test day compressive strength for each set of beams as well as the design strength of the beams. These values were used to normalize the peak stresses developed in the beams prior to bond rupture. The average square root normalized stresses for each set of beams are also plotted in **Figure 5.25**. A boxplot indicating the spread of the square root normalized

beam splice results is provided in **Figure 5.26**. Likewise, the average fourth root normalized stresses for each set of beam are plotted in **Figure 5.27**, and a boxplot indicating the spread of the data is shown in **Figure 5.28**.

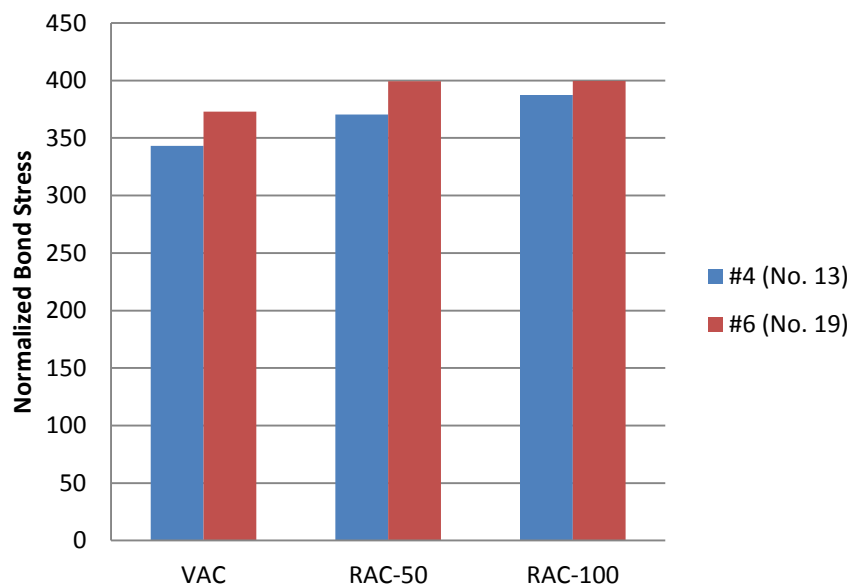


Figure 5.24: Comparison of #4 (No.13) and #6 (No. 19) Fourth Root Normalized Pull-out Results

A comparison of the square root normalized results indicates that 50% RCA beams had a slight increase in developed stress in the steel of 5.9% over the VCA control. However, the 100% RCA beams had a decrease in stress of 16.9% over the VCA control. A comparison of the fourth root normalized results shows that generally, both RCA beam sets had a lower stress in the steel. The 50% RCA beams decreased by 5.0%, and the 100% RCA beams decreased by 19.5%.

A parametric statistical analysis was performed on the normalized peak stresses between both RCA mix beams and the control beams for both normalization techniques. The analysis used an independent, two-sample, student's t-test assuming unequal variances and a 95% confidence interval. For the square root normalized results, the t-test

showed that the 50% RCA beam results are statistically the same as the control beam results. However, the same student's t-test showed that the 100% RCA beam results are different from the control beams under square root normalization. This statistical analysis verifies that the slight percent increase between the 50% RCA beams and the control beams is well within the test variability, whereas the 100% RCA beams exhibited diminished bond strength over the control beams. For the fourth root normalization, the t-test likewise showed that the 50% RCA beam results are statistically the same as the control beam results, and the 100% RCA beam results are different from the control beams. This statistical analysis verifies that the percent difference between the 50% RCA beams and control beams is within the test variability, whereas the 100% RCA beams exhibited diminished bond strength over the control beams. A summary of this parametric statistical analysis is provided in Appendix D.

Given that the data set for each set of beams was small, a non-parametric statistical analysis was performed to validate the student's t-test. The Mann-Whitney test was utilized to compare the normalized peak stresses between both RCA beam sets and the control beam set with a 95% confidence interval. This test verified the results from the student's t-test that there was no difference between the 50% RCA and the control beams under both normalization techniques. However, the test showed that the difference between the 100% RCA and control beams under both normalization techniques was just barely insignificant. A summary of this non-parametric statistical analysis is provided in Appendix D.

Table 5.8: Normalized Developed Stresses for Beam Splice Specimens

Mix	Specimen	Design Strength (psi)	Test Day Strength (psi)	Peak Stress (ksi)	Square Root Normalized Stress (ksi)	Average of Square Root Normalized Stress (ksi)	Fourth Root Normalized Stress (ksi)	Average of Fourth Root Normalized Stress (ksi)
VAC	VAC-1	4000	4000	63.0	63.01	65.13	63.01	65.13
	VAC-2			70.8	70.79		70.79	
	VAC-3			61.6	61.58		61.58	
RAC-50	RAC50-1	5500	3560	56.5	70.28	68.98	63.04	61.87
	RAC50-2			55.2	68.61		61.54	
	RAC50-3			54.8	68.05		61.04	
RAC-100	RAC100-1	5500	4840	47.3	50.46	54.10	48.87	52.40
	RAC100-2			49.9	53.14		51.47	
	RAC100-3			55.1	58.69		56.85	

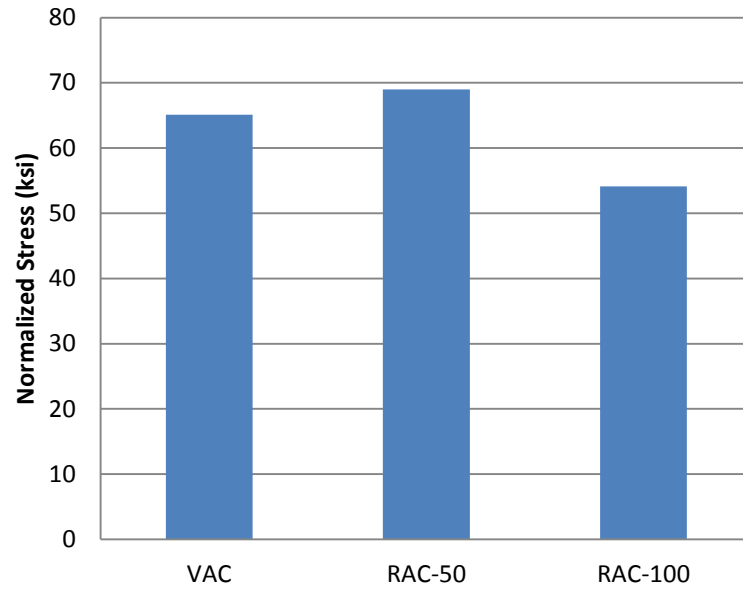


Figure 5.25: Average Beam Splice Peak Stresses by Square Root Normalization

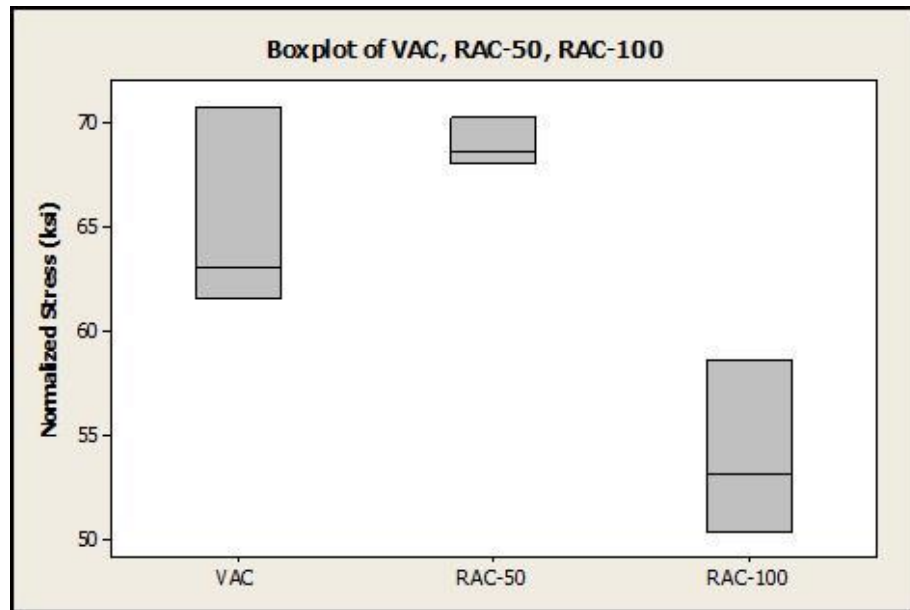


Figure 5.26: Boxplot of Peak Stresses by Square Root Normalization

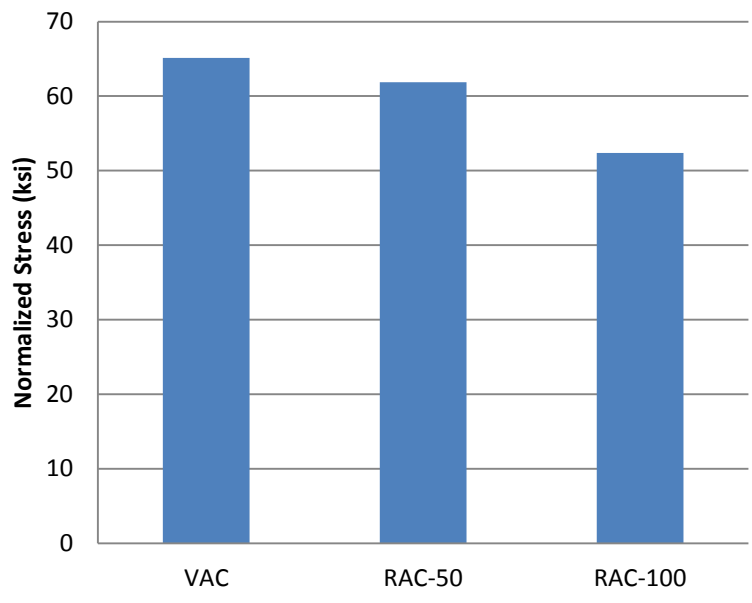


Figure 5.27: Average Beam Splice Peak Stresses by Fourth Root Normalization

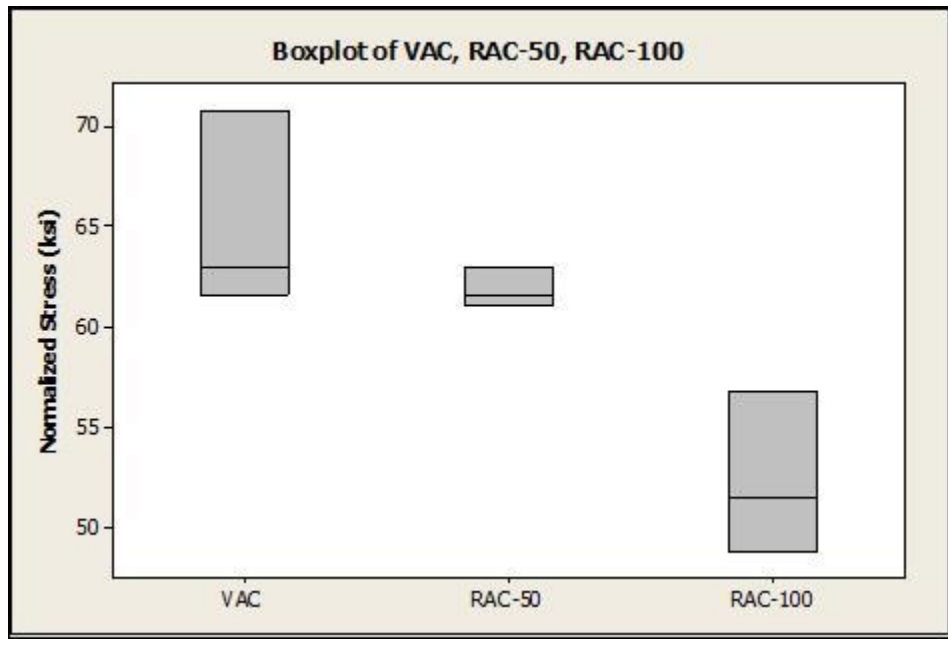


Figure 5.28: Boxplot of Peak Stresses by Fourth Root Normalization

The stress developed in the longitudinal steel was compared to the theoretical values from moment-curvature calculations of the section. This was done in order to further evaluate the validity of the test results and to evaluate the applicability of stress-strain relationships to the 50% and 100% RCA mixes. To calculate the theoretical stress in the longitudinal reinforcement, the moment-curvature program *Response-2000* (Bentz and Collins 2000) was used to evaluate the section under the peak applied moment observed in the specimens. These applied moments were calculated from the average peak loads carried by the beams. Two different stress-strain models were used to describe the concrete. The first was Hognestad's stress-strain relationship, which is recommended by ACI 408R (2003). The second was Popovic, Thorenfeldt and Collins' stress-strain relationship. **Table 5.9** shows the summary of measured and theoretically calculated stress values.

Table 5.9 also shows the ratio of measured to theoretically calculated stress. This ratio provides an indication of how well the measured values were predicted by the theoretical models. The theoretical values slightly underestimated the measured results, as indicated by the ratio values slightly over unity. Despite this small underestimation, the measured stresses were fairly accurately predicted. This analysis indicates that both Hognestad's stress-strain relationship as well as the Popovic, Thorenfeldt and Collins' stress-strain relationship for concrete may be acceptable for use with concrete containing up to 100% RCA replacement for coarse aggregates.

Table 5.9: Comparison of Measured to Theoretical Stress in Beam Splice Specimens

Table reports stress values in ksi

Conversion: 1 ksi = 6.9 MPa

Mix	Specimen	Measured ^a	Average Measured ^a	M- ϕ ^b	Average M- ϕ ^b	$f_{s(\text{measured})}/f_{s(\text{M-}\phi)^b}$	M- ϕ ^c	Average M- ϕ ^c	$f_{s(\text{measured})}/f_{s(\text{M-}\phi)^c}$
VAC	VAC-1	63.01	65.13	58.5	61.53	1.06	58.5	61.37	1.06
	VAC-2	70.79		63.6			63.5		
	VAC-3	61.58		62.5			62.1		
RAC-50	RAC50-1	56.54	55.50	51.7	48.57	1.14	51.5	48.40	1.15
	RAC50-2	55.20		46.4			46.3		
	RAC50-3	54.75		47.6			47.4		
RAC-100	RAC100-1	47.33	50.75	45.8	48.60	1.04	45.8	49.17	1.03
	RAC100-2	49.85		47.5			47.6		
	RAC100-3	55.06		52.5			54.1		

^a Strain (average from strain gages) multiplied by modulus of elasticity

^b Hognestad stress-strain model (ACI 408R-03 recommended method)

^c Popovic, Thorenfeldt, & Collins stress-strain model

The beam splice results were compared to the bond strength prediction equations summarized in ACI 408R 2003. This was done in order to evaluate if the trend of decreasing bond strength with increasing replacement with RCA could be observed under the normalization techniques used in all of these formulae. Further, this analysis was performed to evaluate how closely RCA concrete bond behavior could be predicted by these equations developed for conventional concrete. The prediction ratios were calculated as the measured bond stress over the calculated bond stress. The measured stresses in the steel were normalized as per the technique adopted by each descriptive equation. These ratios are provided in **Table 5.10**. A graphical representation is provided in **Figure 5.29**.

As shown in **Figure 5.29**, the bond stress generally decreases as the amount of RCA increases. Furthermore, all equations underestimate the bond strength for both VAC and RAC-50 on average, whereas RAC-100 is not as conservatively predicted. The equation in ACI 318 2011 for development and splice length of straight reinforcement in tension is based on the equations provided by Orangun, Jirsa, and Breen (1977). For all three levels of RCA replacement, their technique was the most conservative as it underestimated average bond strengths.

Table 5.10: Prediction Ratios for Beam Splice Results

Specimen	Orangun, Jirsa, & Breen (1977)	Darwin et al. (1992)	Zuo & Darwin (2000)	Esfahani & Rangan (1998)	ACI 408 (2003)
VAC-1	1.40	1.34	1.33	1.27	1.31
VAC-2	1.57	1.50	1.49	1.43	1.48
VAC-3	1.37	1.31	1.30	1.24	1.28
Average	1.45	1.38	1.37	1.31	1.36
RAC50-1	1.49	1.36	1.34	1.29	1.33
RAC50-2	1.45	1.33	1.31	1.26	1.30
RAC50-3	1.44	1.32	1.30	1.25	1.29
Average	1.46	1.33	1.32	1.27	1.30
RAC100-1	1.07	1.05	1.04	0.99	1.03
RAC100-2	1.12	1.11	1.10	1.04	1.08
RAC100-3	1.24	1.23	1.21	1.15	1.20
Average	1.14	1.13	1.12	1.06	1.10

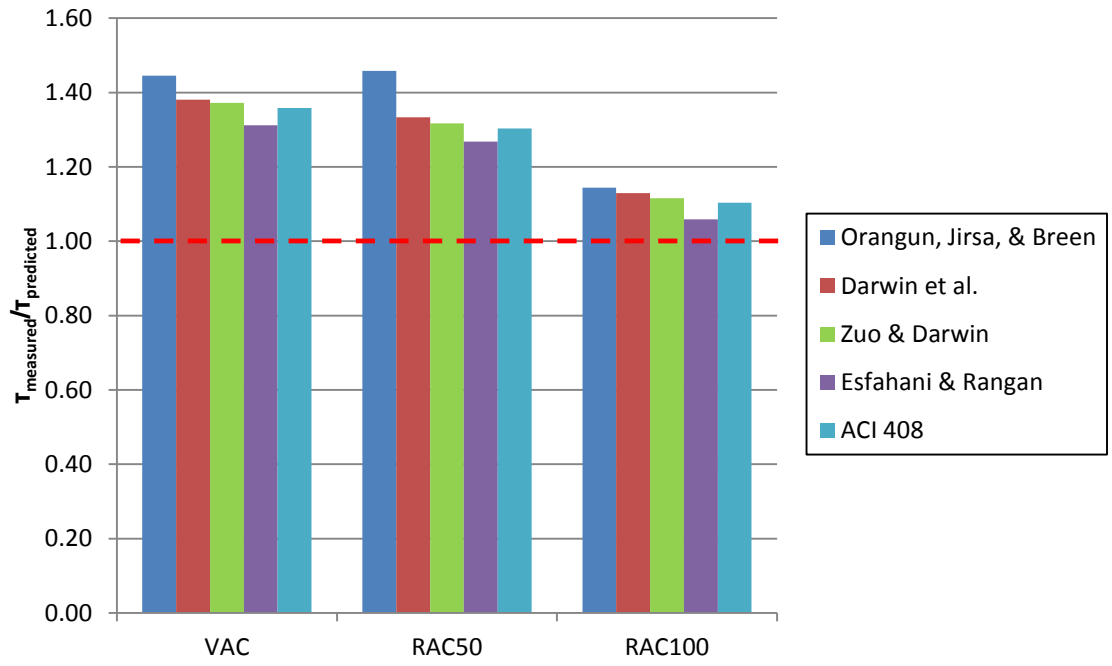


Figure 5.29: Comparison of Prediction Ratios for Beam Splice Results

The beam splice results were compared to the bond database 10-2001 provided by ACI Committee 408 (ACI 408R, 2003) in **Figure 5.30**. The plot below shows those beam splice tests results from similar bond specimens with bottom-cast bars and no transverse confinement in the spliced region. This comparison helps validate the test method from this study as falling within the range of data provided by previous bond researchers. For a given compressive strength of concrete, the beam splice results fit well within the scatter of the data. However, due to the large scatter of this historical bond data, it is difficult to draw a conclusion about the trend of bond strength with concrete compressive strength.

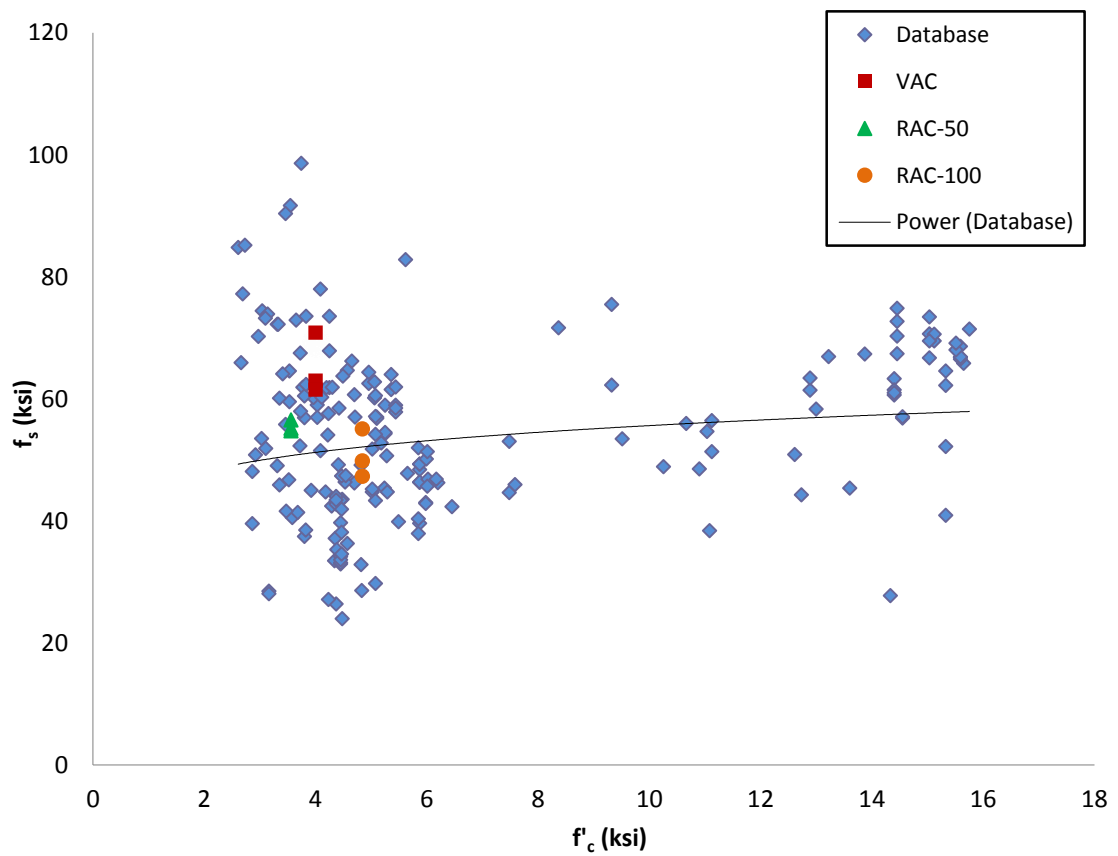


Figure 5.30: Comparison of Beam Splice Results to Database
Conversion: 1 ksi = 6.9 MPa

6. FINDINGS, CONCLUSIONS AND RECOMMENDATIONS

6.1. INTRODUCTION

The objective of this study was to determine the effect of replacing coarse natural aggregates with RCA on the bond strength between deformed steel bars and surrounding concrete. The following section presents the findings, conclusions, and recommendations of this study. The testing program compared mix designs at three different RCA replacement levels, 0%, 50%, and 100%. A standard Missouri Department of Transportation (MoDOT) Class B mix design was used as a baseline mix throughout the study. Two test methods were used to evaluate bond performance. The first method was the direct pull-out test based on the RILEM 7-II-128 *RC6: Bond test for reinforcing steel* (RILEM, 1994). The second method was a full-scale spliced beam tested under third point loading. While the direct pull-out test is a widely used test method for comparing bond performance, the full-scale beam splice specimens are regarded as the most realistic stress state response in evaluating bond performance.

6.2. FINDINGS

6.2.1. Material Properties Testing. All concrete material properties were negatively impacted with increasing replacement of coarse natural aggregates with RCA. The most drastic decreases were seen in splitting tensile strength and fracture energy. The splitting tensile strength decreased 12% and 29% for 50% RCA replacement and 100% RCA replacement, respectively. The fracture energy decreased 14% and 22% for 50% RCA replacement and 100% RCA replacement, respectively.

6.2.2. Direct Pull-Out Testing. A total of 18 direct pull-out specimens were constructed and tested in this study. For each RCA replacement level, three specimens were constructed with a #4 (No. 13) deformed bar and three specimens were constructed with a #6 (No. 19) deformed bar. Comparing average square root normalized data for the #4 (No.13) specimens indicates that there was essentially no difference in peak bond stress between the VAC and RAC-50 specimens and a slight increase of 6.0% in the RAC-100 over the VAC specimens. A comparison of the average square root normalized data for the #6 (No.19) specimens indicates that there was a 1% decrease in peak bond stress in the RAC-50 specimens over the controls and essentially no difference in peak bond stress between the RAC-100 specimens and the VAC specimens.

Comparing the fourth root normalized data for the #4 (No.13) specimens, there was a slight increase in peak bond stress between the control and both RCA replacement levels. The bond stress increased 7.9% in RAC-50 specimens and 12.9% in the RAC-100 specimens. Likewise, comparing the fourth root normalized data for the #6 (No. 19) specimens, there was a slight increase in peak bond stress between the control and both RCA replacement levels. In both RAC-50 and RAC-100 specimens, the average peak bond stress was 7.1% higher than the control.

In all RCA replacement levels, the #6 (No. 19) specimens exhibited higher bond stresses than the #4 specimens. However, as RCA replacement increases, the percent difference between decreased. The percent difference between #4 (No. 13) and #6 (No. 19) was 8.6%, 7.8%, and 3.1% for the VAC, RAC-50, and RAC-100, respectively.

6.2.3. Beam Splice Testing. Three beam splice specimens were constructed and tested for each RCA replacement level. Deformed #6 (No. 19) steel bars were used as

longitudinal reinforcement and no confinement was provided in the spliced region. All beams were cast with longitudinal reinforcement in the bottom of the beam. A comparison of the square root normalized results indicates that 50% RCA beams had a slight increase in developed stress in the steel of 5.9% over the VAC control. However, the 100% RCA beams had a decrease in stress of 16.9% over the VAC control. A comparison of the fourth root normalized results shows that generally, both RCA beam sets had a lower stress in the steel. The 50% RCA beams decreased by 5.0%, and the 100% RCA beams decreased by 19.5%.

6.3. CONCLUSIONS

6.3.1. Direct Pull-Out Testing. Analysis of the direct pull-out data indicates that both 50% and 100% RCA mixes performed comparably or had a slight improvement in bond capacity over the controls. However, a statistical analysis indicates that all mixes performed comparably when normalized by the square root of concrete compressive strength for both #4 (No. 13) and #6 (No. 19) specimens. When normalized by the fourth root of concrete compressive strength, #4 (No. 13) specimens performed comparably across all three mixes, and #6 (No. 19) specimens were comparable between the 50% RCA and control mixes. Only the #6 (No. 19) specimens had a statistically significant difference between the 100% RCA and control mixes, with the 100% RCA showing a 7.1% increase in bond strength.

6.3.2. Beam Splice Testing. Analysis of the beam splice data indicates that both 50% and 100% RCA specimens exhibited diminished bond strength over the control specimens. A statistical analysis indicates that when normalized by either the square root

or fourth root of concrete compressive strength, the 50% RCA specimens performed comparably to the control specimens. However, the 100% RCA specimens exhibited a statistically significant decrease in bond strength from the control specimens, 16.9% based on the square root normalization and 19.5% based on the fourth root normalization. This decrease in bond strength parallels the decrease in splitting tensile strength, 29%, and fracture energy, 22%, both of which are related to the tensile response of the concrete, which governs bond failures where splitting cracks control. These findings indicate that replacing more than 50% of the coarse natural aggregates with RCA may require some modification to the bond and development length to achieve sufficient bond strength between deformed steel reinforcing bars and the surrounding concrete.

6.4. RECOMMENDATIONS

Due to the limited number of studies into the bond behavior of RCA, further research is needed to make comparisons and conclusions across a larger database. To better understand the influence of RCA replacement on the bond behavior of reinforced concrete, additional variables important to design must also be investigated. A list of the testable variables relating to the structural characteristics and bar properties of the reinforced member is given below:

- Perform tests with wider variation in bar sizes to investigate bar size effect
- Perform tests with smooth bars and deformed bars with different rib heights to develop relationship between rib height and bond strength
- Perform tests with different surface deterioration and cleanliness
- Perform tests with epoxy or zinc coated bars

- Perform studies with transverse reinforcement provided in the spliced region to investigate effect of confinement
- Perform studies with splice region cast with more than 12 in. (30.5 cm) of concrete below to investigate “top bar” effect
- Perform tests with noncontact lap splices to evaluate performance with contact lap splices

Testable variables relating to the RCA material itself are listed below:

- Perform studies on RCA from different source structures (pavements, building structures, bridge structures, etc.)
- Perform studies on RCA from different source locations (different geographical regions of the United States)
- Perform studies on RCA from different parent rock material
- Perform studies with varied amounts of chloride contamination
- Perform studies with varied amounts of organic impurities
- Perform studies with varied amounts of fine RCA

APPENDIX A: DIRECT PULL-OUT TEST DATA PLOTS

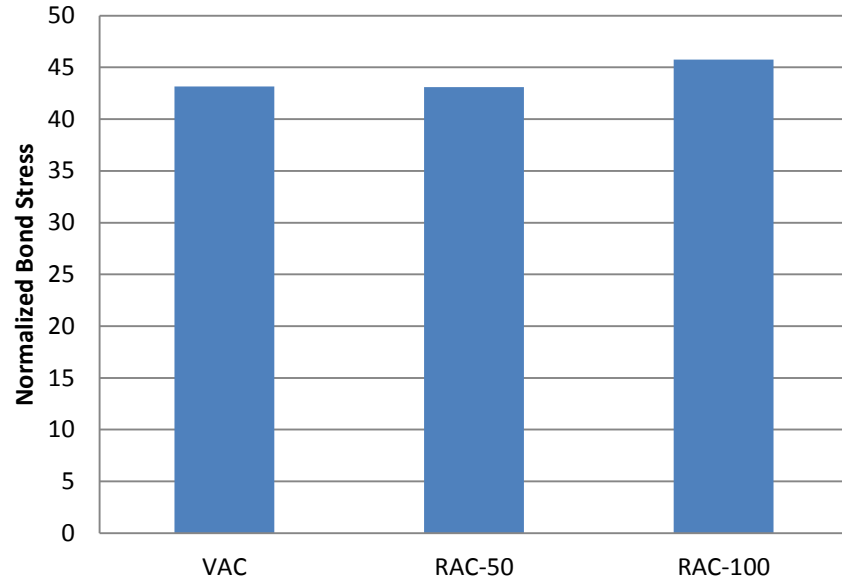


Figure A.1: Bond Stresses for #4 Pull-Out Specimens, Square Root Normalization

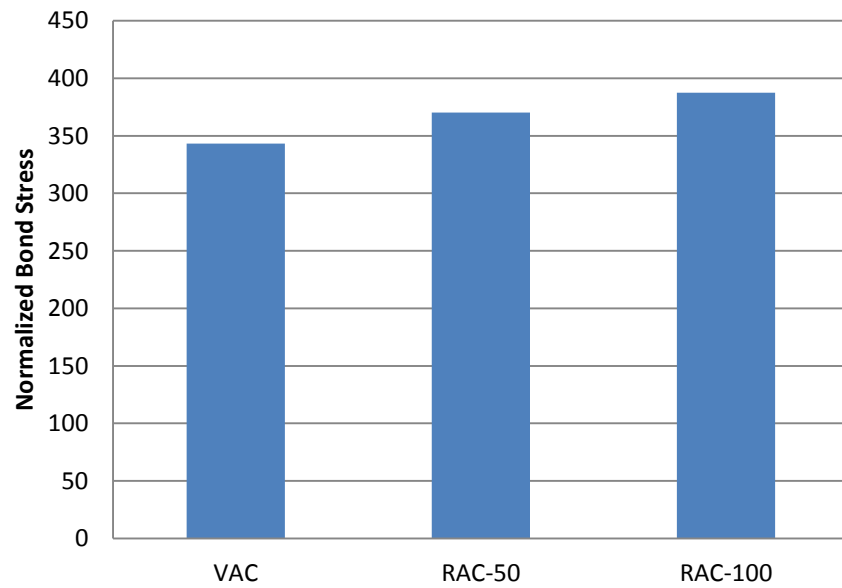


Figure A.2: Bond Stresses for #4 Pull-Out Specimens, Fourth Root Normalization

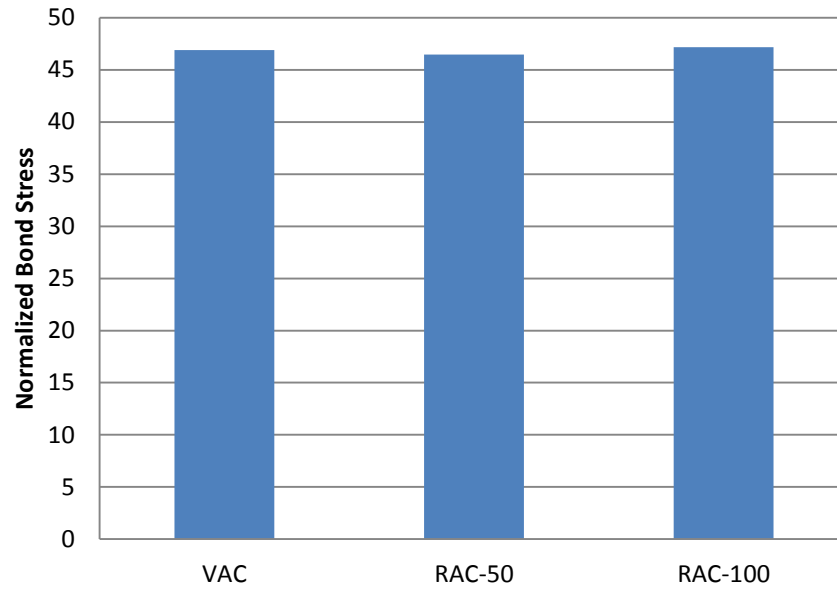


Figure A.3: Bond Stresses for #6 Pull-Out specimens, Square Root Normalization

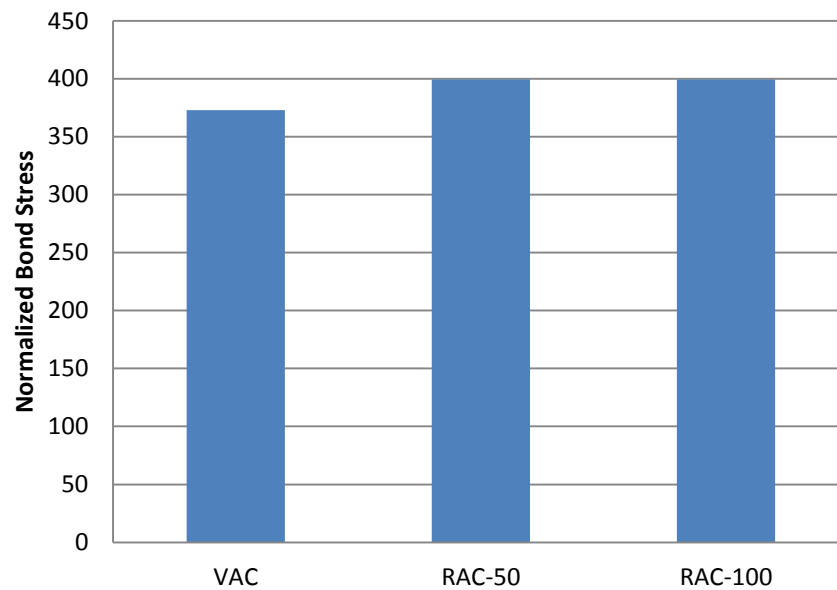


Figure A.4: Bond Stresses for #6 Pull-Out Specimens, Fourth Root Normalization

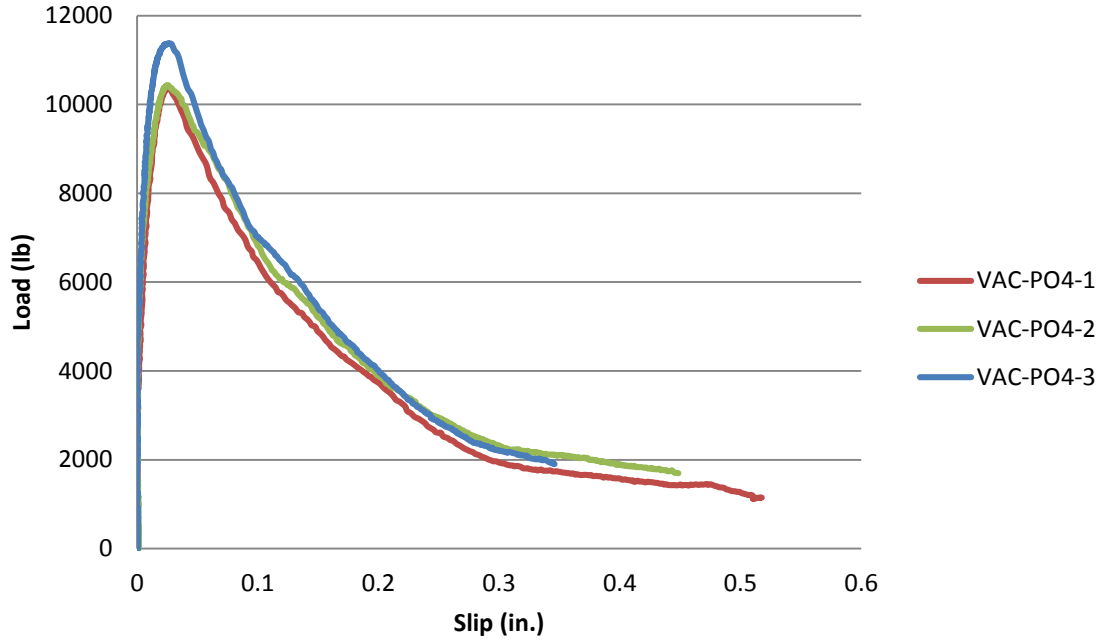


Figure A.5: Applied Load vs. Slip Plot for #4 (No. 13) VAC-PO4

Conversion: 1 in. = 25.4 mm

1 lb. = 4.45 N

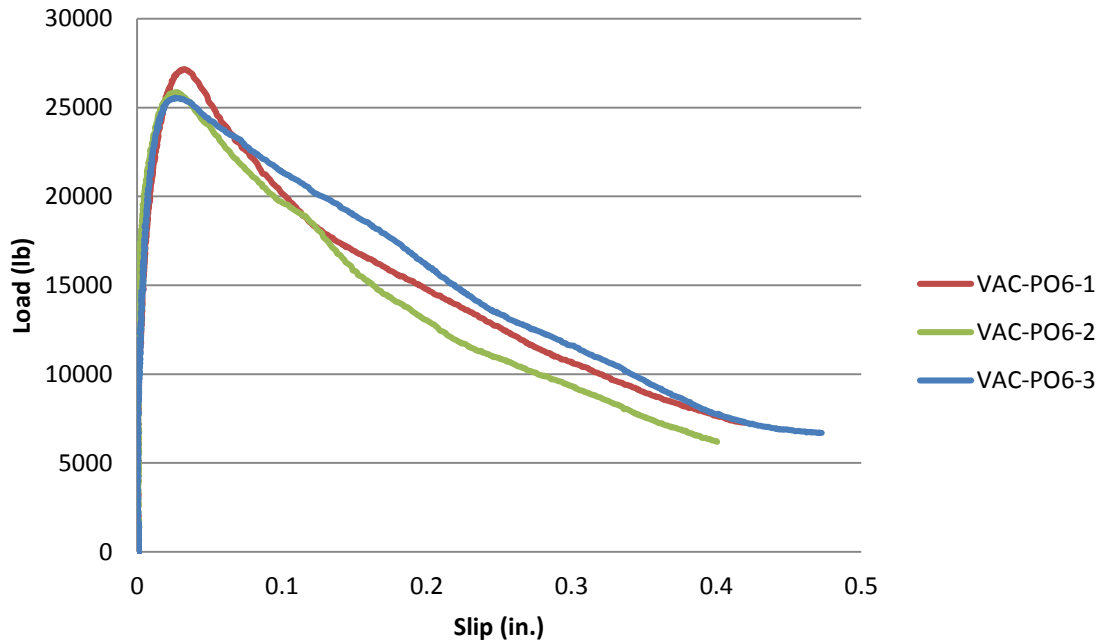


Figure A.6: Applied Load vs. Slip Plot for #6 (No. 19) VAC-PO6

Conversion: 1 in. = 25.4 mm

1 lb. = 4.45 N

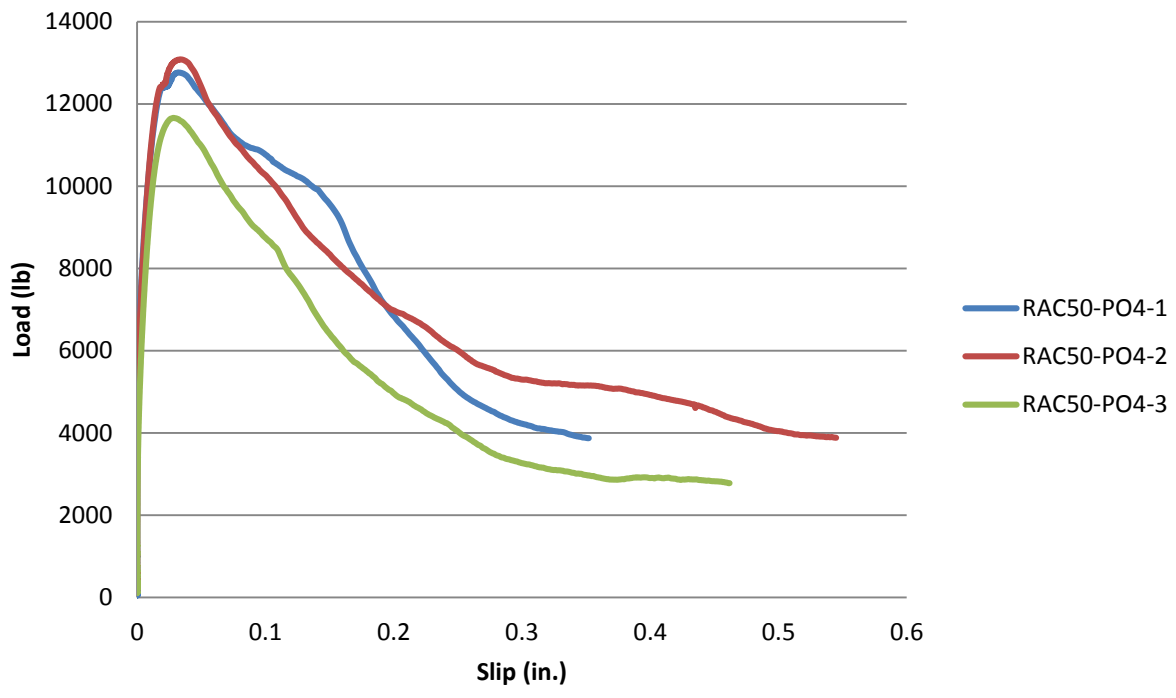


Figure A.7: Applied Load vs. Slip Plot for #4 (No. 13) RCA50-PO4
Conversion: 1 in. = 25.4 mm
1 lb. = 4.45 N

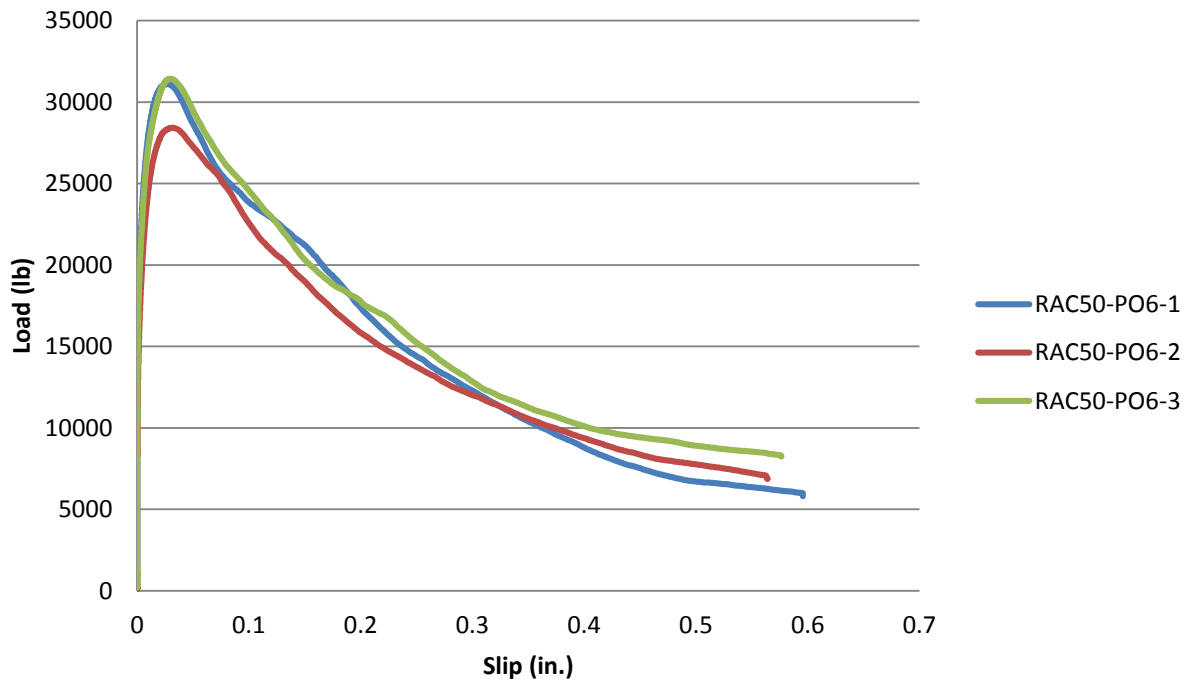


Figure A.8: Applied Load vs. Slip Plot for #6 (No. 19) RCA50-PO6
Conversion: 1 in. = 25.4 mm
1 lb. = 4.45 N

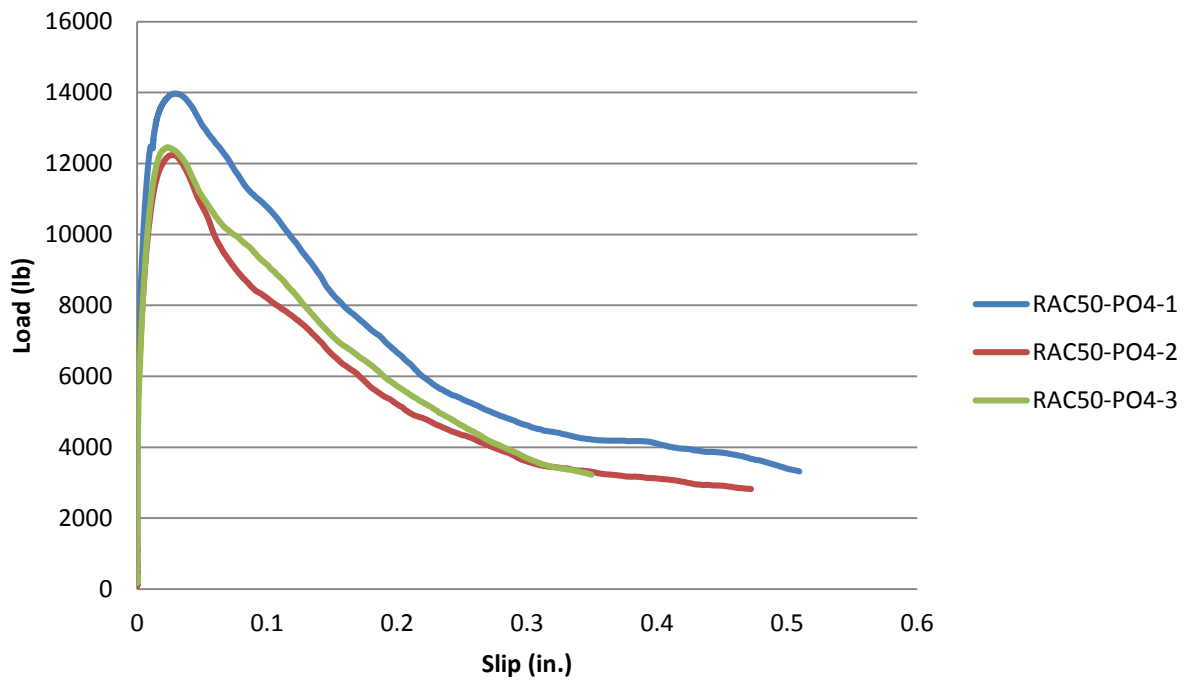


Figure A.9: Applied Load vs. Slip Plot for #4 (No. 13) RCA100-PO4
Conversion: 1 in. = 25.4 mm
1 lb. = 4.45 N

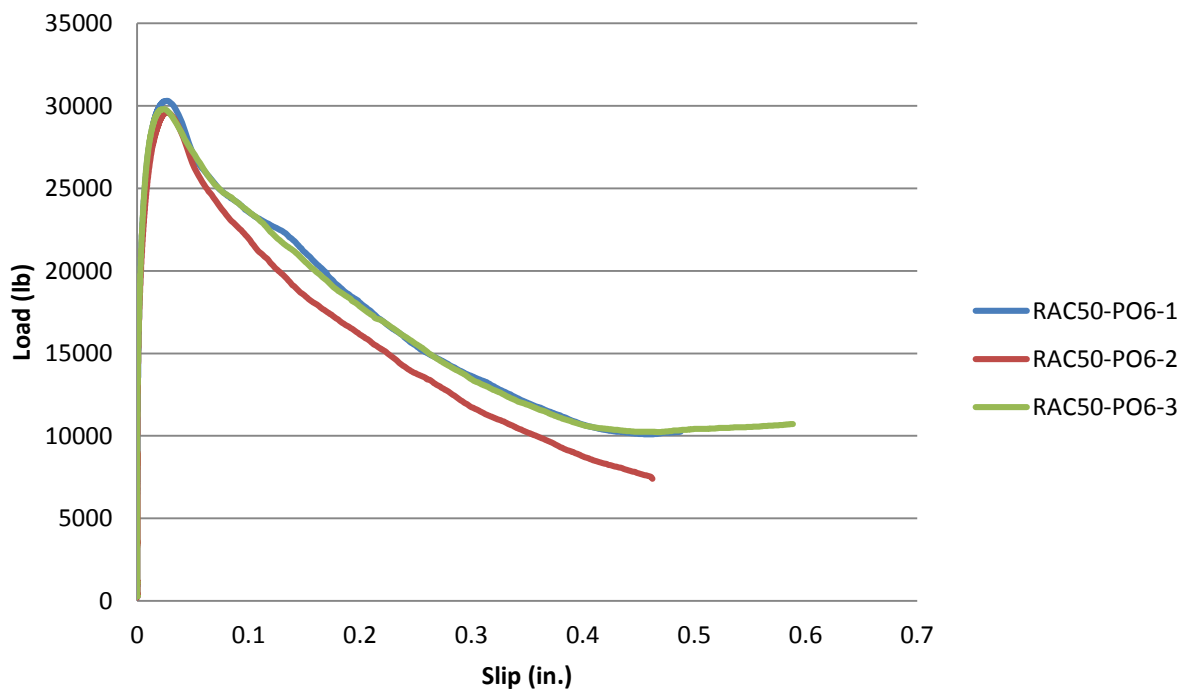


Figure A.10: Applied Load vs. Slip Plot for #6 (No. 19) RCA100-PO6
Conversion: 1 in. = 25.4 mm
1 lb. = 4.45 N

APPENDIX B: BEAM SPLICE TEST DATA PLOTS

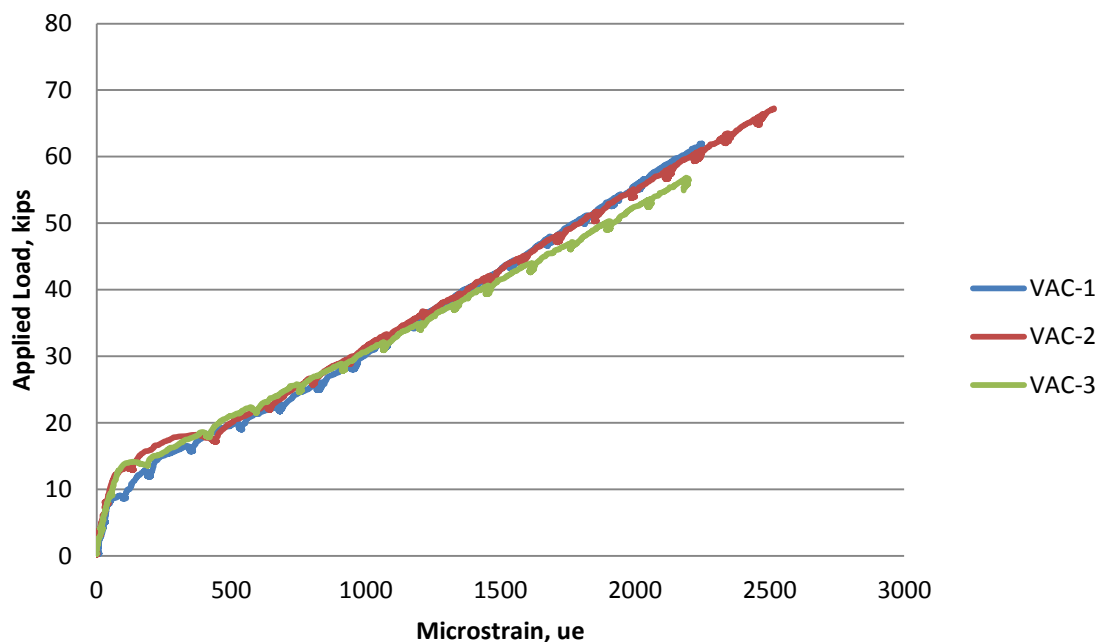


Figure B.1: Applied Load vs. Strain for VAC Specimens

Conversion: 1 kip = 4.45 kN

Note: Average of all gauges per specimen.

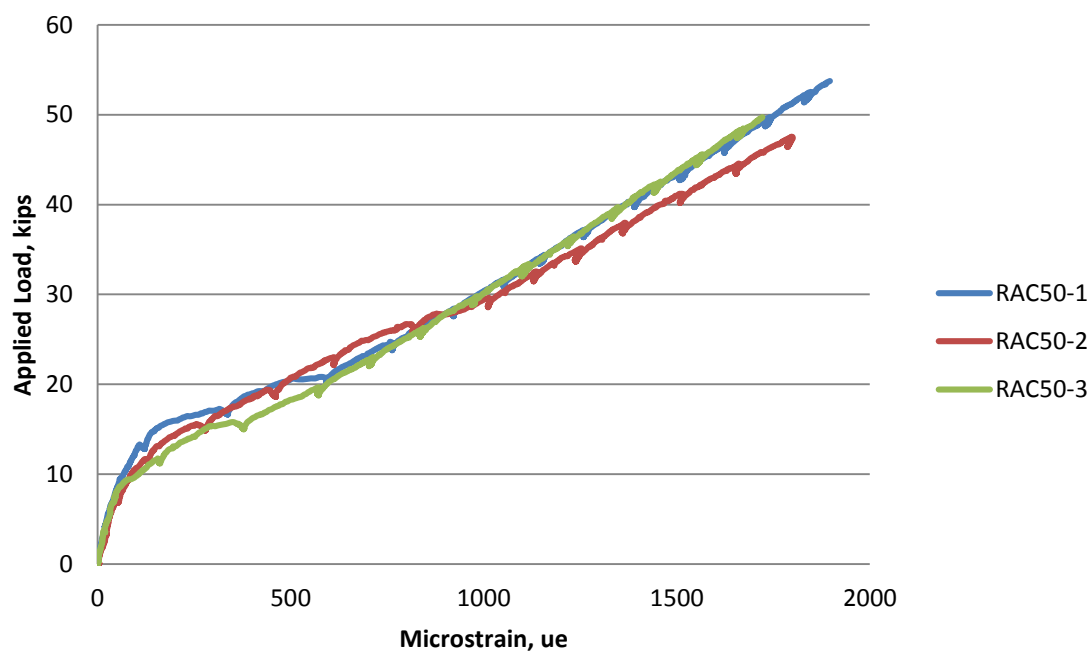


Figure B.2: Applied Load vs. Strain for RAC-50 Specimens

Conversion: 1 kip = 4.45 kN

Note: Average of all gauges per specimen.

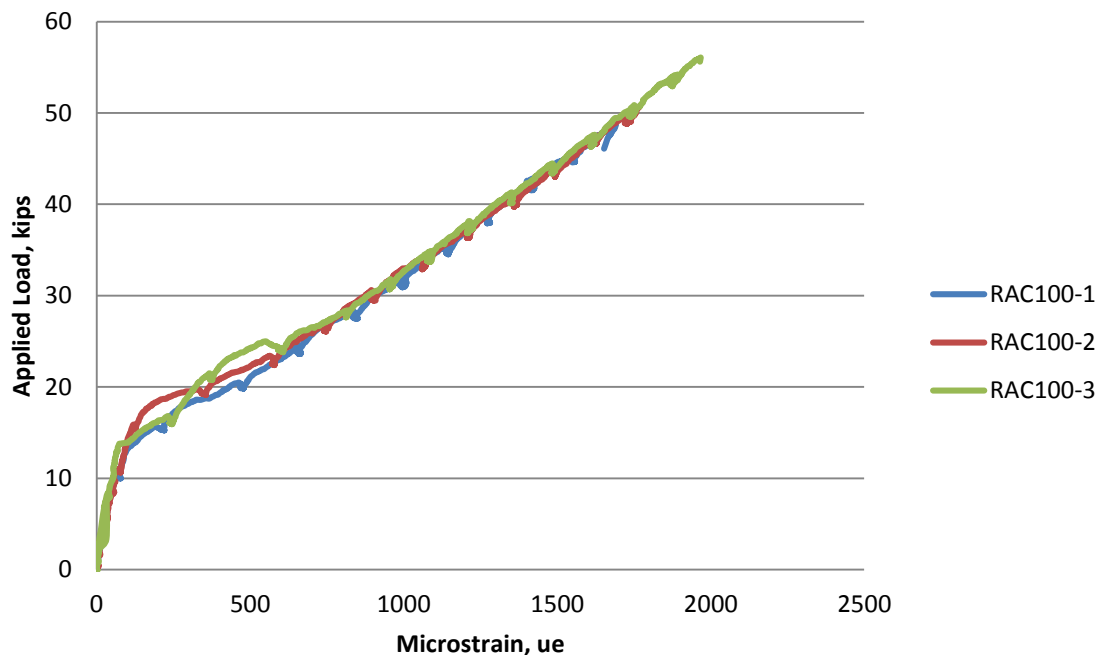


Figure B.3: Applied Load vs. Strain for RAC-100 Specimens

Conversion: 1 kip = 4.45 kN

Note: Average of all gauges per specimen.

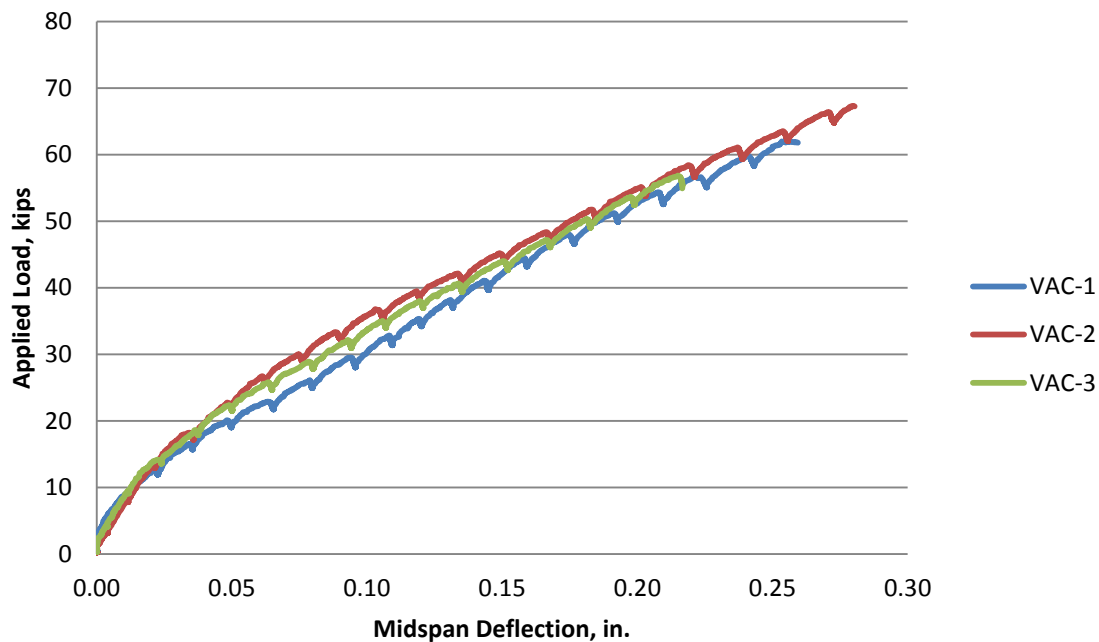


Figure B.4: Applied load vs. Midspan Deflection for VAC

Conversion: 1 in. = 25.4 mm

1 kip = 4.45 kN

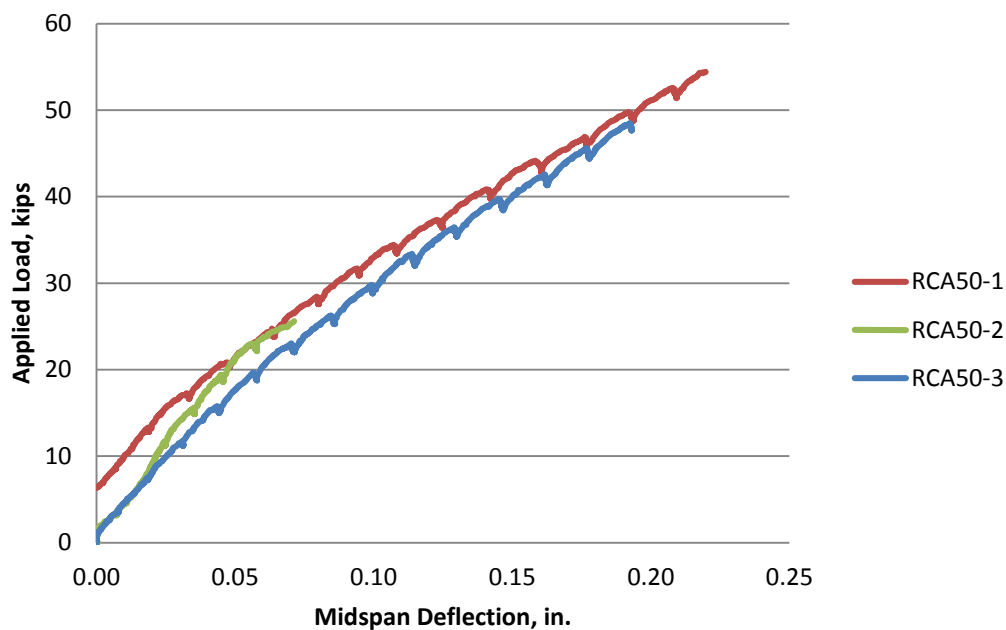


Figure B.5: Applied load vs. Midspan Deflection for RAC-50

Conversion: 1 in. = 25.4 mm

1 kip = 4.45 kN

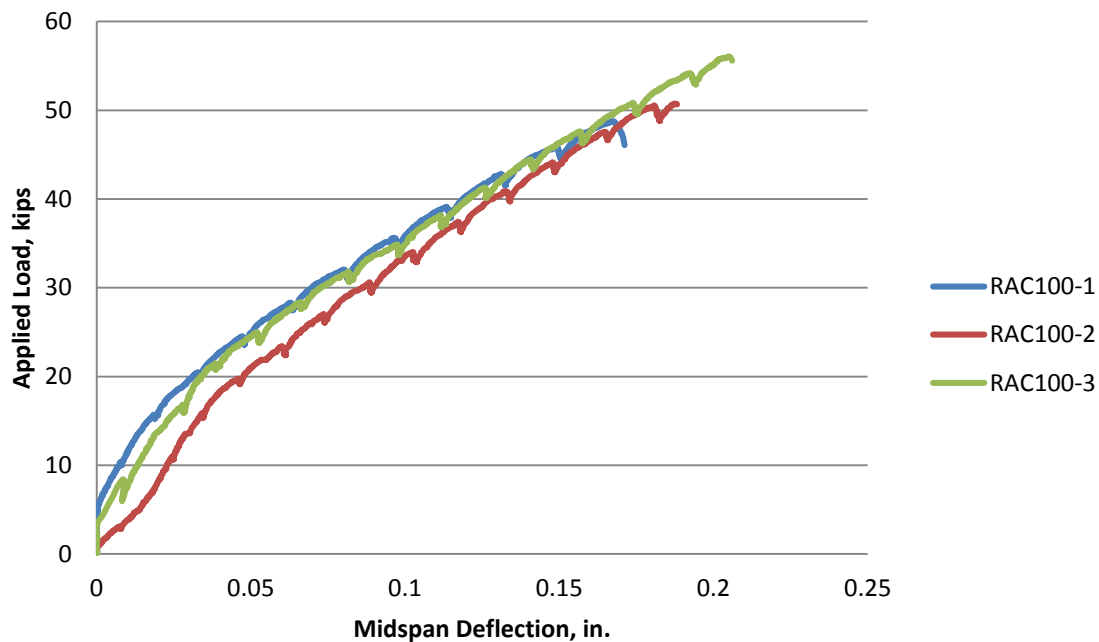


Figure B.6: Applied load vs. Midspan Deflection for RAC-100

Conversion: 1 in. = 25.4 mm

1 kip = 4.45 kN

APPENDIX C: PHOTOGRAPHS OF BEAM SPLICE FAILURES



Figure C.3: Side View of VAC-2



Figure C.4: Bottom View of VAC-2



Figure C.5: Side View of VAC-3



Figure C.6: Bottom View of VAC-3

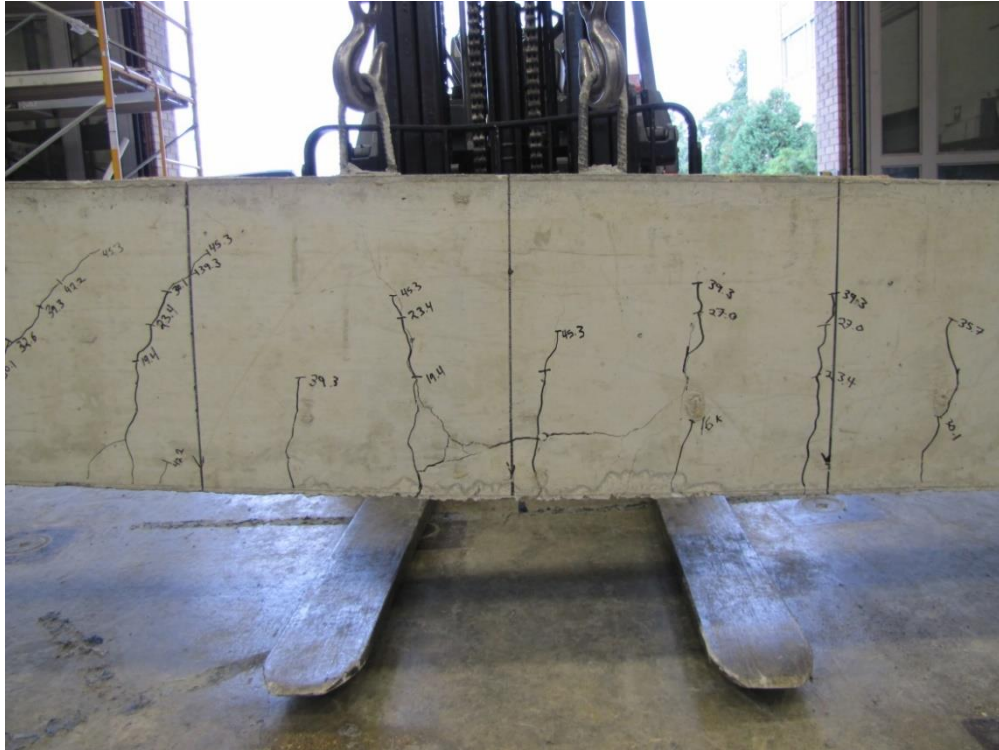




Figure C.9: Side View of RAC50-2



Figure C.10: Bottom View of RAC50-2



Figure C.11: Side View of RAC50-3



Figure C.12: Bottom View of RAC50-3

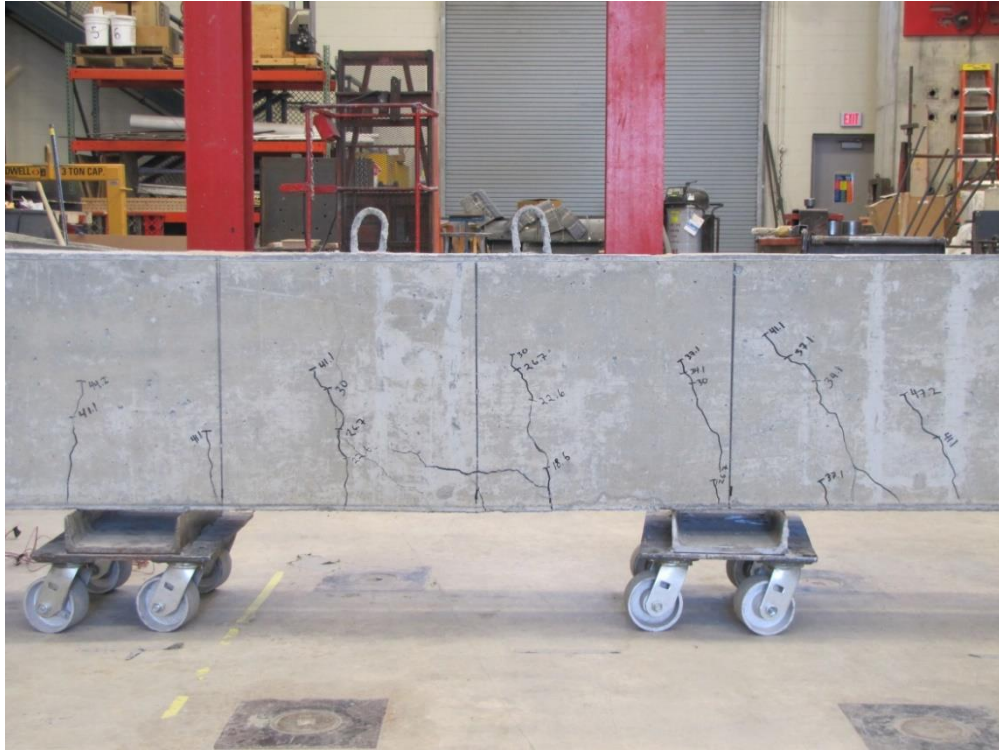


Figure C.13: Side View of RAC100-1



Figure C.14: Bottom View of RAC100-1



Figure C.15: Side View of RAC100-2



Figure C.16: Bottom View of RAC100-2



Figure C.17: Side View of RAC100-3



Figure C.18: Bottom View of RAC100-3

APPENDIX D: STATISTICAL ANALYSIS OF RESULTS

Table D.1: Parametric Analysis of #4 (No.13) Pull-Out Results with Square Root Normalization between VAC and RAC-50

t-Test: Two-Sample Assuming Unequal Variances

	VAC	RAC-50
Mean	43.15965	43.07783
Variance	5.324474	6.639769
Observations	3	3
Hypothesized Mean Difference	0	
df	4	
t Stat	0.040971	
P(T<=t) one-tail	0.484641	
t Critical one-tail	2.131847	
P(T<=t) two-tail	0.969283	
t Critical two-tail	2.776445	

Table D.2: Non-parametric Analysis of #4 (No.13) Pull-Out Results with Square Root Normalization between VAC and RAC-50

Mann-Whitney Test and CI: VAC, RAC-50	
N	Median
VAC 3	42.015
RAC-50 3	43.974
Point estimate for ETA1-ETA2 is 0.729	
91.9 Percent CI for ETA1-ETA2 is (-3.438,5.645)	
W = 11.0	
Test of ETA1 = ETA2 vs ETA1 not = ETA2 is significant at 1.0000	

Table D.3: Parametric Analysis of #4 (No.13) Pull-Out Results with Square Root Normalization between VAC and RAC-100

t-Test: Two-Sample Assuming Unequal Variances

	VAC	RAC-100
Mean	43.15965	45.73487
Variance	5.324474	11.22826
Observations	3	3
Hypothesized Mean Difference	0	
df	4	
t Stat	-1.09633	
P(T<=t) one-tail	0.167254	
t Critical one-tail	2.131847	
P(T<=t) two-tail	0.334509	
t Critical two-tail	2.776445	

Table D.4: Non-parametric Analysis of #4 (No.13) Pull-Out Results with Square Root Normalization between VAC and RAC-100

Mann-Whitney Test and CI: VAC, RAC-100	
N	Median
VAC 3	42.015
RAC-100 3	44.194
Point estimate for ETA1-ETA2 is -2.180	
91.9 Percent CI for ETA1-ETA2 is (-7.932,2.384)	
W = 8.0	
Test of ETA1 = ETA2 vs ETA1 not = ETA2 is significant at 0.3827	

Table D.5: Parametric Analysis of #6 (No.19) Pull-Out Results with Square Root Normalization between VAC and RAC-50

t-Test: Two-Sample Assuming Unequal Variances

	VAC	RAC-50
Mean	46.88684	46.44951
Variance	2.337816	6.39148
Observations	3	3
Hypothesized Mean Difference	0	
df	3	
t Stat	0.256377	
P(T<=t) one-tail	0.407118	
t Critical one-tail	2.353363	
P(T<=t) two-tail	0.814236	
t Critical two-tail	3.182446	

Table D.6: Non-Parametric Analysis of #6 (No.19) Pull-Out Results with Square Root Normalization between VAC and RAC-50

Mann-Whitney Test and CI: VAC, RAC-50	
N	Median
VAC 3	46.292
RAC-50 3	47.648
Point estimate for ETA1-ETA2 is 0.469	
91.9 Percent CI for ETA1-ETA2 is (-2.410,5.080)	
W = 11.0	
Test of ETA1 = ETA2 vs ETA1 not = ETA2 is significant at 1.0000	

Table D.7: Parametric Analysis of #6 (No.19) Pull-Out Results with Square Root Normalization between VAC and RAC-100

t-Test: Two-Sample Assuming Unequal Variances

	VAC	RAC-100
Mean	46.88684	47.17004
Variance	2.337816	0.32679
Observations	3	3
Hypothesized Mean Difference	0	
df	3	
t Stat	-0.30049	
P(T<=t) one-tail	0.391712	
t Critical one-tail	2.353363	
P(T<=t) two-tail	0.783424	
t Critical two-tail	3.182446	

Table D.8: Non-Parametric Analysis of #6 (No.19) Pull-Out Results with Square Root Normalization between VAC and RAC-100

Mann-Whitney Test and CI: VAC, RAC-100	
N	Median
VAC 3	46.292
RAC-100 3	47.017
Point estimate for ETA1-ETA2 is -0.725	
91.9 Percent CI for ETA1-ETA2 is (-2.057,1.933)	
W = 9.0	
Test of ETA1 = ETA2 vs ETA1 not = ETA2 is significant at 0.6625	

Table D.9: Parametric Analysis of #4 (No.13) Pull-Out Results with Fourth Root Normalization between VAC and RAC-50

t-Test: Two-Sample Assuming Unequal Variances

	VAC	RAC-50
Mean	343.236	370.2985
Variance	336.7493	490.6246
Observations	3	3
Hypothesized Mean Difference	0	
df	4	
t Stat	-1.62959	
P(T<=t) one-tail	0.089261	
t Critical one-tail	2.131847	
P(T<=t) two-tail	0.178522	
t Critical two-tail	2.776445	

Table D.10: Non-parametric Analysis of #4 (No.13) Pull-Out Results with Fourth Root Normalization between VAC and RAC-50

Mann-Whitney Test and CI: VAC, RAC-50	
N	Median
VAC 3	334.13
RAC-50 3	378.00
Point estimate for ETA1-ETA2 is -23.21	
91.9 Percent CI for ETA1-ETA2 is (-56.36,19.04)	
W = 7.0	
Test of ETA1 = ETA2 vs ETA1 not = ETA2 is significant at 0.1904	

Table D.11: Parametric Analysis of #4 (No.13) Pull-Out Results with Fourth Root Normalization between VAC and RAC-100

t-Test: Two-Sample Assuming Unequal Variances

	<i>VAC</i>	<i>RAC-100</i>
Mean	343.236	387.3789
Variance	336.7493	805.5445
Observations	3	3
Hypothesized Mean Difference	0	
df	3	
t Stat	-2.26221	
P(T<=t) one-tail	0.054352	
t Critical one-tail	2.353363	
P(T<=t) two-tail	0.108704	
t Critical two-tail	3.182446	

Table D.12: Non-parametric Analysis of #4 (No.13) Pull-Out Results with Fourth Root Normalization between VAC and RAC-100

Mann-Whitney Test and CI: VAC, RAC-100	
N	Median
VAC	3 334.13
RAC-100	3 374.33
Point estimate for ETA1-ETA2 is -40.20	
91.9 Percent CI for ETA1-ETA2 is (-88.70,-3.51)	
W = 6.0	
Test of ETA1 = ETA2 vs ETA1 not = ETA2 is significant at 0.0809	

Table D.13: Parametric Analysis of #6 (No.19) Pull-Out Results with Fourth Root Normalization between VAC and RAC-50

t-Test: Two-Sample Assuming Unequal Variances

	VAC	RAC-50
Mean	372.8773	399.2816
Variance	147.8565	472.2781
Observations	3	3
Hypothesized Mean Difference	0	
df	3	
t Stat	-1.83651	
P(T<=t) one-tail	0.081803	
t Critical one-tail	2.353363	
P(T<=t) two-tail	0.163606	
t Critical two-tail	3.182446	

Table D.14: Non-Parametric Analysis of #6 (No.19) Pull-Out Results with Fourth Root Normalization between VAC and RAC-50

Mann-Whitney Test and CI: VAC, RAC-50	
N	Median
VAC 3	368.15
RAC-50 3	409.59
Point estimate for ETA1-ETA2 is -27.25	
91.9 Percent CI for ETA1-ETA2 is (-50.14,12.37)	
W = 7.0	
Test of ETA1 = ETA2 vs ETA1 not = ETA2 is significant at 0.1904	

Table D.15: Parametric Analysis of #6 (No.19) Pull-Out Results with Fourth Root Normalization between VAC and RAC-100

t-Test: Two-Sample Assuming Unequal Variances

	VAC	RAC-100
Mean	372.8773	399.5349
Variance	147.8565	23.44476
Observations	3	3
Hypothesized Mean Difference	0	
df	3	
t Stat	-3.52778	
P(T<=t) one-tail	0.01935	
t Critical one-tail	2.353363	
P(T<=t) two-tail	0.038701	
t Critical two-tail	3.182446	

Table D.16: Non-Parametric Analysis of #6 (No.19) Pull-Out Results with Fourth Root Normalization between VAC and RAC-100

Mann-Whitney Test and CI: VAC, RAC-100	
N	Median
VAC 3	368.15
RAC-100 3	398.24
Point estimate for ETA1-ETA2 is -30.09	
91.9 Percent CI for ETA1-ETA2 is (-41.10,-8.79)	
W = 6.0	
Test of ETA1 = ETA2 vs ETA1 not = ETA2 is significant at 0.0809	

Table D.17: Parametric Analysis of Beam Splice Results with Square Root Normalization between VAC and RAC-50

t-Test: Two-Sample Assuming Unequal Variances

	VAC	RAC-50
Mean	65.12762	68.98221
Variance	24.56742	1.342879
Observations	3	3
Hypothesized Mean Difference	0	
df	2	
t Stat	-1.3116	
P(T<=t) one-tail	0.159997	
t Critical one-tail	2.919986	
P(T<=t) two-tail	0.319993	
t Critical two-tail	4.302653	

Table D.18: Non-Parametric Analysis of Beam Splice Results with Square Root Normalization between VAC and RAC-50

Mann-Whitney Test and CI: VAC, RAC-50	
N	Median
VAC 3	63.010
RAC-50 3	68.611
Point estimate for ETA1-ETA2 is -5.602	
91.9 Percent CI for ETA1-ETA2 is (-8.700,2.736)	
W = 9.0	
Test of ETA1 = ETA2 vs ETA1 not = ETA2 is significant at 0.6625	

Table D.19: Parametric Analysis of Beam Splice Results with Square Root Normalization between VAC and RAC-100

t-Test: Two-Sample Assuming Unequal Variances

	VAC	RAC-100
Mean	65.12762	54.09878
Variance	24.56742	17.64037
Observations	3	3
Hypothesized Mean Difference	0	
df	4	
t Stat	2.940316	
P(T<=t) one-tail	0.021188	
t Critical one-tail	2.131847	
P(T<=t) two-tail	0.042376	
t Critical two-tail	2.776445	

Table D.20: Non-Parametric Analysis of Beam Splice Results with Square Root Normalization between VAC and RAC-100

Mann-Whitney Test and CI: VAC, RAC-100		
	N	Median
VAC	3	63.01
RAC-100	3	53.14
Point estimate for ETA1-ETA2 is 11.12		
91.9 Percent CI for ETA1-ETA2 is (2.89,20.33)		
W = 15.0		
Test of ETA1 = ETA2 vs ETA1 not = ETA2 is significant at 0.0809		

Table D.21: Parametric Analysis of Beam Splice Results with Fourth Root Normalization between VAC and RAC-50

t-Test: Two-Sample Assuming Unequal Variances

	VAC	RAC-50
Mean	65.12762	61.8741
Variance	24.56742	1.08039
Observations	3	3
Hypothesized Mean Difference	0	
df	2	
t Stat	1.112727	
P(T<=t) one-tail	0.190821	
t Critical one-tail	2.919986	
P(T<=t) two-tail	0.381643	
t Critical two-tail	4.302653	

Table D.22: Non-Parametric Analysis of Beam Splice Results with Fourth Root Normalization between VAC and RAC-50

Mann-Whitney Test and CI: VAC, RAC-50	
N	Median
VAC 3	63.010
RAC-50 3	61.541
Point estimate for ETA1-ETA2 is 1.468	
91.9 Percent CI for ETA1-ETA2 is (-1.459,9.748)	
W = 13.0	
Test of ETA1 = ETA2 vs ETA1 not = ETA2 is significant at 0.3827	

Table D.23: Parametric Analysis of Beam Splice Results with Fourth Root Normalization between VAC and RAC-100

t-Test: Two-Sample Assuming Unequal Variances

	VAC	RAC-100
Mean	65.12762	52.39721
Variance	24.56742	16.54813
Observations	3	3
Hypothesized Mean Difference	0	
df	4	
t Stat	3.438744	
P(T<=t) one-tail	0.013162	
t Critical one-tail	2.131847	
P(T<=t) two-tail	0.026324	
t Critical two-tail	2.776445	

Table D.24: Non-Parametric Analysis of Beam Splice Results with Fourth Root Normalization between VAC and RAC-100

Mann-Whitney Test and CI: VAC, RAC-100		
	N	Median
VAC	3	63.01
RAC-100	3	51.47
Point estimate for ETA1-ETA2 is 12.71		
91.9 Percent CI for ETA1-ETA2 is (4.73,21.92)		
W = 15.0		
Test of ETA1 = ETA2 vs ETA1 not = ETA2 is significant at 0.0809		

BIBLIOGRAPHY

- AASHTO (2007). AASHTO LRFD Bridge Design Specification. Fourth Edition, Washington, D.C.
- Abbas, A., et al. (2008). "Proposed Method for Determining the Residual Mortar Content of Recycled Concrete Aggregates," Journal of ASTM International, Vol. 5, Issue 1, pp. JAI101087.
- ACI 408R (2003). Bond and Development of Straight Reinforcing Bars in Tension. American Concrete Institute, Farmington Hills, MI.
- ACI 318 (2011). Building Code Requirement for Structural Concrete, Farmington Hills, MI.
- ASTM C 29 (2009). Standard Test Method for Bulk Density (Unit Weight) and Voids in Aggregate. American Society for Testing and Materials. West Conshohocken, PA.
- ASTM C 39 (2011). Standard Test Method for Compressive Strength of Cylindrical Concrete Specimens. American Society for Testing and Materials. West Conshohocken, PA.
- ASTM C 78 (2010). Standard Test Method for Flexural Strength of Concrete (Using Simple Beam with Third-Point Loading). American Society for Testing and Materials. West Conshohocken, PA.
- ASTM C 127 (2012). Standard Test Method for Density, Relative Density (Specific Gravity), and Absorption of Coarse Aggregate. American Society for Testing and Materials. West Conshohocken, PA.
- ASTM C 136 (2006). Standard Test Method for Sieve Analysis of Fine and Coarse Aggregates. American Society for Testing and Materials. West Conshohocken, PA.
- ASTM C 138 (2010). Standard Test Method for Density (Unit Weight), Yield, and Air Content (Gravimetric) of Concrete. American Society for Testing and Materials. West Conshohocken, PA.
- ASTM C 143 (2010). Standard Test Methods for Slump of Hydraulic Cement Concrete. American Society for Testing and Materials. West Conshohocken, PA.
- ASTM C 231 (2010). Standard Test Method for Air Content of Freshly Mixed Concrete by the Pressure Method. American Society for Testing and Materials. West Conshohocken, PA.

- ASTM C 469 (2010). Standard Test Method for Static Modulus of Elasticity and Poisson's Ratio of Concrete in Compression. American Society for Testing and Materials. West Conshohocken, PA.
- ASTM C 496 (2011). Standard Test Method for Splitting Tensile Strength of Cylindrical Concrete Specimens. American Society for Testing and Materials. West Conshohocken, PA.
- ASTM E8 (2009). Standard Test Methods for Tension Testing of Metallic Materials. American Society for Testing and Materials. West Conshohocken, PA.
- Bentz, E., Collins, M. (2000). Response-2000 Reinforced Concrete Sectional Analysis. Version 1.0.5. Toronto, Canada.
- Butler, L. et al. (2011). "The effect of recycled concrete aggregate properties on the bond strength between RCA concrete and steel reinforcement," *Cement and Concrete Research*, Vol. 41, Issue 10, pp. 1037-1049
- CEB-FIP Model Code for Concrete Structures (1990). "Evaluation of the Time Dependent Behaviour of Concrete," *Bulletin d'Information No. 199*, Comite European du Béton/Fédération Internationale de la Précontrainte, Lausanne, 1991, pp. 201
- Fathifazl, G. (2008). "Structural performance of steel reinforced recycled concrete members." Ph.D. Thesis, Department of Civil and Environmental Engineering, Carleton University, Ottawa, Ontario, Canada
- Federal Highway Administration. (2004). *Transportation Application of Recycled Concrete Aggregate: Federal Highway Administration State of Practice National Review*, <<http://www.fhwa.dot.gov/pavement/recycling/applications.pdf>>
- Kim, S.W. (2012). "Influence of recycled coarse aggregates on the bond behavior of deformed bars in concrete," *Engineering Structures*, Vol. 48, pp. 133
- Looney, T. (2012). "Bond Behavior of High-Volume Fly Ash and Self-Consolidation Concrete." M.S. Thesis, Missouri University of Science and Technology, Rolla, MO.
- RILEM 7-II-28. (1994). "Bond Test for Reinforcing Steel. 2. Pull-out test." E & FN Spon, London.
- RILEM, TC 50-FMC, (1985). *Fracture Mechanics of Concrete*, "Determination of the Fracture Energy of Mortar and Concrete by Means of Three-Point Bend Tests on Notched Beams," RILEM Recommendation, *Materials and Structures*, V. 18, No. 16, pp. 287-290.

- Shayan, A., and Xu, A. (2003). "Performance and Properties of Structural Concrete Made with Recycled Concrete Aggregate," *ACI Mater. J.*, Vol. 100, No. 5, pp. 371–380.
- Shi-Cong Kou, Chi-Sun Poon , Hui-Wen Wan, Properties of concrete prepared with low-grade recycled aggregates, *Construction and Building Materials* 36 (2012) 881–889.
- Wolfe, M. (2011). "Bond Strength of High-Volume Fly Ash Concrete." M.S. Thesis, Missouri University of Science and Technology, Rolla, MO.
- Zuo, J., and Darwin, D. (2000). "Splice Strength of Conventional and High Relative Rib Area Bars in Normal and High Strength Concrete," *ACI Structural Journal*, V. 97, No.4, July-Aug., pp.630-641